Thermal Evaluation of an Urbanized Watershed using SWMM and MINUHET: a Case Study of the Stroubles Creek Watershed, Blacksburg, VA

Mehdi Ketabchy

Thesis submitted to the faculty of the Virginia Polytechnic Institute and State University
in partial fulfillment of the requirements for the degree of

Master of Science
in
Biological Systems Engineering

David J. Sample, Chair
Theresa M. Thompson, Co-Chair
William C. Hession
Erich T. Hester

Virginia Beach, Virginia

December 20, 2017

Keywords: Stormwater pollution, MINUHET, SWMM, Temperature, Stroubles Creek, Watershed, Thermal

Thermal Evaluation of an Urbanized Watershed using SWMM and MINUHET: a Case Study of the Stroubles Creek Watershed, Blacksburg, VA

Mehdi Ketabchy

Scholarly Abstract

Urban development significantly increases water temperatures within watersheds, primarily from the construction of impervious surfaces for buildings and pavement. While thermally enriched runoff can be harmful to aquatic life, available research and guidance on predicting these effects is limited. The goal of this assessment is to provide guidance on how to achieve necessary temperature regimes that meet aquatic health criteria for sensitive species such as trout. To address this need, the Minnesota Urban Heat Export Tool (MINUHET) and U.S. Environmental Protection Agency's Storm Water Management Model (SWMM) models were utilized to simulate hourly streamflow, water temperature, and heat flux in an urban watershed in Blacksburg, VA for typical summer periods using continuous-based simulation. SWMM and MINUHET were combined in a unique, hybrid approach that emphasized each model's strengths, i.e., SWMM for runoff and streamflow, and MINUHET for water temperature. The watershed is 14.1 km^2, and is portion of Stroubles Creek located near downtown Blackburg, Virginia and the main campus of Virginia Tech. Streamflow, water temperature, and climate data were acquired from Virginia Tech StREAM Lab (Stream Research, Education, and Management) monitoring stations. SWMM and MINUHET were calibrated manually for the summers of 2016, and were validated for the summer of 2015. Model sensitivity analyses revealed that simulations were especially sensitive to imperviousness (SWMM predicted streamflow as outputs) and dew point temperature (MINUHET predicted water temperatures as outputs), both resulted in increased outputs of SWMM and MINUHET models, respectively.

Model performance in simulating streamflow was evaluated using Nash-Sutcliffe Efficiency (NSE) and correlation (R^2). NSE and R^2 values were 0.65 and 0.7 for the SWMM Model and 0.57 and 0.55 for the MINUHET model during the validation period, indicating that SWMM performed better than MINUHET in streamflow simulation. Streamflow temperatures were simulated using MINUHET with a NSE and R^2 statistical values of 0.58, and 0.83, respectively, demonstrating a satisfactory simulation of water temperature. Heat loads were simulated using the MINUHET and Hybrid models, demonstrating less Percent BIAS of the Hybrid approach in simulation of watershed total heat load than MINUHET alone. Furthermore, a number of practices were implemented to reduce thermal loading within a watershed. These included infiltration practices, methods for decreasing absorption of thermal energy primarily by reducing albedo, and increased vegetation canopies. An index titled Percentage of Time Temperature Exceeded 21°C Threshold (PTTET) for trout habitat was used to represent the effectiveness of thermal mitigation practices. Installing concrete pavement (thermal diffusivity: 15×10^{-7} m^2/s, pavement thickness: 0.20 m, and heat capacity: 4.0×10^6 $J/m^{3}\cdot°C$) and Acrylic Coated Galvalume (ACG) roofs for all pavement and roofs, respectively, in the watershed reduced heat load by 45%, and the PTTET index declined 4.5%. Installing bioretention with 61 cm of media thickness, and soil-media infiltration rate of 25 mm/hr. for 53 selected parking lots in the watershed, resulted in 11.1% reduction in watershed heat load and 1.4% reduction in PTTET. Planting forest canopies for the entire pervious area of the watershed, sufficient to shade 90% of all lands, resulted in reduction in heat load by 24% and PTTET by 4.6%.

Thermal Evaluation of an Urbanized Watershed using SWMM and MINUHET: a Case Study of the Stroubles Creek Watershed, Blacksburg, VA

Mehdi Ketabchy

General Audience Abstract

Development within urbanized regions increase impervious surfaces, which further cause significant storm events in watersheds. The increased impervious surfaces result in hotter stormwater particularly during hot summers, which has diverse effects on aquatic health of downstream receiving streams. The main objective of the current study is to evaluate the thermal impact of urbanization on aquatic health habitats in Stroubles Creek Watershed, Blacksburg, Virginia. To aim this goal and achieve the thermal evaluation of the highly urbanized Stroubles Creek Watershed, a U.S. Environmental Protection Agency's Storm Water Management Model (SWMM) and a Minnesota Urban Heat Export Tool (MINUHET) models from scratch of the Stroubles Creek watershed, using Town of Blacksburg and Virginia Tech Physical Facility information were developed. This necessitated combining information from a wide variety of sources, including geologic maps, geodatabases, hydraulic models, computer-aided design (CAD) files, and scanned as-built information. In addition to the models, a hybrid model was developed that combines SWMM and MINHET outputs. The temperatures and heat loads at the downstream of the watershed were predicted using SWMM, MINUHET, and Hybrid models for two summer periods of 2016 and 2015, and the predicted temperature were compared to the criteria for survival of aquatic health such as trout. Furthermore, a number of thermal mitigation strategies such as bioretentions systems, concrete pavements (which has lighter color compared to asphalt pavements), and increased vegetation canopies were simulated within the MINUHET and SWMM models configurations to reduce simulated temperatures and heat loads at the

watershed scale. The simulated temperatures and heat loads represented that concrete pavements results in better performance of thermal mitigation within watersheds than bioretention systems, and increased vegetation canopies.

This thesis is dedicated to my mother, thank you!

ACKNOWLEDGEMENTS

First, I would like to thank my advisors and mentors, Dr. David Sample and Dr. Tess Thompson for giving me the chance to attend graduate school at the Virginia Tech Biological Engineering Department, and for all their valuable advice, input, and guidance throughout this entire process.

I would also like to thank my committee members, Dr. Hester and Dr. Hession for their time and effort, and especially for their professional advice over the last 2 years. I would like to thank specially Dr. William Herb at the University of Minnesota for his advice and comments on my research program throughout the last 1 year. I also thank Dr. Saied Mostaghimi Graduate Dean of our college for being supportive and sympathetic over my career at Virginia Tech.

Thanks to my mom and dad, Farideh Nahreini and Mehran Ketabchi for being understanding and loving parents. Thank also to the rest of my family including my brother Farbod Ketabchi for his supportive personality, and my friend Shima Safinia for making 2 years of my graduate school at Virginia Tech a great time.

Thank you all!

TABLE OF CONTENTS

LIST OF FIGURES

LIST OF TABLES

Chapter 1.0 Introduction

Urban development significantly impacts thermal processes within watersheds primarily through the construction of impervious surfaces for buildings and pavement. These surfaces are typically darker than natural surfaces, and absorb, and hold more thermal energy, thereby raising the temperature of runoff. Higher temperature runoff directly impacts receiving streams. Stream temperature is an important aspect of water quality, playing a critical role in physical, chemical, and biological processes (Caissie, 2006). Water temperature regimes in streams and rivers are influenced by changes in air and groundwater temperatures, shading, and alterations to the hydrologic regime. These changes occur due to stream and land surface modifications, and can be the result of natural and human-induced activities. The principal anthropogenic and natural influences on stream temperature regime are described in Table 1.1. The natural processes affecting stream temperature are solar energy, type of substrate through which the water flows (Johnson, 2004), heat exchanges across the water surface and streambed (Webb and Zhang, 1999) and the water surface and air, and heat advection from tributaries and groundwater flows (Evans et al., 1998).

1.1 Criteria on temperature threshold for trout habitat

The recent rapid increase in the thermal pollution of streams due to urbanization and runoff inputs (which create both intermittent temperature spikes as well as elevating the average water temperature) has prompted the evaluation of thermal effects on aquatic health and the associated monitoring studies (Herb et al., 2009a). The sensitivity of trout to daily average and daily maximum stream temperatures was evaluated (Wehrly et al., 2007). According to the study findings, the threshold maximum daily temperature varies from 27.5°C for a single-day exposure to 25.5°C for a seven-day exposure; Single day maximum temperatures (27.5°C) can be used as

an acute toxicity threshold for trout. Another study indicated that even at very short exposure times (10 min), water at 30°C could be fatal for trout (Elliott and Elliott, 1995). Most trout begin to experience some level of stress at approximately 21°C (Herb et al., 2009a). While many trout species can withstand gradual warming with changes in seasons, rapid changes in temperature can be fatal (Agersborg, 1930); hence, high magnitude temperatures and heat loads spikes should be evaluated.

Table 1.1. The principal anthropogenic and natural influences on stream temperature regime.

Influences	Description	References
Anthropogenic		
Reduced stream shading and riparian vegetation	Increases net radiation, which results in stream temperature rise during summer days up to 10°C.	(Cooter and Cooter, 1990; Hester and Doyle, 2011)
Reduced groundwater exchange	Increased groundwater temperature during baseflow conditions leads to greater stream temperature.	(Taylor and Stefan, 2009)
Increase in impervious surface areas	Warmer surface runoff and consequently warmer streams/rivers immediately after storms during hot summers.	(Hester and Bauman, 2013; Li et al., 2013)
Heat energy of incoming wastewater effluents of industries	Stream temperature increases due to direct heat inflow to the stream/river.	(Hester and Doyle, 2011)
Channelization	Leads to less shading and increases daily and seasonal temperature fluctuations.	(Hester and Doyle, 2011)
Natural		
Type of Substrate	Bedrock substrate cools the stream temperature and dampens diurnal temperature fluctuations.	(Johnson, 2004)
Heat advection	Due to tributaries, and groundwater flows; can have either cooling effect (groundwater flows in summer) or warming effect (groundwater flows in winter or thermally enriched tributaries).	(Evans et al., 1998)

1.2 Research problem and purpose

It is clear that thermally enriched runoff can be harmful to aquatic life; however, only limited research and guidance is available for predicting these impacts at the watershed level. In Blacksburg, Virginia, Stroubles Creek is a stream with a watershed is highly urbanized, particularly in its headwaters, due to the presence of downtown Blacksburg, Virginia and a portion of the campus of Virginia Tech. These urbanized areas impact Stroubles Creek significantly via thermal loads from urban runoff. While several studies (Hester and Bauman, 2013; Long and Dymond, 2014) have investigated thermal loads in Stroubles, none has been conducted at the watershed scale or analyzed mitigation measures. Addressing these impacts on a watershed basis is needed. Stroubles Creek provides an excellent case study site due to extensive monitoring and available geodatabase information, relatively small size, and extensive impervious coverage in headwater regions. Thus, the purpose of this research is to evaluate the thermal processes occurring within the Stroubles Creek watershed and their impacts to downstream aquatic health.

Chapter 2.0 Literature Review

2.1 Human effects on stream thermal processes

Water temperature regimes in streams and rivers are influenced by changes in air and groundwater temperatures and alterations to the hydrologic regime. In addition, land surface temperatures have substantial effects on stream/river temperature. These changes occur because of natural and human-modified energy exchange processes. The sections below discuss the major anthropogenic influences on stream/river temperature.

Altering stream shading by removing vegetation increases net radiation, resulting in daytime stream temperature increases of up to 7°C (Cooter and Cooter, 1990) and 10°C (Hester and Doyle, 2011). This impact is more critical in summer, due to greater solar radiation (Jones and Hunt, 2009).

Groundwater flow is another significant factor in the temperature of gaining streams, especially during periods with low precipitation. On the other hand, if a stream is losing, then stream temperature is unaffected by groundwater temperature. Groundwater flow and temperature are influenced by climate, hydrogeology, and surface water temperature (Taylor and Stefan, 2009). Taylor and Stefan (2009) investigated the effects of land use and climate change on shallow groundwater temperature in Minneapolis-St. Paul, MN. Their analysis showed that pavement is the main controlling factor of groundwater temperature, as documented by a 3°C increase in groundwater temperatures under paved areas, as compared to temperatures in unpaved areas. According to their study, urbanization, which leads to less pervious lands and infiltration, increases groundwater temperature, which leads to increased stream temperatures during baseflow conditions. When urbanization and climate change influences are considered together, groundwater temperature was projected to rise by 5°C, and that during the summer,

groundwater influence on stream temperature is generally greater than climate change influence. Conversely, in another study conducted by Herb et al. (2009a), stream temperature was highly correlated with air temperature, possibly due to low groundwater inputs. As a result of the low groundwater inputs, the stream may be particularly sensitive to climate change.

During warm season storm events, thermal energy, which is absorbed by impervious surfaces and pavements, is conveyed by surface runoff to streams, leading to warmer surface runoff and thus warmer streams and rivers. Thompson et al. (2005) conducted a study on thermal pollution differences between asphalt pavement and turfgrass surfaces under a range of simulated rainfall conditions, using experimental plots. According to their findings, solar radiation was the most important factor affecting asphalt surface runoff temperature. Before the storm event simulations, the asphalt and sod average surface temperatures were 43.6°C and 23.3°C, respectively. Immediately after simulated rainfall events, the pavement and turfgrass surface temperatures declined an average of 12.3°C and 1.3°C, respectively. Increasing turf areas within the watershed was shown to be highly effective in mitigating urban runoff temperature and heat energy (Thompson et al., 2008). In a similar study, the effect of permeable and impermeable pavements on surface temperature reduction and cooling of surface runoff temperature was investigated (Li et al. 2013). The authors assessed three kinds of permeable pavements including interlocking concrete paver, asphalt concrete, and Portland cement concrete, and found that permeable pavement reduced surface temperature and thence runoff temperature; conversely, impervious surfaces led to warmer surface runoff and consequently higher stream temperature. Overall, higher impervious surfaces in urban areas resulted in increased average and peak runoff temperature and variability (Li et al., 2013). Immediately after a summer storm event, stream temperature increases dramatically mainly due to two reasons; 1) warmer surface runoff due to

more developed areas (Li et al., 2013); and 2) less groundwater discharge to the stream due to less infiltration in watersheds (Taylor and Stefan, 2009). Groundwater aquifers play a dampening role, and decrease stream temperature during warm months of the year (Herb, 2008).

Temperature surges in runoff: Temperature surges in runoff are a common phenomenon in urban areas during hot summers, resulting in spikes in receiving stream temperature, health impacts to aquatic biota through rapid changes of temperature, and increased pollutant loading (Hester and Bauman, 2013). Hester and Bauman (2013) monitored urban storm sewer outfalls in Blacksburg, Virginia and assessed runoff temperatures. Temperature surges occurred approximately a dozen times per summer months (during early June to mid-August) ranging up to 8.1°C with average duration of 2 hr. in a stream and up to 11.2°C with average duration of 7 hr. in a detention pond. Surges were more common in the afternoon, but were observed during all times of the day (Hester and Bauman 2013).

Temperature changes due to industrial wastewater effluents, dam releases, and water diversions: Wastewater discharges entering streams are considered continuous sources. Wastewater increases stream temperature over time, mainly because of heat inflow to the stream/river. Increased stream temperature by aforementioned influence (wastewater discharge) is more prominent during the winter seasons, when there is a large gap between stream temperatures and effluent temperatures levels (Xin and Kinouchi, 2013). Releases from reservoirs increases the stream/river temperature during winter, mainly due to water releases from the lower layers of a thermally stratified reservoir. These influences are most prominent in headwater streams. Some anthropogenic influences have cooling effects on stream temperature, such as diverting tributaries (Hester and Doyle, 2011). Xin and Kinouchi (2013) found that the Tama River, a major river system running through central Tokyo had significantly greater water

temperatures in winter due to warm effluent discharges from wastewater treatment facilities. A large water temperature increase was observed due to the effects of water withdrawals, in summer (Xin and Kinouchi, 2013). Results indicated that the largest contributions to water and heat gains were attributable to wastewater effluents, while other factors such as groundwater recharge acted as heat energy sinks, specifically in summer. Heat exchange at the air–water interface contributed less to heat budgets in winter and summer seasons for all river segments. Therefore, the effect of heat exchange through the air–water interface was minor (Kinouchi et al., 2007; Xin and Kinouchi, 2013).

Channelization: Stream channelization causes streamflow to move more quickly, and leads to less shading (mainly because of reduced stream-bank vegetation). Channelization is most prominent is urban areas and increases daily and seasonal temperature fluctuations (Gorney et al., 2012)

2.2 Stormwater control measures to mitigate thermal pollution

One tool for mitigating thermal pollution is infiltrative stormwater control measures (SCMs), also known as urban stormwater best management practices (BMPs). The purpose of BMPs is to mimic predevelopment hydrology, water quality, and temperature of runoff. Infiltrative BMPs may be the most effective technique to mitigate thermal impacts of runoff on the environment. Infiltration recharges the groundwater and becomes part of the baseflow to coldwater streams. In addition to single infiltrative BMP types, infiltrative BMPs in series (such as infiltration ponds and bioretention systems), known as an “infiltrative BMP treatment trains”, provide thermal treatment of runoff.

Restoration of the aquatic habitat in urban streams should consider potential strategies to mitigate thermal pollution from impervious surfaces. Once such BMP is bioretention, which has been shown to be effective in reducing maximum and median runoff temperatures (Jones and Hunt, 2009). However, several studies (Dietz and Clausen, 2005; Hester and Bauman, 2013; Jones and Hunt, 2009; Long and Dymond, 2014) have suggested that these practices alone will likely be insufficient to maintain runoff temperatures from an urban watershed during the summer below the toxicity threshold for trout (21°C).

Jones and Hunt (2010) investigated the effects of wetlands and wet ponds on the urban runoff temperature in western North Carolina for acute toxicity to trout populations. The paved surfaces during summer months absorb and retain the solar radiation, which transfer this thermal energy to urban runoff during rainfall events. The authors found that the volume of enriched runoff could have harmful effects on aquatic systems. Jones and Hunt (2010) found that the parking lot runoff temperatures were far higher than 21°C, which is a threshold for trout. The wetlands and wet ponds raised temperatures between their respective inlets and outlets, indicating these BMPs were a source of thermal pollution, although the wetland outflow temperatures increase in temperature was less than what was observed in the wet pond, mainly due to the effect of wetlands shading vegetation. The authors found that underground pipes that conveyed runoff from the wetland to the receiving stream were effective in cooling discharges (Jones and Hunt, 2010). According to Jones et al. (2012) findings, BMP practices alone cannot be effective separately (or even as a train) in reducing thermal pollution of urban runoff. In other words, with the threshold for acute toxicity for trout being 21°C, current practices were unable to mitigate temperatures to below this level during the summer. Hence, Jones et al. (2012) suggest that other factors related to catchments characteristics and a watershed-scale plan or response can

be used to mitigate thermal pollution. These actions include tree canopies for increased shading of streams to reduce median and maximum surface temperature of the contributing catchment, and light-colored chip seal application to reduce runoff temperatures, in addition to implementation of infiltrative practices such as bioretention. These factors reduce the median and maximum surface runoff of parking lot. Utilizing BMP trains together with in-catchment control factors of stormwater may lead to better mitigation of thermal pollution.

Janke et al. (2009) developed an unsteady, 1-D model to simulate heat transfer within a detention pond to assess thermal pollution of a cold-water stream in Minnesota. The authors simulated the system for six years using observed rainfall events and found the long-term average outflow temperature was 1.2°C higher than the inflow temperature. However, temperature spikes in the stream were reduced mainly due to the reductions in the peak runoff rate. The schematic of stormwater pond and model features is shown in Figure 2.1 (Janke et al., 2009).

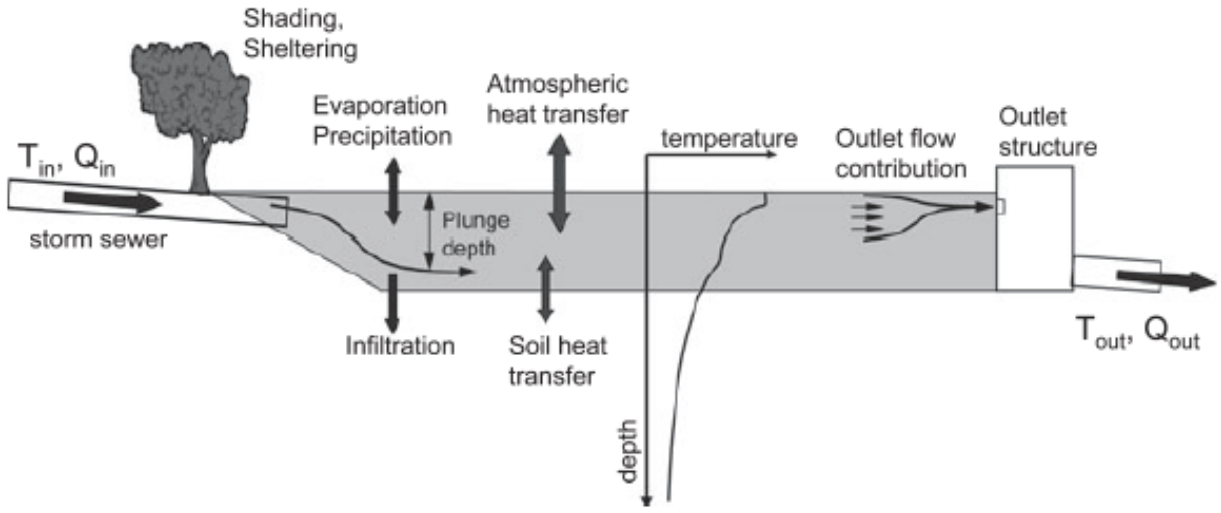

Figure 2.1. Schematic of stormwater pond and model features (Janke et al., 2009)

Jones and Hunt (2009) investigated the effect of bioretention on runoff temperature. The smaller bioretention cells reduced peak and median discharge water temperature significantly. In comparison, the proportionally larger bioretention cell was unable to match the lower temperature of the smaller bioretention cell due to a much larger runoff volume input. This study points out that while small and large bioretention cells provided temperature mitigation and thermal load reduction, outflow temperatures still exceeded 21°C. The authors suggest it will be necessary to implement more bioretention cells, to achieve a healthy stream in a trout habitat. A key finding of Jones and Hunt (2009) study was that deeper bioretention cells lead to cooler runoff temperatures during the summer months.

Dietz and Clausen, (2005) investigated the temperature mitigation of roof runoff by roof gardens in all seasons of a year; while there was no installed control roof to evaluate the effectiveness of roof gardens compared to a baseline scenario. The ANOVA statistical test results on the difference between roof runoff temperature (produced by asphalt shingle roofs) and roof gardens underdrain-systems outflow temperature showed no significant differences between the inflow and outflow temperature among all seasons. Another study in Blacksburg, southwest Virginia by Long and Dymond (2014) was conducted through 10 artificial runoff events generated by a nearby fire hydrant. Runoff median and maximum temperature were reduced by 8.8°C and 8.6°C, respectively, between the inlet and discharge of the bioretention cell. The bioretention reduced runoff volume by 1.4 m^3, or 10%, and reduced heat export from the site by 37 MJ/m^3. Bioretention systems, in comparison to wetlands and wet ponds, increases runoff reduction, and results in less heat export (Jones and Hunt, 2009; Jones et al., 2012; Long and Dymond, 2014). Bioretention systems are particularly effective at runoff and thermal load

reduction when installed in coarse textured soils, such as well sorted gravel, well sorted sand or sand and gravel, which have greater hydraulic conductivity (Long and Dymond, 2014).

2.3 Review of models and empirical equations to simulate water temperature

Numerous process-based models and empirical relationships have been developed for simulating runoff quantity and temperature from urban surfaces during rainfall events. For example, a hydro-thermal model was developed to simulate runoff temperatures from a paved surface (Janke et al., 2009). The authors found that heat export was strongly correlated with the rainfall parameters such as intensity, duration, and temperature; higher intensities resulted in lower runoff temperature. The authors found that any activities that alter the timing or magnitude of streamflow regime likely would alter stream temperature (Janke et al., 2009). A physically based model was assessed to estimate the spatiotemporal variability of river water temperature in summer at a regional scale (Beaufort et al., 2016). Air temperature was used as an index to predict stream temperature (Morrill et al., 2005), using a nonlinear regression equation (Eq. 1).

$$T_s = \mu + \frac{(\alpha-\mu)}{1+e^{(\gamma*(\beta-T_a))}} \quad \text{Eq. 1}$$

Where T_s= estimated stream temperature (°C); T_a = is measured air temperature for the period of interest (°C); μ=minimum stream temperature (°C); α=maximum stream temperature (°C); and β= inflection point, defined as the function of the steepest slope of the T_s function.

Brogan (2003) used Equilibrium Temperature (Eq.T), which is the stream temperature at which the sum of all heat fluxes through the stream is 0.0, as an indicator of stream temperature (ST). The relationship between Eq.T and ST was assessed using an empirical linear regression relationship (Bogan, 2003).

Arrington et al. (2004) developed and applied the Thermal Urban Runoff Model (TURM) to evaluate the impact of urbanized watersheds on stream temperature. TURM predicts surface runoff and runoff temperature from pervious and impervious surfaces. The TURM model uses the curve number method (NRCS, 1986) for simulating runoff, so it is applicable mainly for design storm events.

SNTEMP (Stream Network Temperature Model), a 1-D steady-state heat transport model, simulates daily average and maximum stream temperatures versus downstream distance as function of groundwater inputs, channel geometry, discharge, climate, and riparian shading (Herb et al., 2009a). Current stream temperature models are reach-based models working at daily/hourly time steps. Simple empirical models are inadequate or inappropriate for catchment-scale applications, while spatially distributed physical models require substantial field-measured input data to run.

The Minnesota Urban Heat Export Tool (MINUHET) was developed to address some of the shortcomings of models described above. MINUHET is both an event-based and continuous simulation model that produces a time series of runoff temperature and heat loading at the catchment outlet. MINUHET includes three main simulation modules for hydrologic routing, hydrologic/thermal modeling of watersheds, and hydrologic and thermal effects of SCMs. Runoff is assumed to be thin (sheet flow) and well mixed, with the heat capacity of pure water. MINUHET enables the user to simulate landuse effects on overland runoff temperature and heat loading to a stream, thereby predicting the thermal impact of landuse on receiving streams (Janke et al., 2013). In its current implementation, MINUHET includes all major hydrologic modules and heat transfer processes applicable to a small urban watershed. A schematic diagram showing the balance of runoff and heat flux for each sub-catchment, drainage network, and pond

component in the MINUHET configuration is shown in Figure 2.2 (Herb, 2008; Stefan et al., 2008).

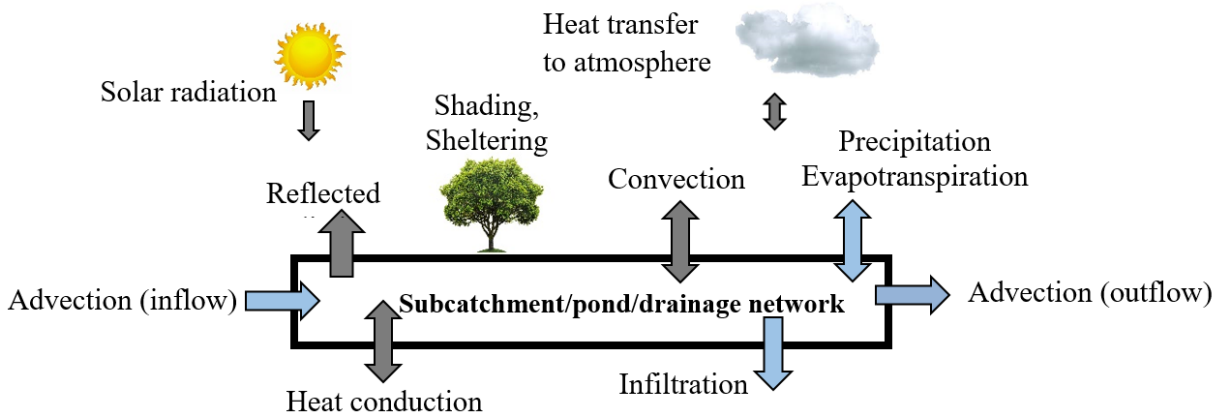

Figure 2.2. Runoff and heat balance diagram for each sub-catchment, drainage network, and pond component, based on Herb (2008).

2.4 MINUHET and SWMM application

The MINUHET model was validated in a case study of a housing development contained within a small urban watershed in Plymouth, MN (Janke et al., 2013). The model exhibited relatively good agreement between observed and simulated water temperatures at the watershed outlet, with an absolute difference of less than 1.5°C. Heat export was also simulated, with similar model performance (Janke et al., 2013). In another study, two residential and commercial watersheds were modeled using MINUHET (Herb, 2008). An infiltration basin and a retention pond were assessed for their capacity for thermal mitigation. Simulation results indicated the infiltration basin was effective at reducing the total heat export from the watershed (primarily by reducing runoff volume), nearly to the pre-development level, while the retention pond increased heat input to the stream (Herb, 2008; Herb et al., 2009c). MINUHET and the U.S. Environmental Protection Agency's Storm Water Management Model (EPA-SWMM) were compared with

respect to runoff generation during a single rainfall event. Both models had similar results for runoff volume (Herb, 2008).

Several public domain hydrologic models are capable of simulating runoff in urban watersheds, e.g., the Hydrologic Modeling Systems, or HMS, Hydrologic Simulation Program-Fortran, or HSPF and SWMM. SWMM is a dynamic hydrology-hydraulic model, which is employed to simulate stormwater quantity and quality for event-based and continuous-based scenarios. The current SWMM configuration determines runoff by evaluating infiltration processes using the Green-Ampt equation (Green and Ampt, 1911), Horton, or Curve Number methods and then makes use of the dynamic wave, kinematic wave, or steady-flow approximations for runoff routing. The capabilities of these models for simulating runoff processes exceed that of MINUHET; the strength of MINUHET is its unique ability to simulate heat export and runoff temperature, thus providing a tool for evaluating the thermal impacts of urban runoff on receiving water bodies.

The limitations of MINUHET and SWMM are shown in Table 2.1. Unlike SWMM, MINUHET does not include a comprehensive aquifer module; however, SWMM does not have the capability to model thermal processes (Table 2.1). While individual MINUHET components have been validated, (Herb, 2008; Janke et al., 2013), to date, MINUHET has not been applied to a larger urbanized watershed which includes open channels, detention/retention ponds, and a variety of urban land covers (Janke et al., 2013).

Table 2.1. MINUHET and SWMM limitations with respect to hydrologic and thermal simulations.

Model	Limitations
MINUHET	No aquifer module; only supporting the groundwater-surface water interaction through a basic algorithm of groundwater inflow/temperature to open channels/streams
	Limited ability to simulate longer times series and large scale/complex watersheds.
	No capability for instream temperature modeling. If the stream is assumed an open channel, MINUHET can model temperature at the outlet of the open channel (with some simplifications such as not modelling the in-channel thermal processes).
	No atmospheric heat transfer for the routing elements and no junction losses. Hence, not being appropriate to simulate long open channel drainage networks (Janke et al., 2009).
	Limited choice of conductivity values for each subwatershed, since MINUHET only uses HSG (Hydrologic Soil Group) categories for each subwatershed.
SWMM	No capability to model thermal processes beyond simple mixing.
	SWMM Aquifer module does not capture the groundwater discharge pattern to the streams appropriately (Ketabchy, et al. 2017).

Chapter 3.0 Research Objectives

Despite the significance of thermal issues associated with urban runoff, only a few tools exist that are capable of simulating runoff temperature and heat loads. The best available tool, MINUHET, has a limited ability to simulate complex urban watersheds; such analyses are often performed using SWMM. The current SWMM configuration has no capability to model thermal processes. The objective of this research is to apply MINUHET and SWMM to a medium-sized urban watershed, Stroubles Creek, in Blacksburg, Virginia. Stroubles Creek has several monitoring locations at which streamflow, groundwater level, climatological data, and water temperatures have been recorded for several years at the Virginia Tech Stream Research, Education, and Management Lab (StREAM Lab) (https://www.bse.vt.edu/research/facilities/StREAM_Lab.html). The StREAM Lab is a nationally recognized research facility that monitors streamflow quantity and quality data. MINUHET and SWMM models were developed, calibrated, and validated using data from two StREAM Lab monitoring stations. Model sensitivity was assessed and event-based and continuous streamflow estimates by models were compared. Then SWMM-simulated streamflow and water temperature from MINUHET were combined in a unique, hybrid approach to simulate heat export from the watershed (Hybrid model). In the next step, the comparison of MINUHET and Hybrid models capabilities for simulating heat export was conducted. Lastly, the effects of retrofitting the watershed for thermal mitigation using infiltration practices and increased canopy shading were evaluated. While these practices have a demonstrated ability to mitigate downstream water temperatures, this effect has not been assessed at the watershed scale. The primary purpose of the assessment is to provide guidance in achieving temperature regimes that meet aquatic health criteria for sensitive species such as trout. This standard is likely going to be

difficult to achieve. To address this issue, a more general approach was developed to assess the relationship between downstream heat loads as a function of upstream infiltration capacity, and thermal mitigation practices such as cool pavement installations.

Chapter 4.0 Materials and Methods

4.1 Site Description of the Case Study

The 58-km^2 Stroubles Creek watershed is located in Montgomery County, Virginia and is tributary to the New River, part of the Ohio-Mississippi River-Gulf of Mexico system. The study was conducted on a 14.1-km^2 upstream portion of the Stroubles Creek watershed (Figure 4.1a).

A monitoring station operated by the Virginia Tech StREAM Lab is located at the watershed outlet as is shown on Figure 4.1a. Land cover is primarily urbanized (75%), with 21% agricultural and 4% forest, based on the 2011 National Land Cover Database (Figure 4.1a). The Duck Pond (Figure 4.1a) acts as a divider between the highly urbanized headwater portion (approximately 7.8 km^2 in area) and the downstream agricultural and forested portion of the Stroubles Creek watershed, the entirety of which is referred to as the Main watershed. The Central Branch and the Webb Branch are the two tributaries that merge at the Virginia Tech Duck Pond to form Stroubles Creek (Figure 4.1a).

Many forms of channel modification exist throughout the watershed, including piped stream reaches, ponds, and channelization. The Town of Blacksburg land use classifications (http://www.gis.lib.vt.edu/gis_data/Blacksburg/GISPage.html) and geographic information system (GIS) data were used for the watershed (Table 4.1 and Figure 4.1b). The breakdown of imperviousness across the watershed and imperviousness distribution, computed by tracing aerial photography (http://www.gis.lib.vt.edu/gis_data/Blacksburg/GISPage.html) are shown in Table 4.2 and Figure 4.1c, respectively. Imperviousness of the entire watershed is 32%, with buildings and parking lots constituting approximately 61% of the total impervious area (Table 4.2).

Characterized by limestone and dolomite formations, the Stroubles Creek streambed is formed of gravel and cobbles and has alluvium-floodplain deposits of stratified clay, sand, and silt (Mostaghimi et al., 2003). The dominant Hydrologic Soil Group of the upstream of watershed is category C (NRCS, 2007), while downstream of Duck Pond consists mainly of category B, or silt loam and loam (Refer to Appendix A for the Stroubles Creek geologic map and respective description). The depth to the water table in the downstream portion of the watershed is approximately 1 m and mean annual precipitation is approximately 1030 mm (Hofmeister et al., 2015).

Table 4.1. Land use categories of the case study watershed.

Land use type	**Percentage**
Commercial/Industrial	4.0
Very low density residential and agricultural	12.8
Low density residential	17.1
Medium density residential	4.0
High density residential	7.0
University	25.4
Park land/Opens spaces	3.3
Civic	5.5
Others	20.9

Table 4.2. Impervious cover of the case study watershed.

Impervious land cover type	**% of Impervious areas**
Building	28.4
Sidewalks	10.3
Ponds	1.8
Streets	22.4
Parking lots	31.3
Driveways	4.1
Others	1.7
Percent imperviousness of StREAM Lab watershed	32.0

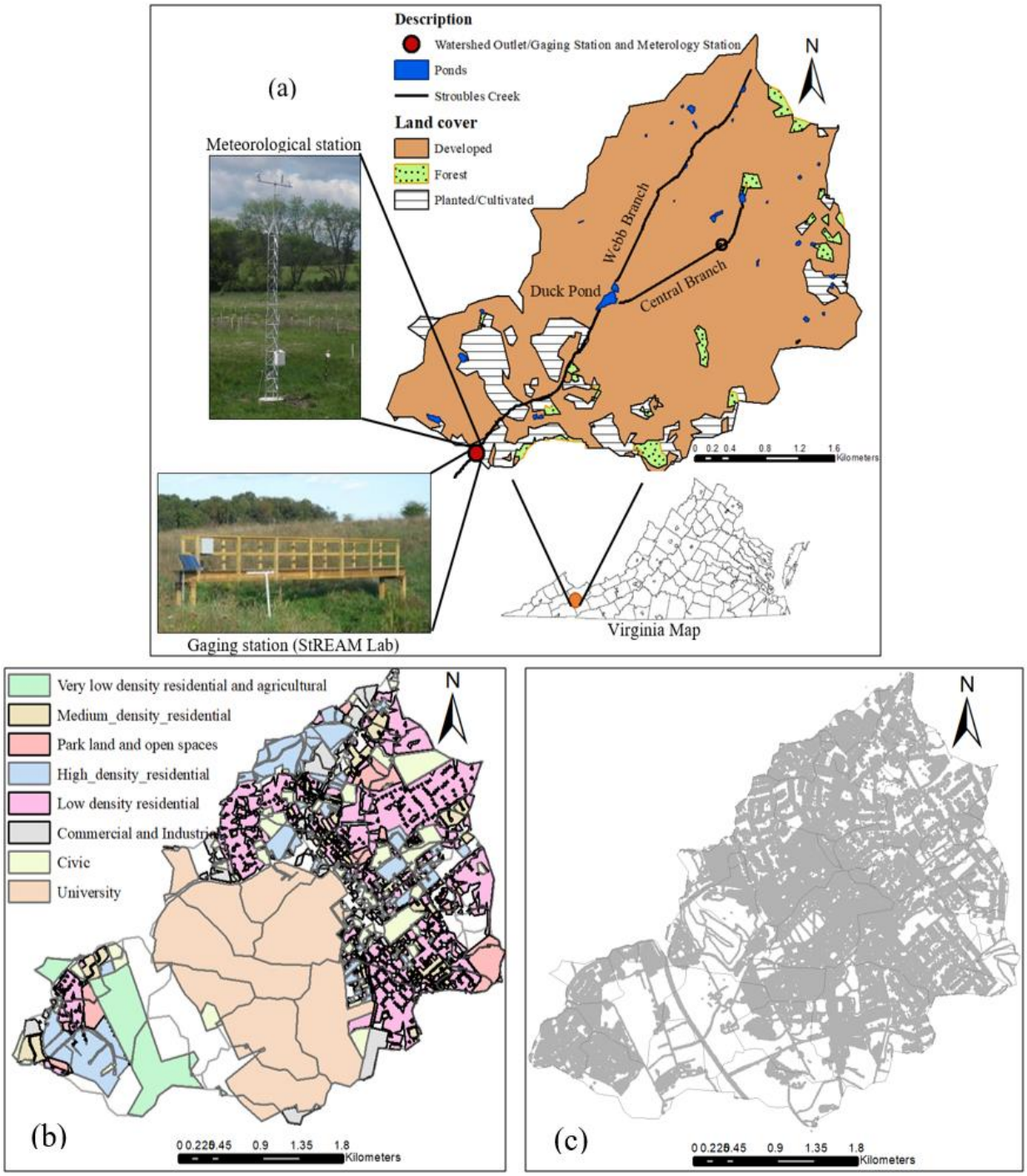

Figure 4.1. (a) Land cover map of the Stroubles Creek watershed (NLCD, 2011) with gaging station location; (b) Land use (the white portions of land use map are the lands with other applications); (c) imperviousness distribution (the grey portions of the imperviousness map represents impervious lands).

4.2 Data Collection

The Town of Blacksburg and Virginia Tech provided storm sewer and surface elevation GIS data. Soil information was acquired from the Soil Survey Geographic Database (SSURGO) of Natural Resources Conservation Service (NRCS) (https://websoilsurvey.sc.egov.usda.gov/App/HomePage.htm), at the watershed scale. At the StREAM Lab monitoring station, a pressure transducer (CS451, Campbell Scientific Inc., Logan, UT, U.S.A., water level resolution: 0.0035% FS) and a datalogger (CR1000, Campbell Scientific Inc., U.S) record stream stage every 15 minutes (Figure 4.1a). Stage is converted to discharge using a rating curve, which was developed based on Stroubles Creek stage-discharge historical data. In addition, an YSI Sonde (6920 V2, Xylem Analytics, U.S, +/- 0.15°C) records water temperature. Temperature measurements are checked against a calibrated thermometer to calibrate the Sonde. Precipitation is recorded by Town of Blacksburg and the meteorology station of the StREAM Lab, on 15 minutes time steps. A tipping bucket rainfall sensor (TR-525USW, Texas Electronics, Inc., Dallas, TX, +/- 1%) is to monitor precipitation at the Town of Blacksburg weather station. Solar radiation, wind speed, relative humidity, and air temperature are measured in every 30 minutes at the StREAM Lab weather station, located approximately 300 m downstream of the Stroubles Creek monitoring station (Figure 4.1a). StREAM Lab sensor specifications are as follows: (1) rain, TE525, Campbell Scientific, U.S, 1.0% up to 2 in/hr.; (2) wind speed, 034A/034B, Campbell Scientific, U.S, 0.1 m/s; (3) air temperature and relative humidity, CS215, Campbell Scientific, U.S, ±2% at 25°C); and (4), solar radiation, CS300, Campbell Scientific, U.S, ±5% for daily total radiation. A datalogger (CR1000, Campbell Scientific Inc., U.S), and a radio modem as the communication equipment (Digi X-Tend 1 W 900mHz spread spectrum, Digi International Inc., MN) are used to store and transmit the weather

station data at StREAM Lab. Cloud cover data every 20 minutes were acquired through NOAA (https://www.ncdc.noaa.gov/cdo-web/). The depth to groundwater is measured every 10 minutes in two piezometers installed in the floodplain adjacent to weather station using two similar water level loggers (CS451, Campbell Scientific, U.S, water-level resolution: 0.0035% FS). The data-sampling period was split into two warm periods of mid-June to late September, for 2015 and 2016. The 2015 warm period was drier and relatively cooler than the 2016 warm period. The total rainfall and average hourly temperature during the two measurement periods were 20.6 cm and 20.1 +/-5°C and 34.5 cm and 21.0 +/- 4.6°C for 2015 and 2016, respectively. The mean discharge for Stroubles Creek during the 2015 and 2016 warm periods was 0.15 and 0.24 m^3s^{-1}, respectively. Groundwater is assumed to be the main control of discharge (Hofmeister et al., 2015); hence, due to minimal precipitation, the stream was at baseflow during much of the two monitoring periods.

4.3 SWMM and MINUHET Models Setup

A total of 43 subwatersheds and 30 detention/retention ponds were delineated within the watershed. The urbanized portion of the watershed (upstream of the Duck Pond) is more complex than the watershed downstream of the Duck Pond due to presence of intensive urban development. Hence, the subwatershed delineation was conducted manually in the urbanized portion of the watershed based on the locations of the ponds and the stormwater drainage network/infrastructure. Downstream of the Duck Pond, elevation data were used to delineate the subwatersheds using a GIS application (the watershed extension) (Ketabchy et al., 2016a). Stroubles Creek was modeled as a pervious open-channel system with irregular cross-sections in downstream and impervious rectangular cross-sections beneath the Virginia Tech campus, for both the MINUHET and SWMM configurations. The outlet of each pond was modeled as a weir

structure. Routing computations were conducted for each pond, and the stage-storage (bathymetry) characteristics of ponds were computed through Town of Blacksburg information and the watershed data elevation models (DEMs). The lengths of the impervious and pervious areas of each subwatershed were estimated from the longest overland runoff paths, while these runoff paths were used to calculate the hydraulic width of each subcatchment, a required SWMM parameter of each subcatchment. Green-Ampt infiltration and dynamic wave methods were used for the infiltration and routing models of SWMM, respectively. Groundwater table elevation was quantified using geological maps of Geology and Mineral Resources Division of Commonwealth of Virginia (Appendix A) (https://www.dmme.virginia.gov/dgmr/mapspubs.shtml), and data from the StREAM Lab pre-installed floodplain piezometers. To build the model structure and conduct the sensitivity analysis, PC-SWMM was used to directly import spatial information and attributes from a geodatabase GIS. MINUHET was used to simulate the time series of runoff temperature for the impervious and pervious sections of a subcatchment. Based on these two simulated time series, the watershed thermal module of MINUHET uses a simple mixing method to produce composite hydrograph and time series of runoff temperature. The schematic of SWMM and MINUHET graphic user interfaces (GUIs) and structures are shown in Figure 4.2.

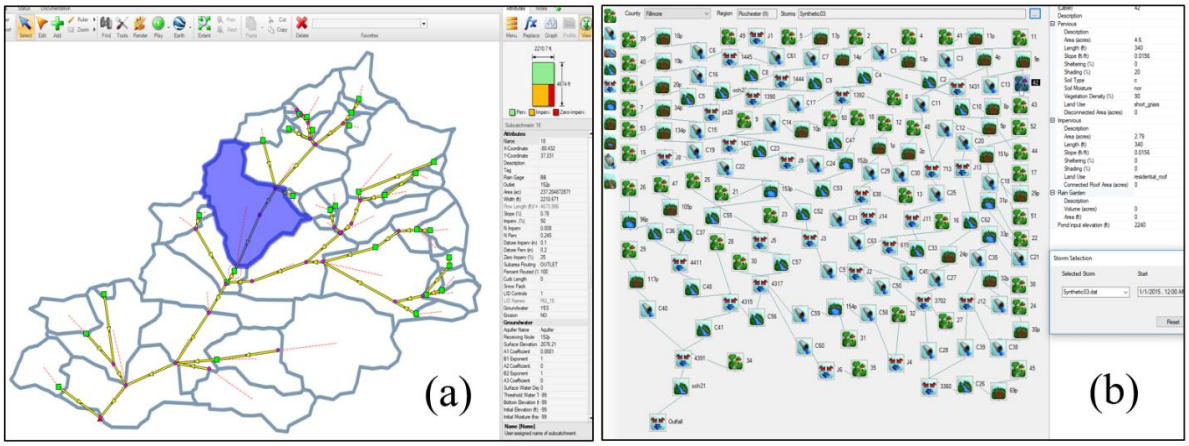

Figure 4.2. The schematic of models layouts and environment of the GUIs, (a) SWMM, (b) MINUHET (with streamflow proceeding towards the lower left corner).

4.4 Sensitivity Analysis

A sensitivity analysis was conducted to assess the influence of individual model input parameters on model (SWMM and MINUHET) streamflow and temperature output. To perform the sensitivity analysis and identify the crucial input parameters, the value of a particular input parameter was varied while holding all other parameters constant during the simulation. Identification of the most sensitive parameters focuses the calibration on a subset of input parameters (Ahmadisharaf et al., 2016; Janke et al., 2013; Nayeb Yazdi et al., 2015).

The sensitivity of the following SWMM and MINUHET model outputs were quantified: average total streamflow and streamflow-averaged temperature, throughout the calibration period (summer 2016). The sensitivities of streamflow and temperature to the input parameters can be represented by the sensitivity coefficient (Eq. 2).

$$S_r = \left(\frac{x}{y}\right)\left(\frac{y_2 - y_1}{x_2 - x_1}\right) \quad \text{Eq. 2}$$

Where x is the input parameter and y is the simulated output. Variables x_1 and x_2 correspond to maximum and minimum ranges of the initial default value and y_1 and y_2 are the corresponding output values (James and Burges, 1982). The greater the S_r, the more sensitive the output parameter is to that particular input parameter. Positive values of sensitivity coefficients represent the direct relationship between the parameters and the outputs, while the negative values represent vice versa. Selected models input parameters and the potential range of values based on literature and field data are shown in Table 4.3.

Table 4.3. Ranges of selected models input parameters based on literature and field data.

Parameter	Unit	Value Range	References
SWMM			
Imperviousness	%	±15% of each subwatershed	(Kong et al., 2017)
Hydraulic width (H.W.)	m	±10% of each subwatershed	(James et al., 2010)
Impervious Manning roughness	-	0.01–0.03	(Wanielista MP, 1997)
Pervious Manning roughness	-	0.02–0.45	(Huber and Dickinson, 1988)
Impervious depression storage	mm	0.3–4.0	(Huber and Dickinson, 1988)
Pervious depression storage	mm	2.5–7.5	(Huber and Dickinson, 1988)
Conductivity	mm/hr.	±20% of initial values	U.S Department of Agriculture
MINUHET			
Heat capacity of pavements	$J/m^3.°C$	$1.9\text{-}3.7\times10^{6}$	(Kavianipour and Beck, 1977)
Thermal diffusivity of pavements	m^2/s	$4.42\times10^{-7}\text{-}14.4\times10^{-7}$	(Luca and Mrawira, 2005)
Pavement thickness	m	0.102-0.203	(Kavianipour and Beck, 1977)
Saturated hydraulic conductivity	m/s	3.61×10^{-7} (HSG: D) - 2.75×10^{-5} (HSG: A)	(Rawls, 2006)
Subwatersheds degree of shading	%	±15% of initial estimate	Aerial photos and field data
Open channels degree of shading	%	±15% of initial estimate	Aerial photos and field data
Dew point temperature	°C	±2°C of initial calculated values	(Stefan et al., 2008)

4.5 Calibration and Validation at the Watershed Outlet

SWMM and MINUHET inputs were chosen for the models calibration process based upon the sensitivity analysis, current manuals, field data, model defaults, and literature sources. Sensitivity analysis indicated the most sensitive parameters, which were adjusted to optimize agreement between the simulated and observed values. Measured streamflow at StREAM Lab between June 15 and September 30 of 2016 were selected to represent summer conditions and were used to calibrate the models; streamflow for the same period in 2015 was used for model validation. The focus is on the summer periods because this is the critical period for temperature in terms of sensitive species, such as trout. The goal of model validation was to assess whether

the calibrated model was able to mimic streamflow behavior for events outside of the calibration period.

To build and run the thermal module of MINUHET, the tool requires climate data as an input, including solar radiation, air temperature, relative humidity, wind speed, cloudiness, and precipitation. Climate files for the calibration and validation periods were built using 15 minute-intervals. The MINUHET model was calibrated for thermal processes by adjusting the heat capacity of pavement, thermal diffusivity of pavement, and pavement thickness to match observed water temperature.

Goodness of fit criteria: The efficacy of calibration and validation results were evaluated using a group of goodness-of-fit tests that are described in the following sections.

Nash-Sutcliffe efficiency (NSE): NSE specifies the relative magnitude of the observed data variance compared to the residual (observed-simulated) variance (Nash and Sutcliffe, 1970). It represents how well the plot of predicted versus observed data fits a 1:1 line. NSE is calculated as shown in Eq. 3.

$$NSE = 1 - \left[\frac{\sum_{i=1}^{n}\left(Y_i^{obs} - Y_i^{sim}\right)^2}{\sum_{i=1}^{n}(Y_i^{obs} - Y^{mean})^2}\right] \quad \text{Eq. 3}$$

Where Y_i^{obs} is the i^{th} observation for the observation data set, Y_i^{sim} is the i^{th} predicted value for the simulated data set, Y^{mean} is the mean of observed data set, and n is the total number of observations. NSE equal to 1.0 is the optimal value, while NSE ranges between $-\infty$ and 1.0.

Percent bias (PBIAS): PBIAS calculates the average tendency of the simulated data set to be smaller or larger than the observed data set (Gupta et al., 1999). The optimal value of PBIAS is 0.0, with lower values representing more accurate model prediction. Negative values represent

model over-prediction bias, while positive values represent model under-prediction bias. It is calculated as shown in Eq. 4.

$$PBIAS = \left[\frac{\sum_{i=1}^{n}\left(Y_i^{obs} - Y_i^{sim}\right) * 100}{\sum_{i=1}^{n}\left(Y_i^{obs}\right)}\right] \quad \text{Eq. 4}$$

RMSE-observations standard deviation ratio (RSR): RMSE (Eq.5) is an error index statistic (Moriasi et al., 2007; Singh et al., 2004), which is standardized through the standard deviation of the observations and named RSR (standard deviation ratio). RSR was calculated as the ratio of the RMSE and standard deviation of observed data set, as shown in Eq. 5.

$$RSR = \frac{RMSE}{STDEV_{obs}} = \left[\frac{\sqrt{\sum_{i=1}^{n}\left(Y_i^{obs} - Y_i^{sim}\right)^2}}{\sqrt{\sum_{i=1}^{n}\left(Y_i^{obs} - Y^{mean}\right)^2}}\right] \quad \text{Eq. 5}$$

By definition, RSR cannot be less than zero. The optimal value of the standard deviation ratio is 0.0, which indicates zero RMSE and hence perfect model performance. Therefore, the lower the RSR, the better the model prediction.

Regression method: This method was conducted by fitting a line using linear regression between the predicted and observed values where the slope of the fitted line is compared to the 1:1 slope (perfect match). Generally, the best calibration performance requires that the coefficient of determination (r^2) and the fitted slope be as close to 1.0 as possible.

Statistical Analysis: To assess the equality of the observed and simulated sample means, student's t-test (as a parametric analysis test) and the Wilcoxon rank sum test (as a non-parametric analysis test) can be used. The t-test assumes the underlying population is normally distributed and the data are independent. Most data that are recorded over time (weather data,

streamflow, etc.) are temporally (serially) correlated. Therefore, they are not independent. To assess if the data are serially correlated, the differences of observed and simulated data sets (model errors) can be used. To investigate the normality of differences, a Shapiro-Wilk test may be used to see if the differences are from a normal distribution. Then, the differences can be plotted versus time, to see if a wave-like pattern was present. If the differences distribution was normal and a wave-like pattern was not observed, then t-test can be used. Otherwise, if the differences distribution was not normal and a wave-like pattern was not observed, then the Wilcoxon rank sum test would be applied to see if the differences are significantly different from zero. Lastly, if a wave-like pattern was observed, it is not appropriate to conduct t.test, Wilcoxon test, and Shapiro-Wilk test.

Model performance evaluation: To evaluate the model performance, a qualitative performance rating system (Table 4.4) was developed. It provides a means to qualitatively compare the simulated data set with the observed data set based on the values provided from the aforementioned statistical methods (Moriasi et al., 2007).

Table 4.4. Model performance rating system (Moriasi et al., 2007).

Statistical Method	Value Range	Model Performance Rating
R^2	≥ 0.8	Good
	≥ 0.6	Satisfactory
	< 0.6	Unsatisfactory
NSE	> 0.65	Good
	> 0.50	Satisfactory
	≤ 0.50	Unsatisfactory
RSR	≤ 0.55	Good
	≤ 0.70	Satisfactory
	> 0.7	Unsatisfactory
PBIAS	$\leq \pm 15\%$	Good
	$\leq \pm 25\%$	Satisfactory
	$> \pm 25\%$	Unsatisfactory

4.6 The Hybrid Model

The objective of the development of the SWMM and MINUHET models are to assess the thermal impact of urbanization on Stroubles Creek. Heat export, which represents the heat content of the streamflow/runoff, has been indicated as a reliable index for assessing aquatic health responses to temperature impacts from urbanization (Janke et al., 2009). Heat export is defined as a function of temperature and streamflow/runoff in a given time interval (Eq. 6).

$$H_{exp} = \rho_w C_{P,w} Q (T_{out} - T_{ref}) \quad \text{Eq. 6}$$

Where H_{exp} = heat export, J; Q = the volumetric streamflow/runoff at the watershed outlet, m^3/s; T_{out} = the outlet water temperature, ºC; T_{ref} = reference temperature, ºC; $C_{P,w}$ = heat capacity of streamflow/runoff (for water = 4.184 J/(ºC·kg)); and ρ_w = water density, kg/m^3. Total heat export from a rainfall event is the sum of the heat export for every time interval of the event. The reference temperature, T_{ref}, can be chosen such that the heat load represents the heating load above a significant value of temperature (e.g. a temperature above which trout experience thermal stress, such as 21ºC). The average streamflow temperatures were between 18 and 19ºC (for the current study), for simulated and observed values, resulting in a negative heat export. Hence, an arbitrary reference temperature of 17ºC was used to ensure that heat export remained positive during the calibration and validation periods (Janke et al., 2013).

Heat export (load) was simulated using two methods, which are diagrammed in Figure 4.3. The first method uses MINUHET alone, the second, a hybrid of SWMM and MINUHET. MINUHET estimates heat export at each time step given a pre-determined reference temperature. The hybrid method uses water temperatures from MINUHET and streamflow from SWMM to produce a heat load according to Eq. 6. In other words, rather than development of a

de-coupled model (streamflows from SWMM input into MINUHET and then running MINUHET), which is not feasible in MINUHET configuration, Eq. 6 was utilized to simulate heat export based on SWMM outputs (streamflow) and MINUHET outputs (temperature).

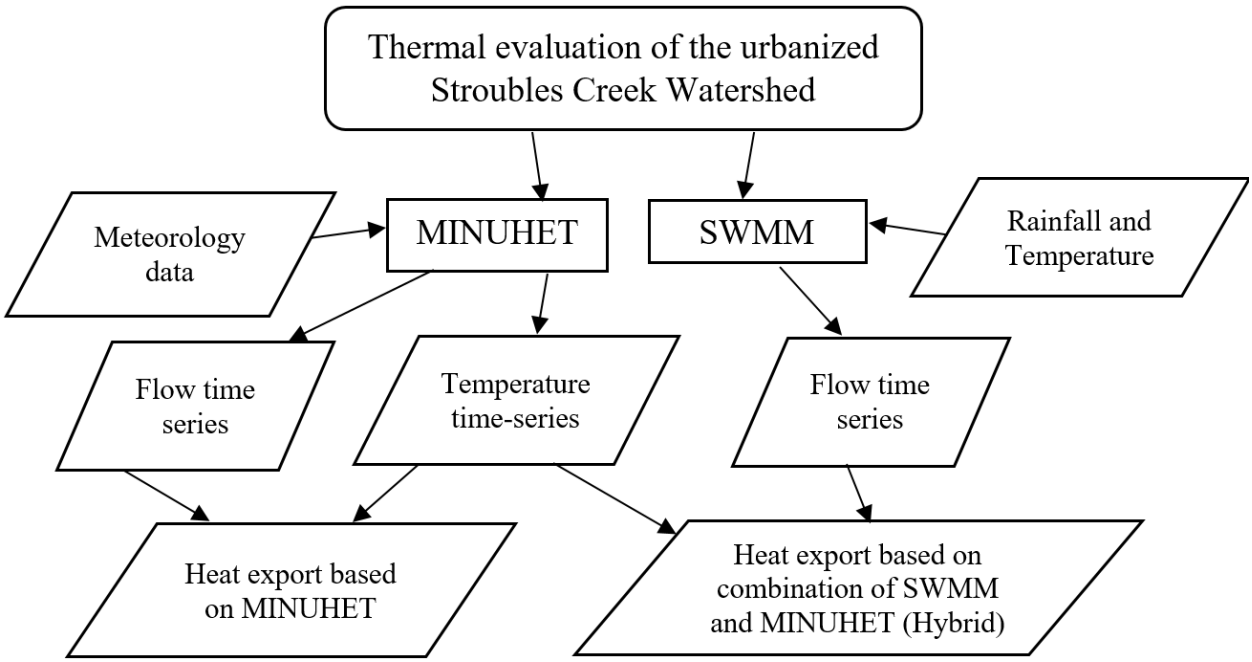

Figure 4.3. Diagram of the heat export simulation methods.

Chapter 5.0 Comparison of SWMM, MINUHET, and Hybrid Models for the Stroubles Creek Watershed

In this Chapter, the sensitivity of predicted streamflow to inputs to the MINUHET and SWMM models was investigated. Downstream streamflow was then simulated using both the SWMM and MINUHET models and the results were compared. The MINUHET model was also employed to predict temperature downstream to evaluate the exceedance threshold temperature for trout habitat. Lastly, heat loads were predicted by the MINUHET and hybrid models, and the respective results were compared.

5.1 Sensitivity Analysis Results

A sensitivity analysis was conducted based on similar studies (Alamdari et al., 2017; Xing et al., 2016) and the results are provided in Table 5.1. The average total streamflow volume was most sensitive to imperviousness (S_r=0.380), followed by impervious depression storage (S_r=-0.110), and subwatershed hydraulic width (S_r=0.030). The parameters in Table 5.1 are ordered based on the absolute values of level of sensitivity, from high to low. Unlike similar studies (Barco et al., 2008), the SWMM model of the Stroubles watershed was not very sensitive to the Green-Ampt infiltration parameter (conductivity, S_r=-0.007). Likewise, it was also not sensitive to Manning's roughness for pervious and impervious surface and depression storage for pervious lands.

The MINUHET Stroubles watershed model predicted water temperature exhibited a high sensitivity to dew point temperature (S_r= 0.762, calculated from air temperature and relative humidity) compared to other thermal parameters, such as heat capacity and thermal diffusivity of pavements (Table 5.1). This was especially true during conditions free of large atmospheric or ground heat fluxes, which commonly occur early in the morning. One of the key reasons that the

MINUHET thermal module is sensitive to dew point temperature is because it assumes that rainfall temperature is equal to dew point temperature (Janke et al., 2013). Dew point temperature equation used in the MINUHET configuration is provided in Eq. 7.

$$T_D = \frac{ln(\frac{RH}{100}+\frac{17.625*T}{243+T})}{17.625-ln(\frac{RH}{100})-\frac{17.625*T}{243+T}} \quad \text{Eq. 7}$$

Where RH is relative humidity (percentage) and T is dry-bulb temperature (°C) (dry-bulb temperature, or DBT is the actual thermodynamic temperature of air; DBT is the air temperature which is measured using a thermometer that is exposed to air but shielded from moisture and radiation). Water temperature was relatively insensitive to pavement thermal diffusivity and thickness (Table 5.1). Likewise, model results were insensitive to shading and sheltering values of open channels, ponds, and subcatchments and not considered for model calibration; hence, the dew point temperature and heat capacity of pavement were the most important parameters affecting water temperature in the MINUHET model. Climate data were collected very near to the study site. This should reduce errors in the dew point temperature calculation. The MINUHET model average streamflow demonstrated a high sensitivity to saturated hydraulic conductivity (S_r=-0.510), mainly due to the increased magnitude of infiltration from pervious areas, thereby reducing runoff from the watershed.

Table 5.1. Sensitivity coefficients of each parameter tested for the SWMM and MINUHET models.

Level of Sensitivity	Parameter	S_r
	SWMM	
High	Imperviousness	0.380
↕	Impervious depression storage	-0.110
↕	Hydraulic width	0.030
↕	Pervious Manning roughness	-0.008
↕	Conductivity	-0.007
↕	Pervious depression storage	-0.004
Low	Impervious Manning roughness	0.001
	MINUHET (Temperature)	
High	Dew point temperature	0.762
↕	Heat capacity of pavements	-0.023
↕	Thermal diffusivity of pavements	-0.009
↕	Pavement thickness	0.008
↕	Open channels degree of shading	-0.002
Low	Subwatersheds degree of shading	-0.002
	MINUHET (Streamflow)	
	Saturated hydraulic conductivity	-0.510

5.2 Calibration and Validation for Streamflow

The sensitivity analysis (Section 5.1) assisted in identifying the most sensitive parameters; this information was later used in developing sets of calibrated parameters, provided in Tables B.1 and B.2 in Appendix B. As described in Table 2.1, there is a limited choice of conductivity values for each subwatershed in MINUHET, as MINUHET only uses HSG (Hydrologic Soil Group) categories for determination of each subwatershed soil hydraulic conductivity. Hence, a specific hydraulic conductivity is attributed to each HSG category (based on NRCS, SSURGO database and model calibration) (Table 5.2 and Figure 5.1f). The calibrated parameter results are summarized in Table 5.2 for the MINUHET and SWMM models; a map of each model by subcatchment is provided in Figure 5.1.

Table 5.2. SWMM and MINUHET hydrologic calibrated input parameters for simulating streamflow.

Parameters	Unit	Values range
SWMM		
Percentage of impervious surfaces	%	7.00-68.67
Total width of subcatchments	m	72-1160
Subcatchments hydraulic conductivity	mm/hr.	0.1-44.7
Impervious depression storage	mm	2.5
Pervious Manning's n	-	0.218-0.388
Impervious Manning's n	-	0.008-0.014
MINUHET		
Saturated hydraulic conductivity	m/s	HSG:B = 2.7×10^{-6}
		HSG:C = 1.8×10^{-6}

After calibration, simulated streamflow matched the observed values well for the models for both the calibration and validation periods. The goodness-of-fit results (model performance) for the calibration and validation periods are summarized in Table 5.3. The simulated and observed hydrographs for the calibration and validation periods are shown in Figure 5.2. As shown in Table 5.3, SWMM provides a better estimate in terms of average percent difference between observed and simulated streamflow. Judging from the relatively high values of NSE and low values of PBIAS, the SWMM model was considered well calibrated and validated for streamflow estimation at StREAM Lab (Table 5.3) monitoring location.

Table 5.3. Goodness-of-fit test results for assessing the reliability of calibration and validation results of SWMM and MINUHET models for streamflow.

Parameter	SWMM		MINUHET	
	Calibration	Validation	Calibration	Validation
	Model performance (hourly)			
NSE	0.67(G*)	0.65(G)	0.62(S)	0.57(S)
R^2	0.7(S*)	0.65(S)	0.65(S)	0.55(S)
RSR	0.58(S)	0.58(S)	0.61(S)	0.69(S)
PBIAS (% differences)	-0.26%(G)	-8.2%(G)	-14.5%(G)	-16.6%(S)

* G: Good; S: Satisfactory

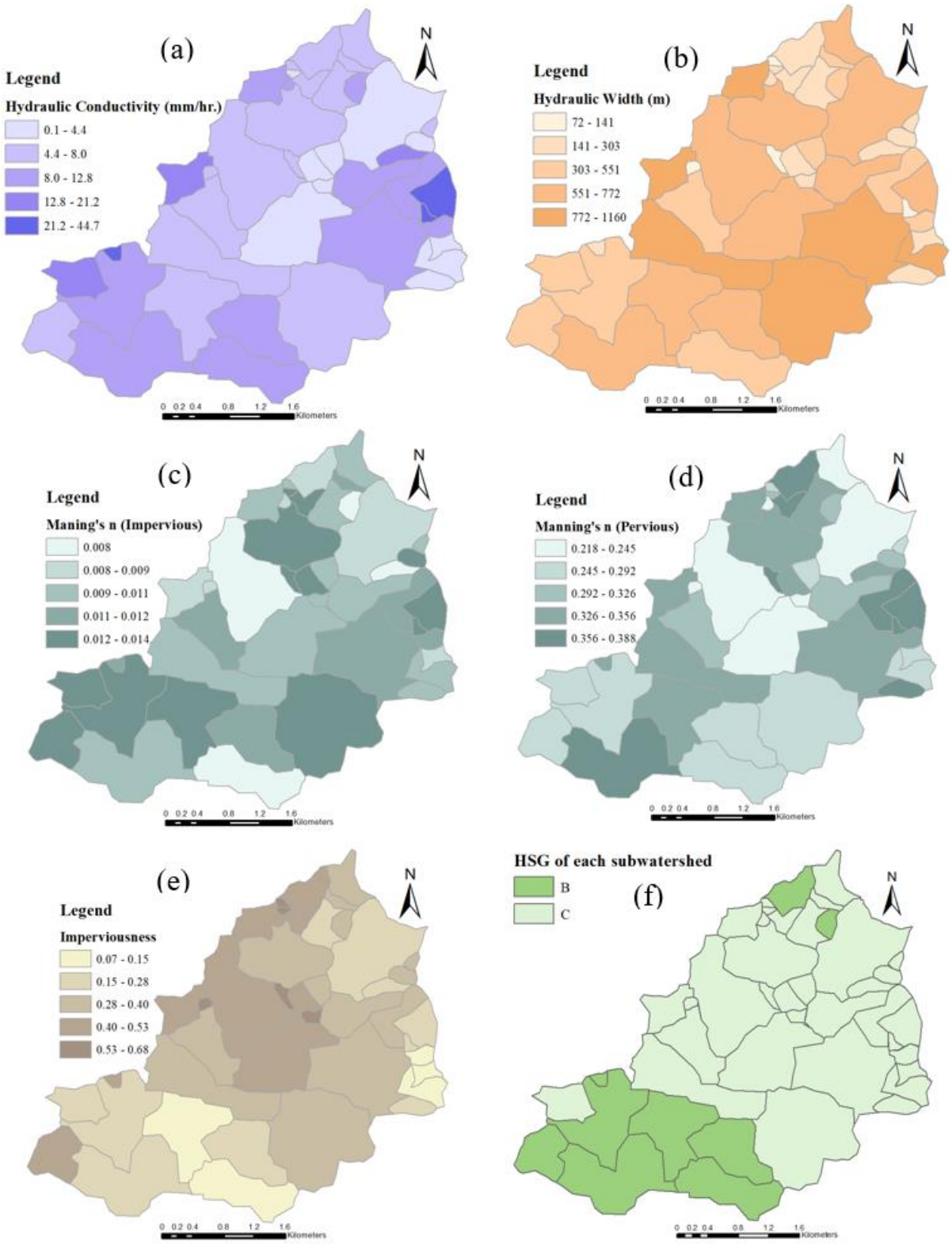

Figure 5.1. Calibrated model parameters by subwatersheds, (a) Hydraulic conductivity for SWMM (mm/hr.); (b) hydraulic width for SWMM (m); (c) Manning's n (of impervious portion) for SWMM; and (d) Manning's n (of pervious portion) for SWMM; (e) Imperviousness for SWMM; and (f) HSG by subwatersheds for MINUHET.

Since the value of PBIAS for SWMM is very close to zero during the calibration period, the model appears to be reasonably accurate; however, the negative value of PBIAS during the validation period indicates a slight overestimation bias. The R^2 values of the calibration and validation periods, 0.7 and 0.65, indicate that the model matches up well between simulated and observed values. Evaluating model performance across events, the SWMM model predicted the observed data set well during the calibration period (Figure 5.2a), but underpredicted streamflow during high intensity storm events in the validation period, i.e., the storm events of July 5 and September 29 (Figure 5.2b). This underprediction could possibly be due to the fact that our criterion was to evaluate all streamflow, including baseflow and storm events, rather than focusing strictly on storm events. Streamflow simulation using SWMM was considered satisfactory by RSR index (Table 5.3)

Based on the values of NSE and PBIAS (Table 5.3), the MINUHET model was considered satisfactorily calibrated and validated for streamflow. The negative value of PBIAS during the calibration and validation periods indicates an overestimation bias. RSR is sufficiently low to receive a satisfactory rating. Simulated and observed values for streamflow were correlated, and R^2 values of the calibration and validation periods were 0.65 and 0.55, respectively. Model performance during the calibration and validation periods matched streamflow of simulated and observed values reasonably well (Table 5.3). The MINUHET model predicted the observed streamflow data set well during the calibration period, except for the first 15 days. This is likely due to dry antecedent conditions (Figure 5.3a). Furthermore, MINUHET predicted streamflow reasonably well during intense events with less dry antecedent periods in the validation period. Specifically, the verified simulation captured the peak streamflow relatively well during the storm events of July 5 and September 29, 2015 (Figure 5.3b). Due to

longer than typical antecedent dry periods for two events (Sep 10 and Aug 6, 2015) that resulted in a reduced effective drainage area and increased surface storage, MINUHET overpredicted peak streamflow for the Sep 10 and Aug 6 storm events (Figure 5.3b). Overall, and according to the Sep 10 and Aug 6 events (the events with significant antecedent dry periods), SWMM appears to better capture the effects of pervious and impervious depression storage of surface areas than MINUHET.

In addition, as shown in Figure 5.2a, SWMM captured most of the streamflow peaks, particularly the highly intense storms of late September, when there was storm with a 10-yr return period. Goodness-of-fit was assessed by plotting the simulated vs. observed values of streamflow as shown in Figure 5.3. The slope of the regression lines in Figure 5.3 for the calibration and validation periods are very close to 1.0 for the SWMM model. As shown in Figures 5.3a and 5.3c, SWMM replicated many of the storm event peaks reasonably well. The slope of the regression line for the MINUHET calibration (Figure 5.3b) was close to 1.0, while that of for validation period (Figure 5.3d) was less than 1.0 (0.83), indicating stream discharge was underpredicted by MINUHET during the validation period.

The errors for hourly streamflow for the calibration and validation of SWMM and MINUHET indicated that the errors were lower during dry periods than wet periods. During the storm events of the calibration period, SWMM errors tended to be positive, while the opposite was true for the MINUHET model.

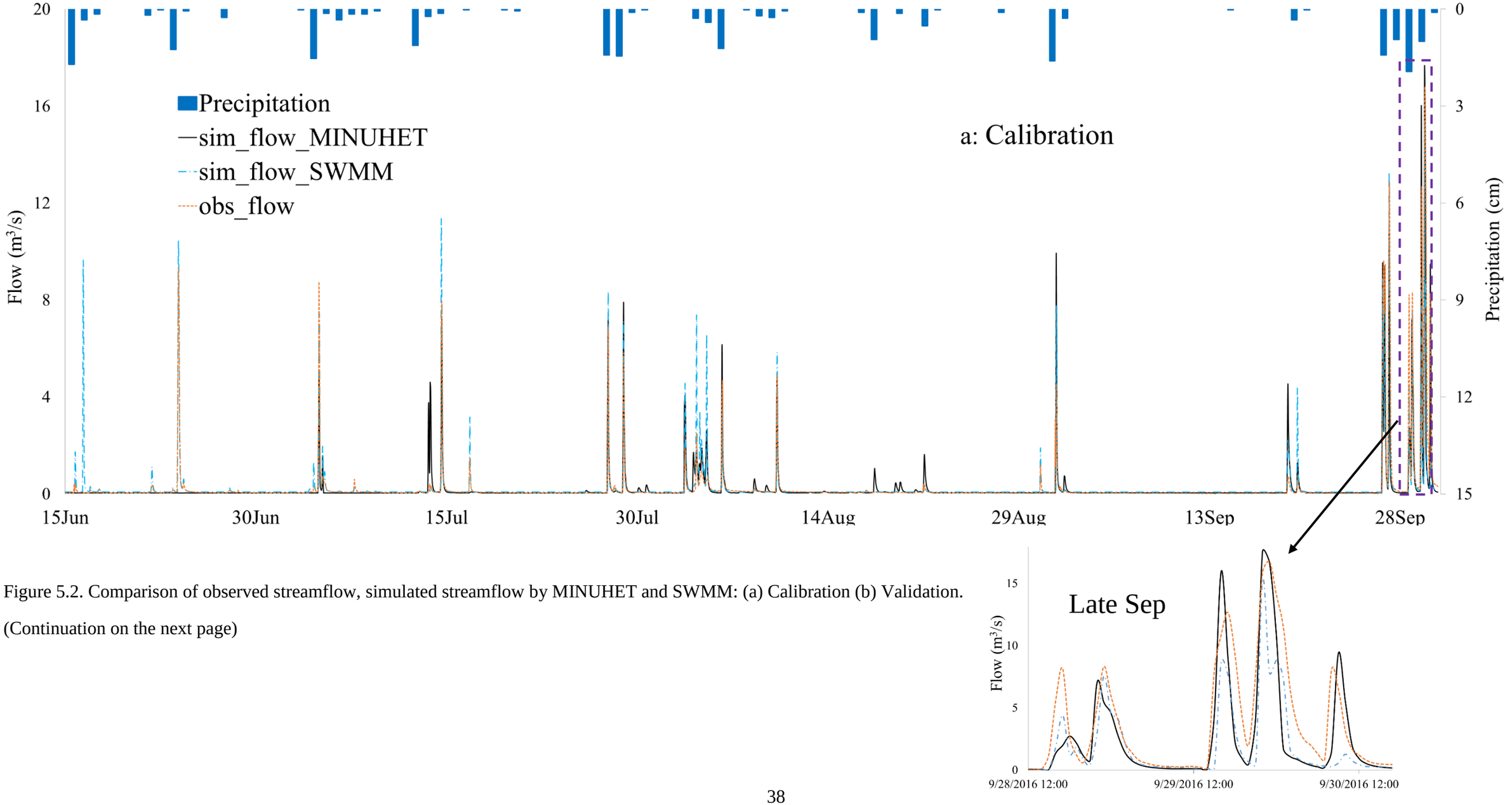

Figure 5.2. Comparison of observed streamflow, simulated streamflow by MINUHET and SWMM: (a) Calibration (b) Validation.

(Continuation on the next page)

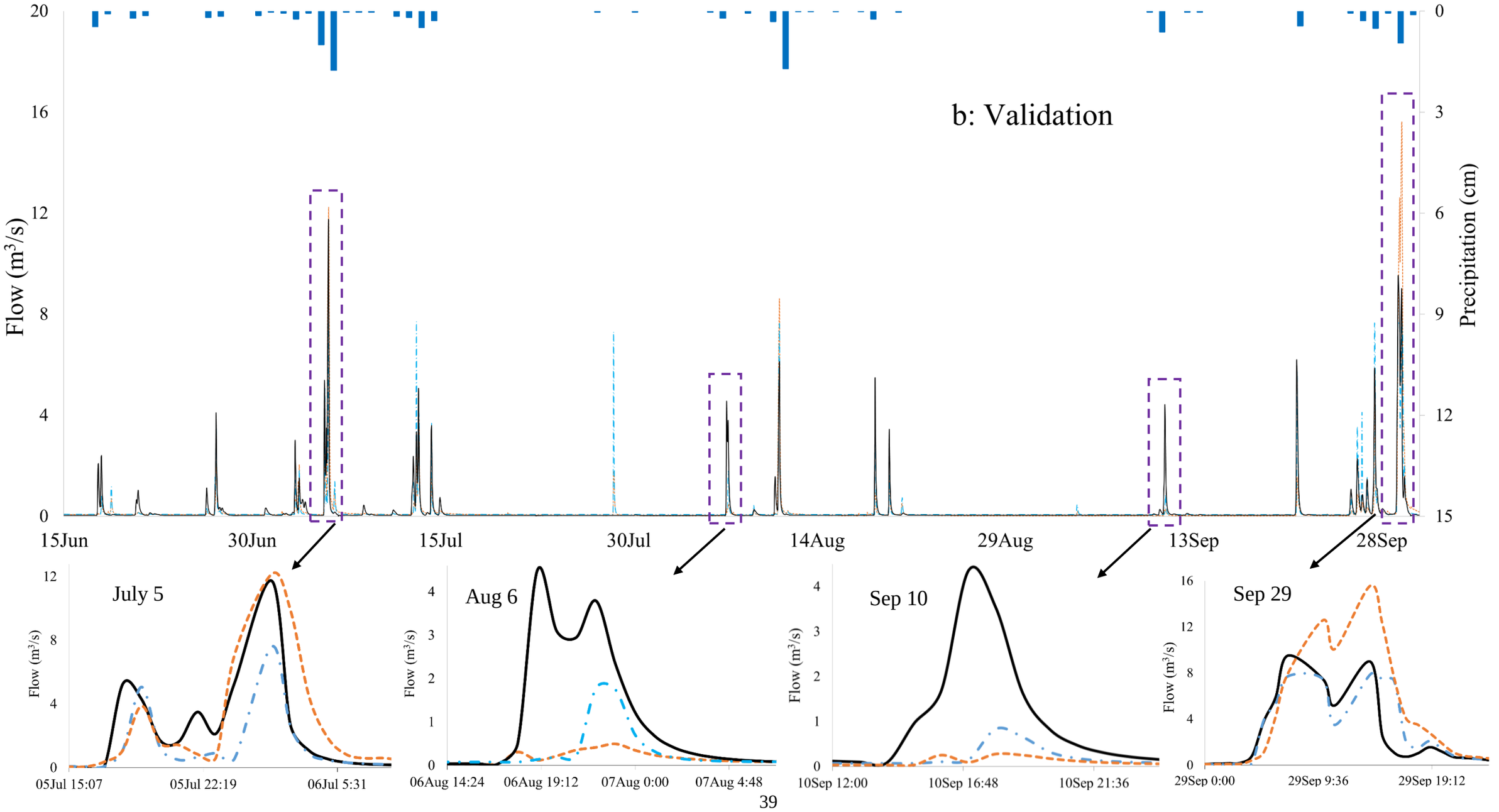
b: Validation
Flow (m3/s)
Precipitation (cm)
20
16
12
8
4
0
0
3
6
9
12
15
15Jun
30Jun
15Jul
30Jul
14Aug
29Aug
13Sep
28Sep
July 5
Flow (m3/s)
12
8
4
0
05Jul 15:07
05Jul 22:19
06Jul 5:31
Aug 6
Flow (m3/s)
4
3
2
1
0
06Aug 14:24
06Aug 19:12
07Aug 0:00
07Aug 4:48
Sep 10
Flow (m3/s)
4
3
2
1
0
10Sep 12:00
10Sep 16:48
10Sep 21:36
Sep 29
Flow (m3/s)
16
12
8
4
0
29Sep 0:00
29Sep 9:36
29Sep 19:12

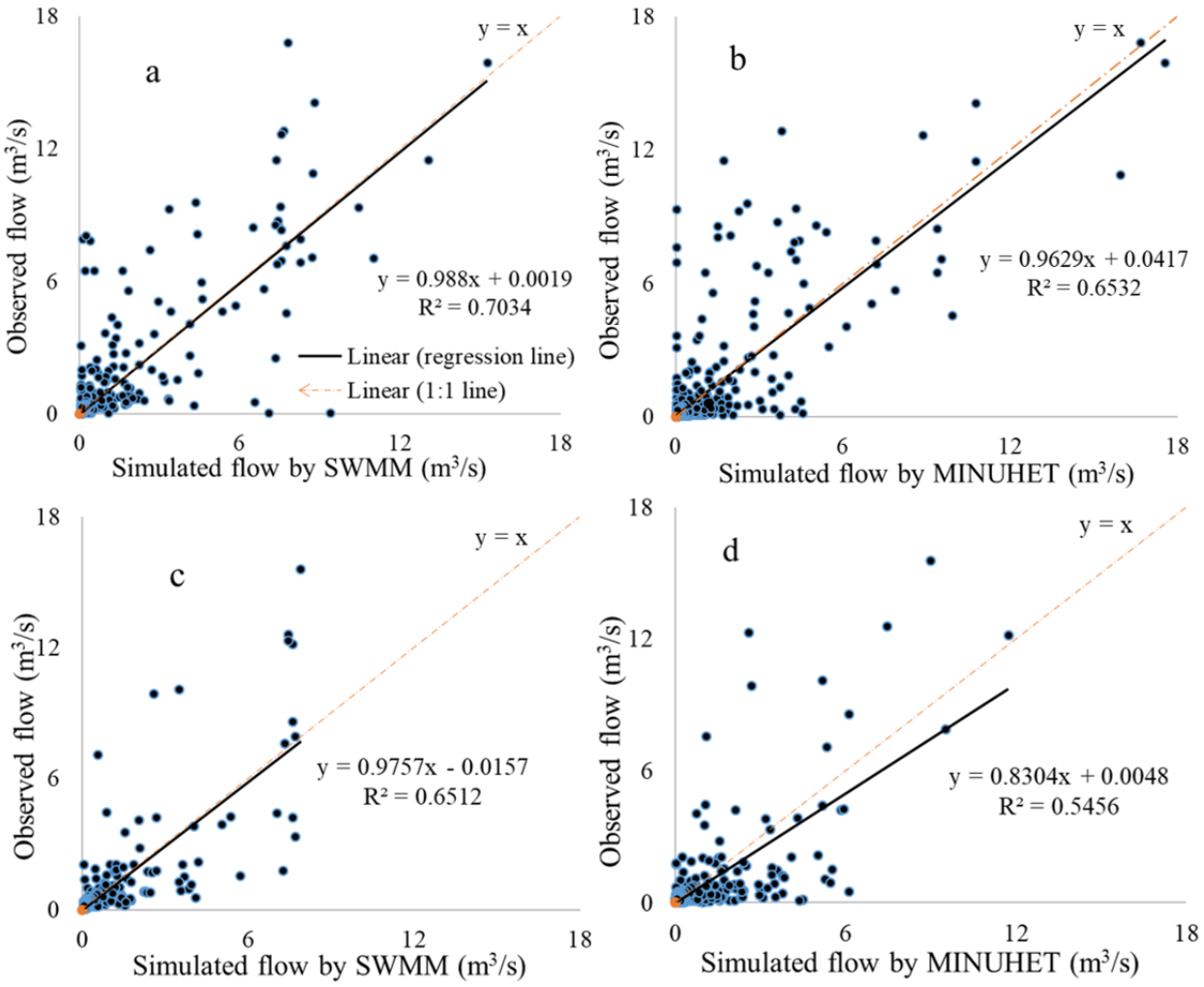

Figure 5.3. Scatter plots of observed and simulated hourly streamflow: (a) Calibration for SWMM; (b) Calibration for MINUHET; (c) Validation for SWMM; and (d) Validation for MINUHET.

As is apparent in the scatter plots (Figure 5.3), some of the errors may be due to the inability of the models to match streamflow peaks for some of the events. To analyze the error data, the Shapiro-Wilk test was first conducted on the errors of simulated and observed discharge (for calibration and validation steps), to see whether the errors are normally distributed. The p-values of Shapiro-Wilk tests were obtained less than 0.05 for models, indicating the validation and calibration errors were not normally distributed. Hence, a non-parametric Wilcoxon test conducted to see if the medians of the errors obtained from SWMM and MINUHET were

significantly different from zero. According to the corresponding calculated p-values for SWMM errors (for validation and calibration steps), the median of the errors was significantly different from zero (<0.05), likely due to the storm events during wet periods, which resulted in higher errors as compared to dry periods. Based upon the p-value for the MINUHET calibration (<0.05), the median of the errors is also statistically different from zero. Regarding MINUHET validation, The Wilcoxon test, which was conducted on the errors of MINUHET model (p-value=0.44>0.05), indicates that the median streamflow errors may not be different from zero.

To further explore differences in predicted and observed discharge values for each model, flow-duration curves (Figure 5.4) as cumulative frequency plots were developed. The observed flow, simulated streamflow by SWMM, simulated streamflow by MINUHET, and baseflow (that representing the groundwater contribution to streamflow) were plotted as shown on Figure 5.4. Two-parameter filter method was used as the baseflow separation method in the current study to generate baseflow and baseflow index (Figure 5.4); The description concerning Eckhardt method is provided in Appendix D (Eckhardt, 2008). The flow-duration curves indicated that the SWMM and MINUHET models simulated streamflow reasonably well during the calibration period. During the calibration period (Figure 5.4a) and for small flows (less than 0.1 m^3/s), the SWMM simulation results were slightly greater than the observed discharges and MINUHET simulations. As shown in Figure 5.4a, for MINUHET and observed results, the groundwater contribution (which is assumed equal to baseflow) is the main source for streamflow when flows are less than 0.05 m^3/s, mainly because the groundwater discharge was an input. However, simulated and observed flows less than 0.1 m^3/s make up more than 80% of all flows. The validated SWMM and MINUHET models resulted in lower agreement of observed and simulated streamflow than during the calibration period (Figure 5.4b). However, simulation

using MINUHET experienced greater periods of streamflow >0.1 m^3/s than SWMM and observed flows.

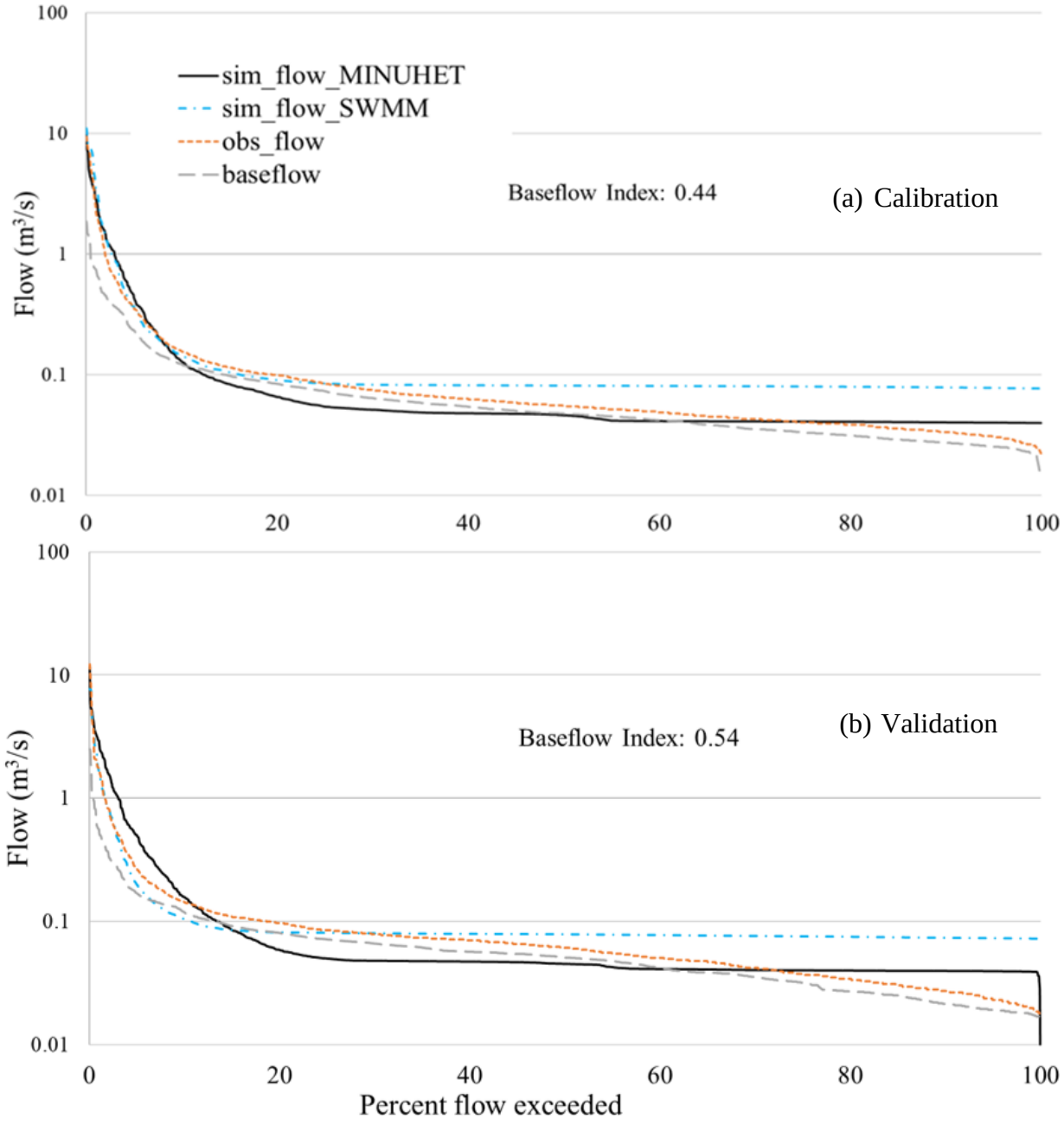

Figure 5.4. Comparison of flow-duration curves of observed streamflow, simulated streamflow by MINUHET, simulated streamflow by SWMM, and baseflow: (a) Calibration (b) Validation.

Monthly variations of hourly streamflows for the summer were compared using a radar plot (Figure 5.5). SWMM results appear to reflect a relatively better agreement with observed streamflow than MINUHET during July and August for the calibration and validation periods. The percentage difference between the simulated streamflow and the observed hourly mean streamflow ranged from 1% to 25%, which may be classified as very good to relatively good results (Al-Abed and Al-Sharif, 2008). The exception to this is in September; during which the percent differences in hourly streamflows predicted by MINUHET were slightly lower than by SWMM (for calibration and validation).

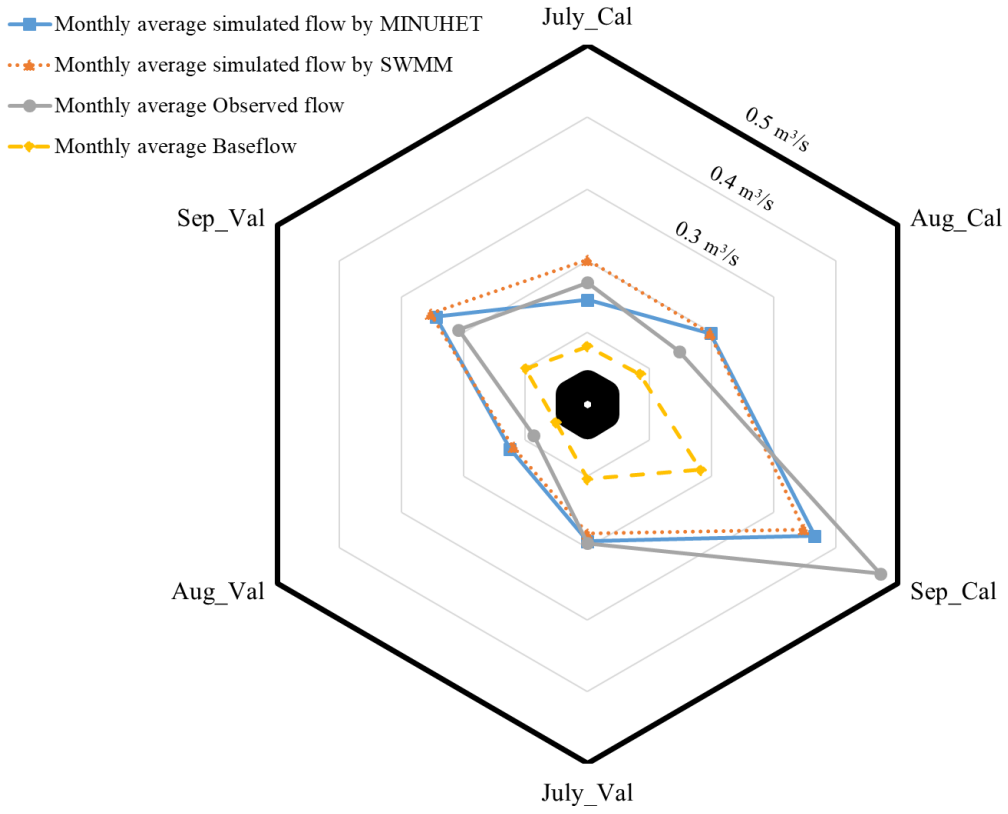

Figure 5.5. Analysis radar plot for hourly mean streamflow in each month; Val: Validation, Cal: Calibration.

The calibrated and validated models were used to simulate streamflow for a total of ten storm events, as listed in Table 5.4. Runoff fractions were calculated as the runoff depth

(volume) divided by rainfall depth (volume). During the less intense storm events of the calibration period, the MINUHET model had a lower computed runoff fraction than SWMM. In contrast, during larger storm events, the MINUHET model demonstrated much greater runoff fractions than the SWMM model. Moreover, MINUHET had a better peak streamflow response to the storm event of No. 5 (which was approximately a 10-yr rainfall event) than SWMM. Overall, the SWMM model was a better predictor of runoff fraction than MINUHET model for the calibration period. During all the storm events of the validation period (Table 5.4), MINUHET resulted in far greater runoff fractions than the runoff fractions obtained from observed data and SWMM model results. SWMM was closer to observed values of runoff fraction for the validation period.

Table 5.4. Observed runoff fraction and predicted runoff fraction by SWMM and MINUHET, for 10 storm events, during the calibration and validation periods.

Storm No.	Storm date	Rainfall Intensity (mm/hr.)	Rainfall Depth (mm)	Runoff Fraction		
				Observed	SWMM	MINUHET
Calibration						
1	7/4/2016	5.9	29.50	0.17	0.14	0.13
2	7/14/2016	7.0	37.60	0.16	0.17	0.12
3	8/3/2016	1.2	39.60	0.13	0.31	0.25
4	8/31/2016	8.4	61.00	0.05	0.05	0.12
5	9/29/2016	3.5	73.15	0.71	0.37	0.63
Validation						
6	7/5/2015	2.5	36.60	0.32	0.23	0.60
7	7/12/2015	1.7	43.70	0.12	0.16	0.18
8	8/10/2015	1.5	13.21	0.37	0.58	0.94
9	9/3/2015	1.3	11.18	0.02	0.04	0.01
10	9/29/2015	4.6	111.7	0.20	0.22	0.48

While storm events 8 and 9 were similar in terms of rainfall depth, storm event No. 9 resulted in a far lower runoff fraction than storm event No. 8 (Figure 5.6 and Table 5.4). The

period prior to storm event 9 was much drier than the period proceeding storm event 8. Hence, there was more depression storage (in impervious and pervious areas) and greater infiltration excess (in pervious areas) to reduce runoff, which resulted in a lower observed runoff fraction during storm event No.9. The duration of rainfall affected the runoff fraction as well. Notwithstanding the relative similarity between rainfall depths for Storm Events No. 6 and No. 7, the runoff fractions of storm event No. 7 were less than those for Storm Event No. 6. This may be due to the difference in duration between these two events (27 hrs. and 14 hrs. for storm No. 7 and No. 6, respectively).

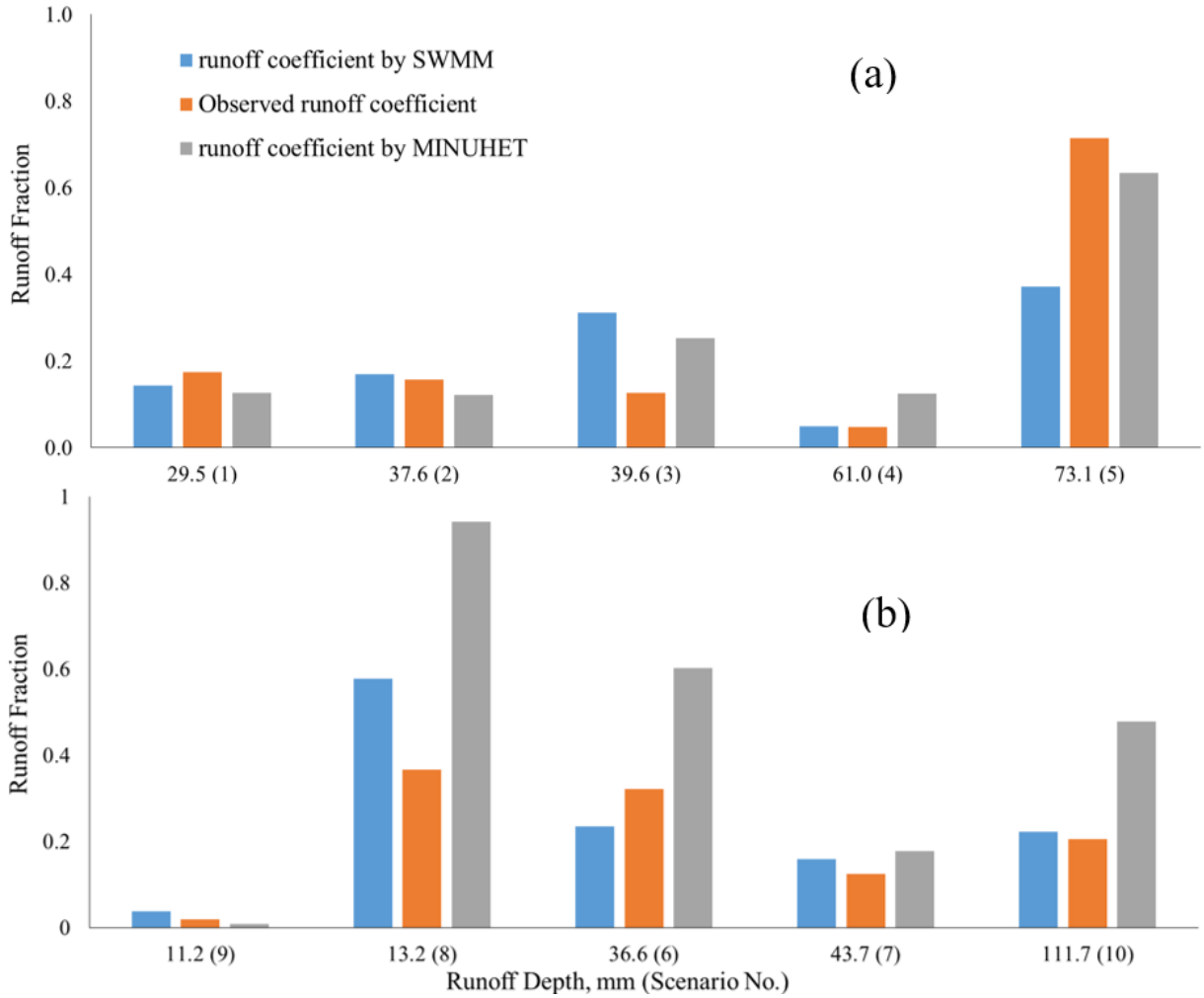

Figure 5.6. A schematic comparison of the runoff fraction conceptualized through SWMM, MINUHET and observed data sets; (a) Calibration, (b) Validation.

5.3 Temperature Simulation in the Watershed Downstream using MINUHET

Streamflow temperatures were simulated using MINUHET for the watershed downstream. After calibration, the water temperature at the watershed outlet predicted by MINUHET matched reasonably well with the observed values for the calibration and validation periods. Goodness-of-fit results for water temperature for the calibration and validation periods are summarized in Table 5.5 and the simulated and observed temperatures for the calibration and validation periods are shown in Figure 5.7. In general, the simulation captures the overall pattern/trend of the observed water temperatures. Additionally, the absolute value of percent differences of simulated and observed mean temperature (PBIAS) for the calibration period is greater than the validation period (Table 5.5), mainly due to the better prediction of water temperature in the validation period.

Table 5.5. Goodness-of-fit test results for assessing the reliability of calibration and validation results of MINUHET model for temperature, mean temperature of simulation and observation for periods, and percent differences of simulation.

Parameter	**Calibration**	**Validation**
	Model Performance	
NSE	0.55(S*)	0.58(S)
R^2	0.70(S)	0.83(G**)
RSR	0.54(G)	0.68(S)
PBIAS (Percent differences)	5.60%(G)	4.80%(G)
	Mean Water Temperature (°C)	
Simulated	20.2	19.8
Observed	21.4	20.8
	Average Daily Maximum Water Temperature (°C)	
Simulated	22.0	21.8
Observed	24.0	23.7
	Errors calculations (°C); Simulated-observed	
Min error	0.0	0.0
Max error	-5.48	-5.6
Mean error	-1.16	-0.99

*S: Satisfactory; **G: Good

The MINUHET model was considered satisfactorily calibrated and validated for water temperature based on NSE and PBIAS. The positive values of PBIAS during the calibration and validation periods indicates an underestimation bias. RSR indicated a good calibration and satisfactory validation. In terms of correlation, R^2 values during the calibration and validation periods were 0.70 and 0.83, or satisfactory and good performance, respectively. Surprisingly, the model performed better in the validation period than in the calibration period, likely because for the case study conditions, there is strong dependence (sensitivity) of simulated temperature to dew point temperatures.

The factors driving the thermal regime in Stroubles Creek are illustrated by the storm event of September 10, 2015. During the initial portion of the September 10 storm event (in the afternoon), which had a significant antecedent dry period (Figure 5.7b), previously heated and stored water in the Duck Pond was released to the stream. The Duck Pond is the largest pond in the watershed in terms of surface area, and being downstream from most of the urbanized watershed, is capable of capturing peak flows (Figure 4.1). However, during this event, a release occurs as a result of the arrival of heated runoff from upstream impervious areas, which mixes with and pushes out the stored, heated water in the Duck Pond, creating the second peak in Figure 5.7b; the initial broad rise was due to diurnal temperature changes.

Water temperature at the watershed outlet was primarily influenced by dew point temperature (according to sensitivity analysis results), except during large storm events. The correlation between water temperature at the watershed outlet and dew point temperature is strong during the beginning of high magnitude floods (e.g. September 29 of the validation period), when there is significant surface runoff (Figure 5.7b). In this case, there is likely enough surface runoff that any heat absorbed from the pavement is diluted by the large runoff volume

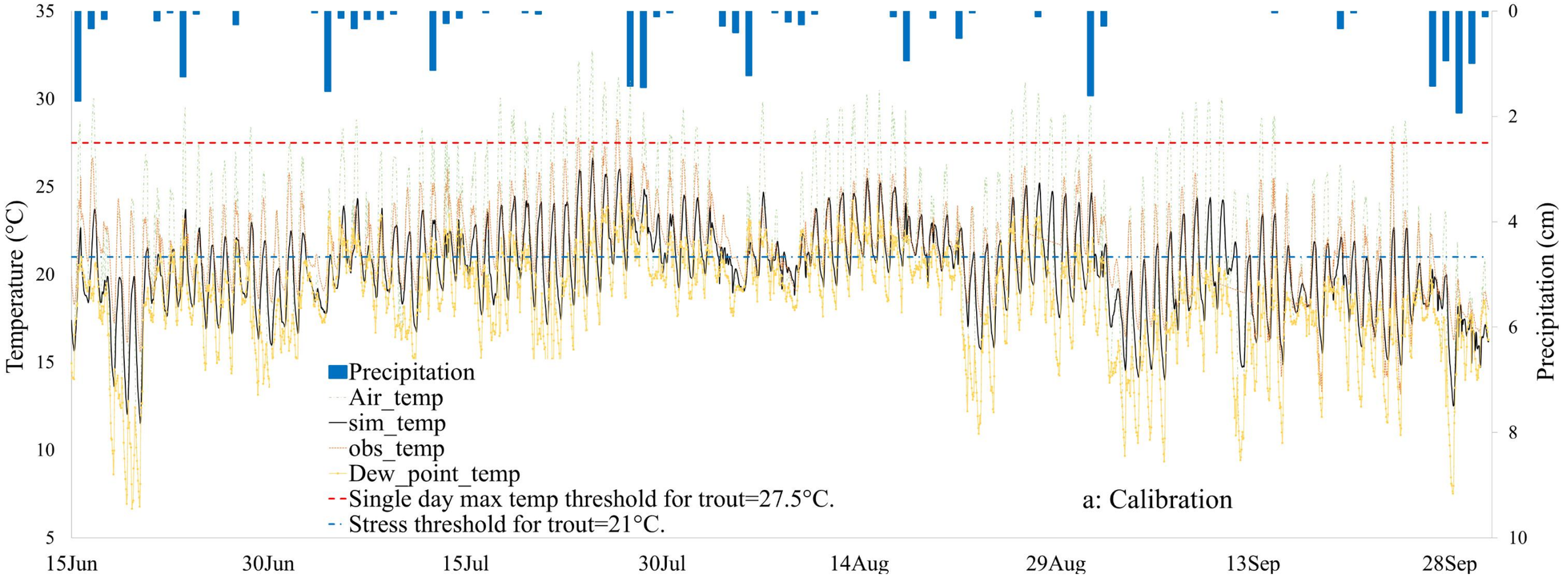

Figure 5.7. Simulated (by MINUHET) and observed temperature: (a) Calibration (b) Validation.

(Continuation on the next page)

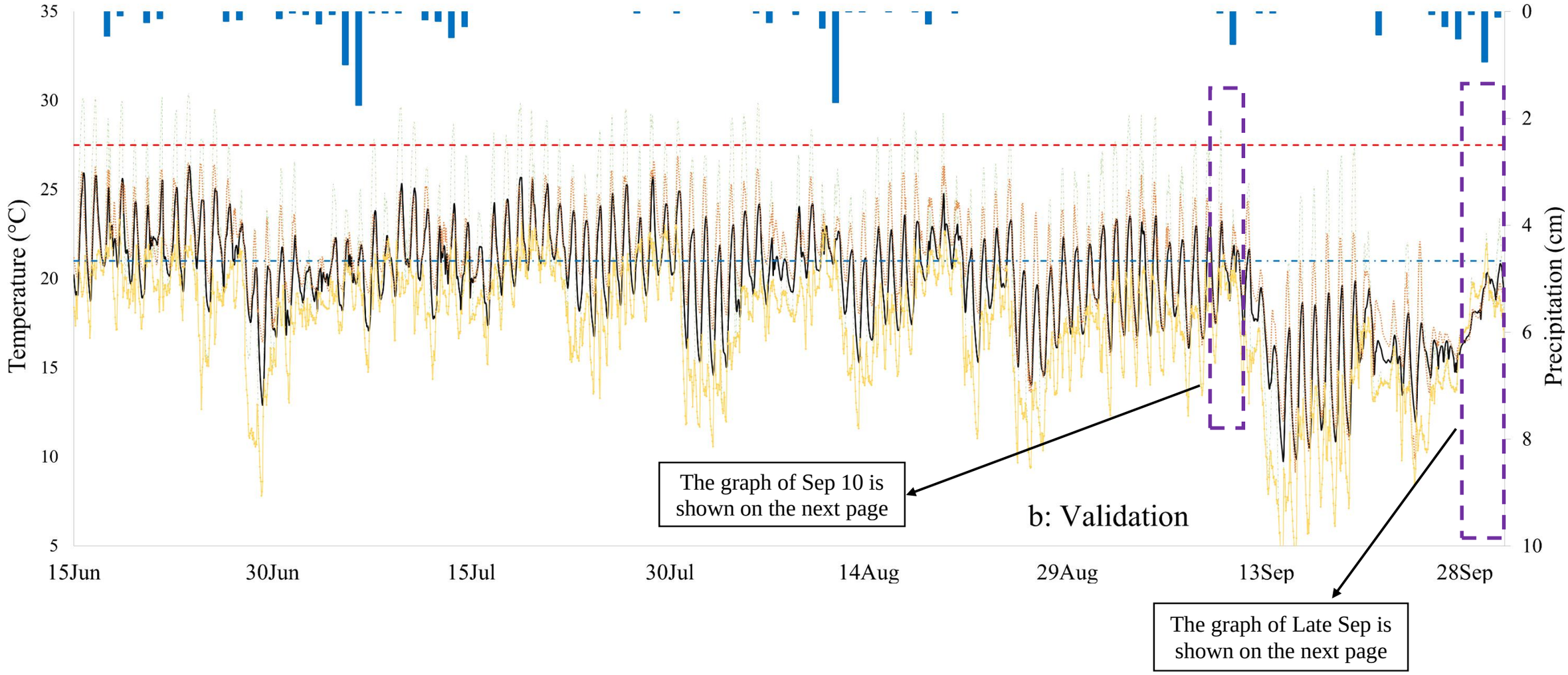

(Continuation on the next page)

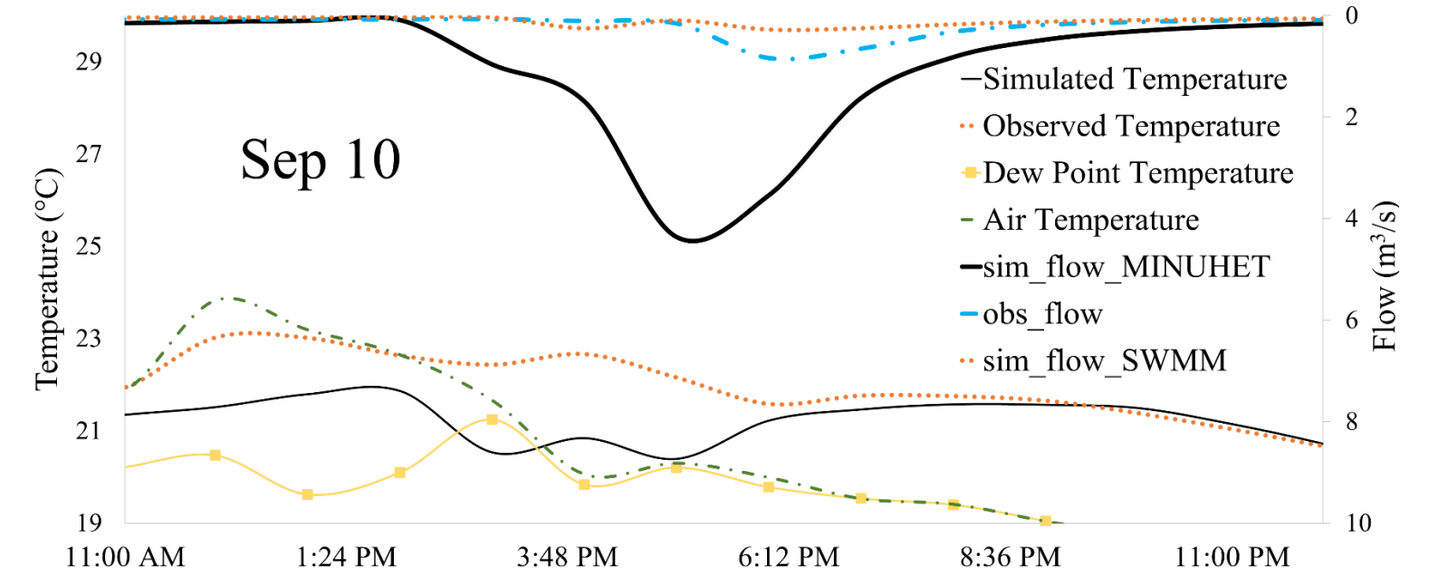
Sep 10
Temperature (°C)
Flow (m³/s)
Simulated Temperature
Observed Temperature
Dew Point Temperature
Air Temperature
sim_flow_MINUHET
obs_flow
sim_flow_SWMM
29
27
25
23
21
19
0
2
4
6
8
10
11:00 AM
1:24 PM
3:48 PM
6:12 PM
8:36 PM
11:00 PM

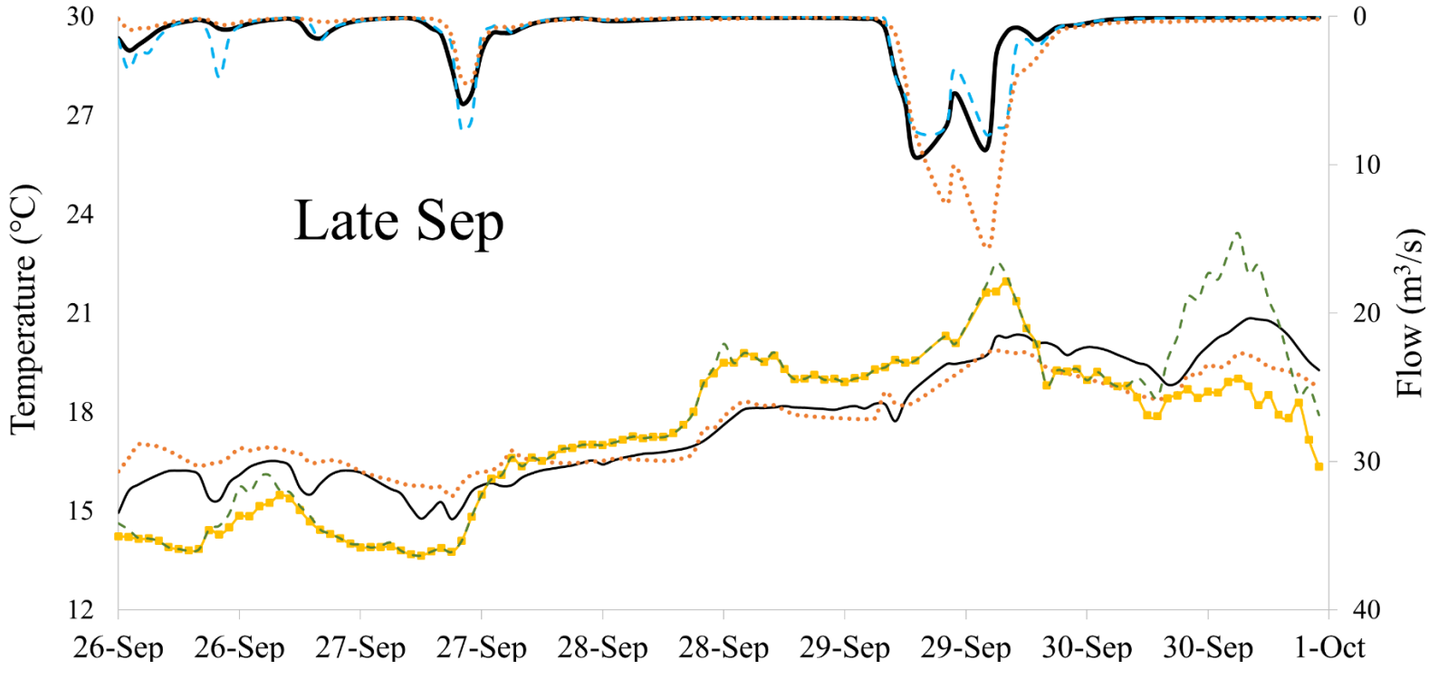
Late Sep
Temperature (°C)
Flow (m³/s)
30
27
24
21
18
15
12
0
10
20
30
40
26-Sep
26-Sep
27-Sep
27-Sep
28-Sep
28-Sep
29-Sep
29-Sep
30-Sep
30-Sep
1-Oct

and is relatively unaffected by its temperature. In addition, as the rainwater falls, water condenses and releases heat energy and the surface water (streamwater) temperature and air temperature values become closer than dry period (as shown in the last three days of calibration and validation periods, Figure 5.7). Overall, the dew point temperature and observed and simulated temperatures match relatively better during flood (defined as high magnitude storm events with runoff topping stream banks) compared to dry periods (Figure 5.7b). During floods, the dew point temperature matches the air temperature well since the air is completely saturated (Figure 5.7b). In contrast, during the initial hours of lesser magnitude storm events (Sep 27 of the validation period), water temperature (simulated and observed) was well above dew point temperature since water temperature during baseflow is strongly influenced by the groundwater temperature which was warmer than the dew point temperature at that time (Figure 5.7b). However, towards the end of the lesser magnitude storms, as most of the available heat was absorbed from the ground surface by the runoff, water temperature at the watershed outlet tended to approach dew point temperature, likely because the bulk of the streamflow towards the end of the storm stems from surface water, rather than groundwater (Figure 5.7b).

Model performance was also assessed by plotting the simulated vs. observed values of temperature as shown in Figure 5.8. Looking at calibration and validation graphs, the model under-predicts water temperature at low temperatures, which are, presumably, baseflow temperatures, likely because it is expected the baseflow to be warmer than stormflow in the summer. In addition, for the calibration period, there seems to be two different sets of data. In one set, the model is over-predicting and in the other instance, it is under-predicting. In other words, there seems to be two “lines” of data at lower temperatures (these areas were highlighted with black boxes). The slope of the regression line during calibration was 0.79, while the slope

for the validation period was greater (0.90). The higher slope indicates better model predictions during the validation period than the calibration period. Moreover, and according to the Shapiro-Wilk test results, all four simulated and observed temperature data sets of calibration and validation periods are not normally distributed and the temperature data sets are serially correlated as well. Hence, it not appropriate to apply a t-test/Wilcoxon statistical tests.

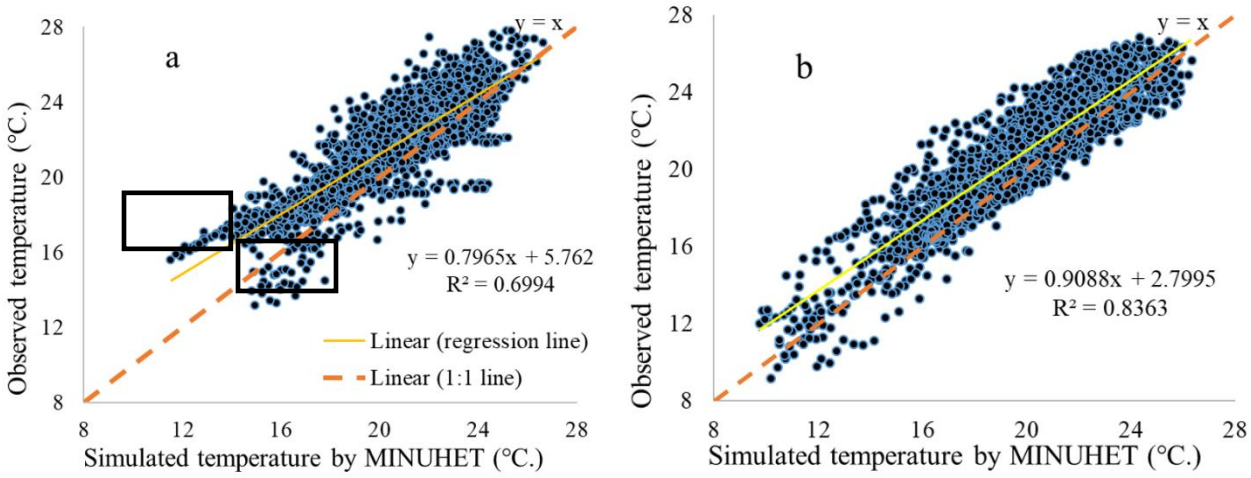

Figure 5.8. Scatter plots of observed and simulated hourly temperature: (a) Calibration (b) Validation.

The model errors time series for hourly water temperature for calibration and validation with precipitation are represented in Figure 5.9. During calibration and validation, the temperature error was negative much of the time, reflecting model under-prediction. The mean temperature simulation error during the wet periods and dry periods of the validation time span were -0.78°C and -1.0°C, respectively; a similar pattern occurred for the calibration time span, indicating the MINUHET model errors were less during wet periods than dry periods. Since the stream temperature model errors were serially correlated (not independent), the statistical tests such as Shapiro-Wilk test and Wilcoxon test cannot be conducted on the datasets to statistically evaluate if the model errors are significantly different from zero.

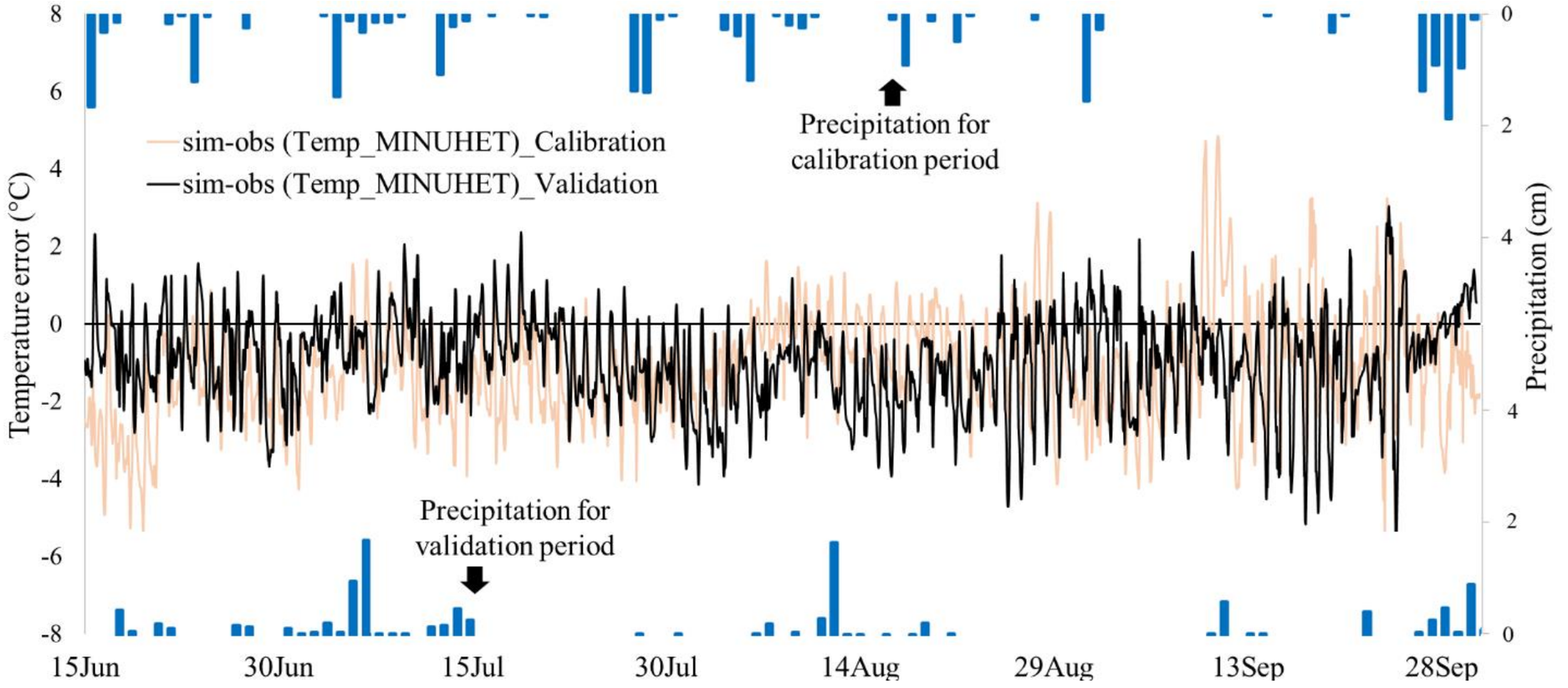

Figure 5.9. Model errors time series plot (simulated−observed) for hourly temperature, during calibration and validation periods.

To evaluate the effects of streamflow simulation on temperature simulation, temperature error vs MINUHET streamflow error was plotted (Figure 5.10). Despite the errors in simulated streamflow, the model generally predicted the overall pattern of stream temperature well. The errors in stream temperature may be the result of errors in streamflow prediction, since errors in the volume of streamflow could result in incorrectly modelled stream temperature, even if the remaining heat fluxes are accurately simulated. The dominant processes controlling stream temperature are advection (associated with streamflow during high flows), and surface heat fluxes (during low flows). During high flows of the validation period when MINUHET streamflow error was positive, temperature error tended to be negative (underestimation of temperature), while during low flows and reduced streamflow errors, the opposite pattern was observed (Figure 5.10).

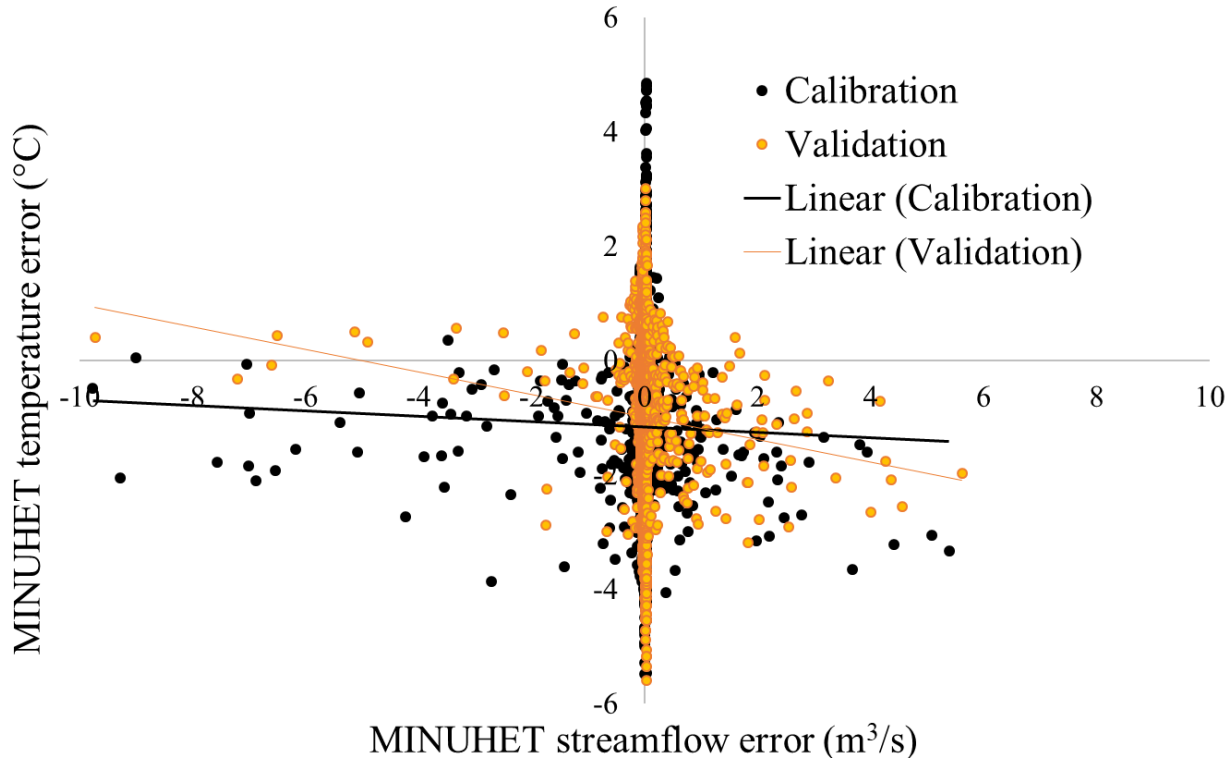

Figure 5.10. Temperature error versus MINUHET streamflow error for the calibration and validation periods.

Comparing the simulated versus observed values (Figure 5.8), it is apparent that the simulation underestimated water temperature during calibration and validation periods; this could be the result of any of the many assumptions made in the model. For example, errors in the estimation of effective impervious area would affect partitioning of precipitation between surface runoff and groundwater, resulting in errors in stream temperature predictions. Another consideration was that Blacksburg is located at an elevation of ~670 m; however, the calculation of dew point temperature, equation (Eq. 7), assumes standard atmosphere (i.e. sea level). Although the input parameters of dew point temperature equation (air temperature and relative humidity) were measured onsite (at the StREAM Lab meteorological station), for a given relative humidity, the dew point temperature at sea level is approximately 2.4°C higher than at an elevation of 670 m. This difference could be a source of systematic bias in the calculation of dew point temperature.

The under-prediction of water temperature could have been the result of the model assumption that the temperature of the precipitation was the dew point temperature. In reality, water droplets condense high in the atmosphere (i.e. clouds) and only fall to the ground once the droplets become large enough to overcome the force from the wind that keeps them in the air. Since air temperature decreases with altitude/elevation, the air where the raindrops form is significantly colder than the air below it. Hence, as the water droplets fall, they move through air that is warmer than the air where they formed. Therefore, it would not be unreasonable to assume that the temperature of the water droplets increases as they fall. In addition, as water vapor condenses, it releases energy, which increases the air temperature. Thus, there may be many reasons why the raindrops are likely warmer than the dew point temperature by the time they reach the ground.

5.4 Implications for Trout Habitats

Trout toxicity threshold values of 27.5°C and 21°C are plotted in Figure 5.7 to assess the impact of water temperature on aquatic health. Simulated water temperature exceeded the trout stress threshold (21°C) during 39% and 38% of calibration and validation periods, respectively, while the observed temperature exceeded the threshold 59% and 53% of the time for the calibration and validation periods, respectively. Quantiles of simulated and observed hourly stream temperatures representing the calibration and validation periods were developed (Table 5.6) to estimate how often water temperatures exceeded the trout stress threshold. Stream temperature in summer is the most critical factor affecting production of trout (Selbig, 2015). Each cell in Table 5.6 is shaded proportionately to increasing stress to trout as a function of stream temperature. Trout mortality due to water temperature can occur outside of this standard, as the degree of thermal stress outside of these tolerance ranges is a function of the rate and exposure duration. Thus, restoration of the aquatic habitat of Stroubles Creek should consider potential strategies to mitigate thermal pollution from impervious surfaces. An example of such practices are bioretention cells, tree canopy restoration for increased shading of streams, and installation of light-colored chip seal pavement.

Table 5.6. Quantile estimation of simulated hourly stream temperature compared to measured stream temperature, for calibration and validation periods.

	Percentile								
	1%	**5%**	**10%**	**25%**	**50%**	**75%**	**90%**	**95%**	**99%**
Calibration									
Sim.**	14.0	15.9	17.0	18.7	20.3	21.8	23.3	24.1	25.2
Obs.***	15.5	17.5	18.6	19.8	21.5	22.9	24.4	25.3	26.6
Validation									
Sim.	11.3	14.7	15.8	18.1	20.2	21.9	23.2	24.1	25.3
Obs.	11.8	15.7	16.7	19.4	21.2	22.8	24.2	25.1	26.0

***** Threshold maximum daily temperature for a seven-day exposure (>25.5°C), Initial thermal trout stress (>21°C); **Sim. = Simulated streamflow temperature; ***Obs. = Observed streamflow temperature.

5.5 Comparison of Hydro-Thermal Streamflow Analysis of MINUHET and Hybrid Models

Total heat export was calculated by the MINUHET and Hybrid models, on an hourly basis, for the calibration and validation periods and is shown in Table 5.7. Clearly, the MINUHET and the Hybrid heat export outputs have not been calibrated and validated based on observed heat export, therefore the subsequent analysis and discussion on heat export is based upon calibrated streamflow and temperature models.

During the calibration period, there was a considerable difference between the simulated and observed heat exports, the result of a large discrepancy between observed and simulated streamflow and a significant under-estimation of streamflow temperature. The simulated total heat export by the hybrid method was closer to the observed total heat export than MINUHET alone, for both calibration and validation periods. The goodness-of-fit results for calibration and validation periods are summarized in Table 5.7.

Table 5.7. Goodness-of-fit test results for assessing the reliability of simulated heat export by Hybrid and MINUHET models and total heat export calculations throughout the calibration and validation periods.

Parameter	**Hybrid**		**MINUHET**	
	Calibration	**Validation**	**Calibration**	**Validation**
	Model Performance (hourly)			
NSE	0.62(S*)	0.56(S)	0.23(U)	0.45(U)
R^2	0.63(S)	0.57(U*)	0.25(U)	0.46(U)
RSR	0.63(S)	0.66(S)	0.69(S)	0.74(U)
PBIAS	20.9%(S)	18.1%(S)	51.5%(U)	36%(U)
Total heat export** (J)	2.6×10^{13}	1.8×10^{13}	1.6×10^{13}	1.4×10^{13}

*S: Satisfactory; U: Unsatisfactory; G: Good. **Total observed heat export for the calibration and validation periods were 3.3×10^{13} and 2.2×10^{13} J, respectively.

The hybrid model can be considered satisfactorily calibrated and validated for estimation of heat export based on NSE and R^2 (Table 5.7). In contrast, the MINUHET model shows poor agreement and correlation between simulated and observed heat export for the calibration period (low NSE and R^2), with improved agreement and correlation for the validation period (i.e. greater NSE and R^2 compared to the calibration period). The improved model predictions during the validation period are likely due to the better water temperature predictions in the validation period, as compared to the calibration period. RSR is satisfactory for the hybrid model for calibration and validation; however, MINUHET did not perform satisfactorily for the validation period. The PBIAS positive values indicate that the MINUHET and the Hybrid models under-predicted observed total heat exports (Figure 5.11).

Goodness of fit for the Hybrid model was assessed by plotting the simulated vs. observed values of heat export as shown in Figure 5.12. The slope of the regression line during validation was very close to 1.0, while that of for calibration period was greater (1.24). It shows that the two data sets (during the calibration period) may be slightly different from zero, compared to the validation period. Overall, predicting heat export by the Hybrid method was better than simulating heat export by MINUHET alone (Table 5.7, Figures 5.11 and 5.12).

The radar plot of hourly mean heat export for the summer months (Figure 5.13) indicates that the Hybrid model results in lower percent differences than MINUHET during July and August for both calibration and validation periods. The percentage difference between the simulated hourly mean heat export and the observed hourly mean heat export ranged from 7% to 35%, which may be classified as very good to poor (Al-Abed and Al-Sharif, 2008). Heat export for September simulated by MINUHET and Hybrid was far less than the observed values for

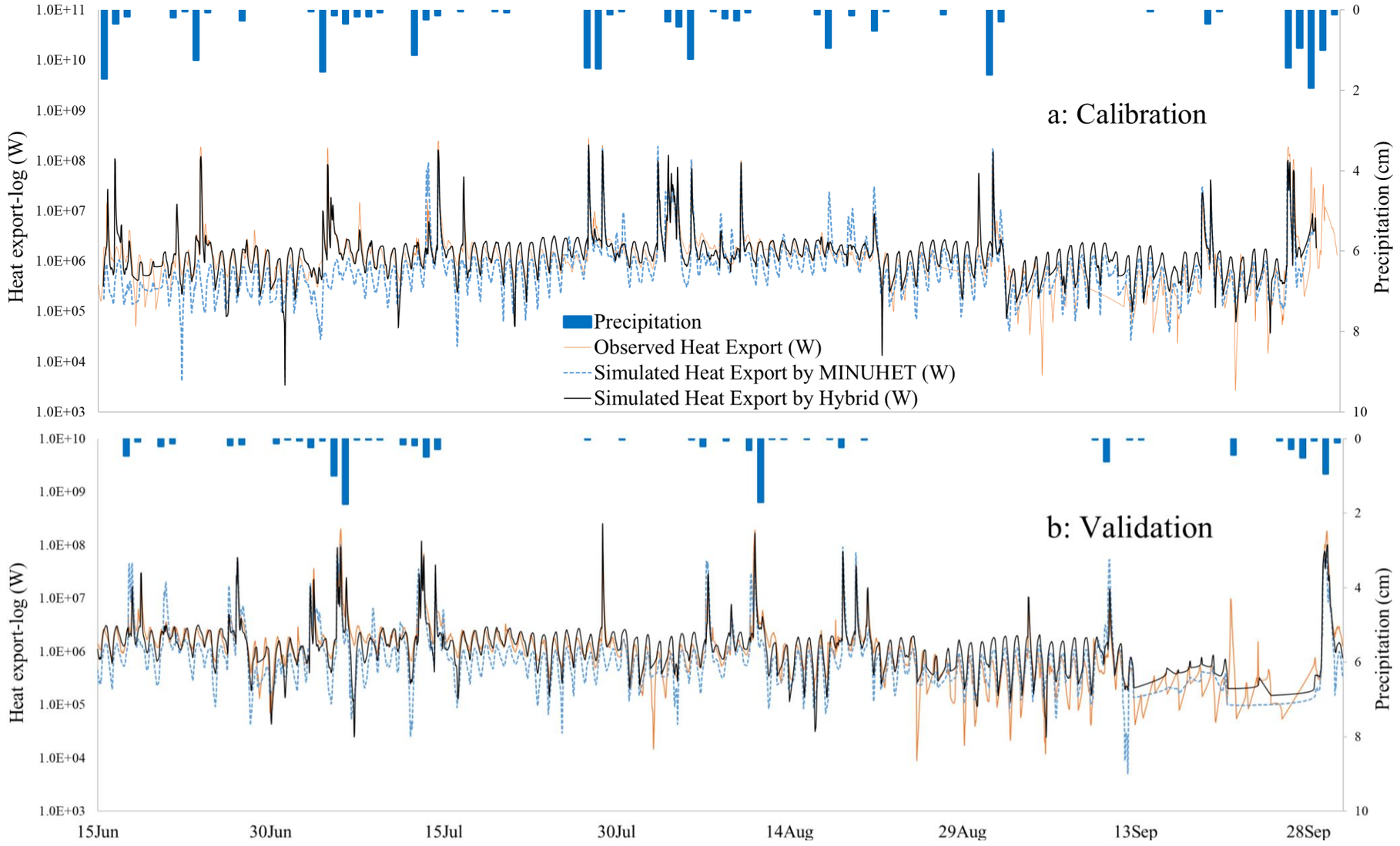

Figure 5.11. Comparison of hourly heat export simulation by MINUHET and Hybrid models: (a) Calibration (b) Validation (heat export unit is Watt as it defined to the energy consumption rate of one joule per second

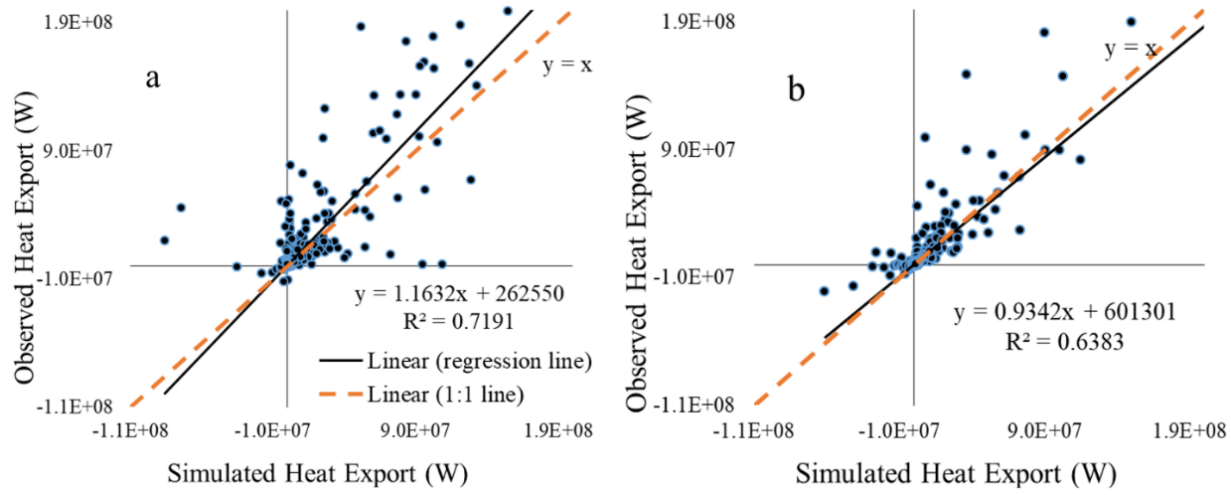

Figure 5.12. Scatter plots of observed and simulated (by Hybrid) heat export: (a) Calibration (b) Validation.

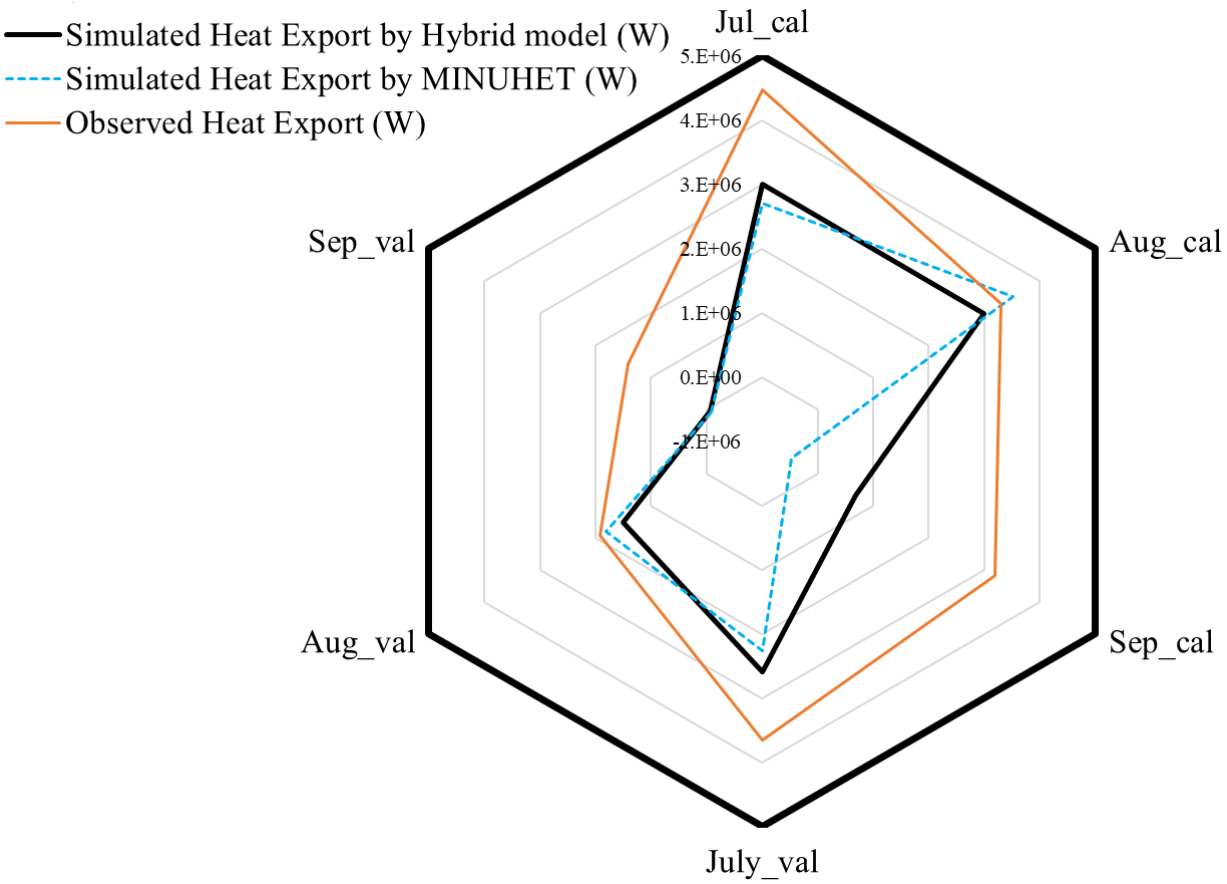

Figure 5.13. Analysis radar plot for hourly mean heat export in each month, for calibration and validation periods; val: Validation, cal: Calibration.

both calibration and validation periods. This likely stems from MINUHET's under-predicting water temperature in September, for calibration and validation periods.

It is apparent that the heat export simulation by Hybrid underestimated observed heat export during calibration and validation periods. The existing percentage difference value (PBIAS) between observed and simulated heat export by the Hybrid model (Table 5.7) may be due to the existing relatively long open channels (Stroubles Creek) in the watershed, and the aforementioned uncertainties in simulating streamflow in MINUHET. Since MINUHET does not model open channel thermal processes, simulated water temperature at the outlet of the watershed may have some uncertainties and error. Another consideration is using all streamflow rather than storm events to simulate streamflow by SWMM, which resulted in underestimation of observed streamflow peaks (because SWMM was mainly developed to simulate storm events); Hence, simulation using Hybrid model underestimated observed heat export, and can be considered as a relatively non-conservative model.

MINUHET was applied to a simple, small watershed and predicted total heat export with error less than 15% (Janke et al., 2013). In this study, with a much more complex and larger watershed, the error was larger. The Hybrid model resulted in better percent differences of total heat export than MINUHET, for calibration and validation periods (Table 5.7). The percent differences for heat export obtained by the Hybrid model were approximately similar to the values simulated by MINUHET in the Janke et al., (2013) study. This suggests using the Hybrid model of SWMM and MINUHET for complex urban watersheds, would likely result in better agreement between observed and simulated heat export than MINUHET alone.

5.6 Simulating Temperature and Heat Loads at the Watershed-Scale

The temperature and heat export results of the calibrated MINUHET and the Hybrid models were plotted based upon respective values at the outlet of each subwatershed (Figure 5.14). Based on these plots, two storms (Table 5.8) were selected from the validation period to assess the impact of storm events antecedent dry periods (ADPs) on temperature and heat load simulation and the ability of MINUHET and Hybrid models in simulation of temperature and heat load, respectively, in watershed-scale, with regards to imperviousness percentage of each subwatershed. These two were the only storms of the validation period that produced runoff at the all subwatershed outlets during the simulation by both MINUHET and SWMM, and these storms had the shortest and longest antecedent dry periods (ADPs). Thus, they were selected for maximum contrast (Table 5.8).

Mean temperature at the outlet of each subwatershed (MTOES) for each storm was compared to assess each models' capabilities at a range of ADPs and air temperatures. The Shapiro-Wilk test was conducted on each data sets of MTOES to check for normality; p-values were less than 0.05, thus the data do not appear to be normally distributed. Hence, the Wilcoxon test was used to compare the median ranks of each data set; p-values were less than 0.05, indicating that the median temperature of subwatershed data sets for the two storms was significantly different (Table 5.8). The simulated mean/average temperature of all subwatersheds outlet runoff for the Aug 11 storm was greater than that of storm Sep 29 due to greater ADP (which led to greater absorbed heat from the pavement), greater mean air temperature, and less surface runoff volume (Table 5.8). The Sep 29 storm experienced only 2 days of ADP, while ADP was 28 days for the Aug 11 storm. The Sep 29 storm produced far greater runoff than Aug 11 storm, which consequently resulted in greater total heat export.

The temperature, heat export, and imperviousness maps of the watershed for the Sep 29 and Aug 11 storms of summer 2015 are provided in Figure 5.14. The red colors of the temperature and heat export maps of each subwatershed represent the respective values at the outlet of each subwatershed. Since MINUHET was mainly developed to simulate urbanized watersheds, and the central and eastern sections of the urbanized portion of watershed are highly urbanized (Figure 5.14e), the urbanized portion of watershed imperviousness pattern corresponds relatively well with the temperature map of Sep 29 storm (simulated by MINUHET) as shown in Figure 5.14a.

The temperature map of the downstream portion of the Stroubles Creek Watershed during Sep 29 storm is not consistent with the imperviousness map (Figures 5.14a and e), due to the mitigating effects of agricultural and forestry land cover downstream. The heat export maps (simulated by the Hybrid model) of Sep 29 and Aug 11 events (Figures 5.14b and d) are approximately consistent with the imperviousness map (Figure 5.14e) at the watershed-scale; this may be due to the more accurate simulation of runoff at each subwatershed outlet by SWMM. The temperature map of Aug 11 storm (Figure 5.14c) does not match Figure 5.14e, possibly because there is far less runoff at the subwatershed outlets in the Aug 11 than the Sep 29 event, resulting in uncertainties in temperature simulation.

Overall, MINUHET and the hybrid models can be considered reliable indexes/models in developing the temperature and heat export maps of urbanized watersheds, respectively, during large storm events.

Table 5.8. Hydrologic and thermal characteristics of the selected storms for the validation period.

Parameter	**Storms Date**	
	9/29/2015	**8/11/2015**
Intensity (mm/hr.)	9.46	5.10
ADP* (day)	2	28
Mean air temperature during ADP (°C)	18.24	21.57
Total Precipitation (mm)	108.71	13.20
Total runoff volume (m^3)	1.37×10^5	1.65×10^4
Simulated Mean temperature** (°C)	19.16	20.33
Total heat export by Hybrid model (J)	1.04×10^{12}	2.46×10^{11}
P-value of Shapiro-Wilk test for temperature at the subwatersheds outlets	<0.05	<0.05
P-value of Wilcoxon test for the temperatures of storms	<0.05	

*Antecedent Dry Period; **Mean temperature of all subwatersheds runoff.

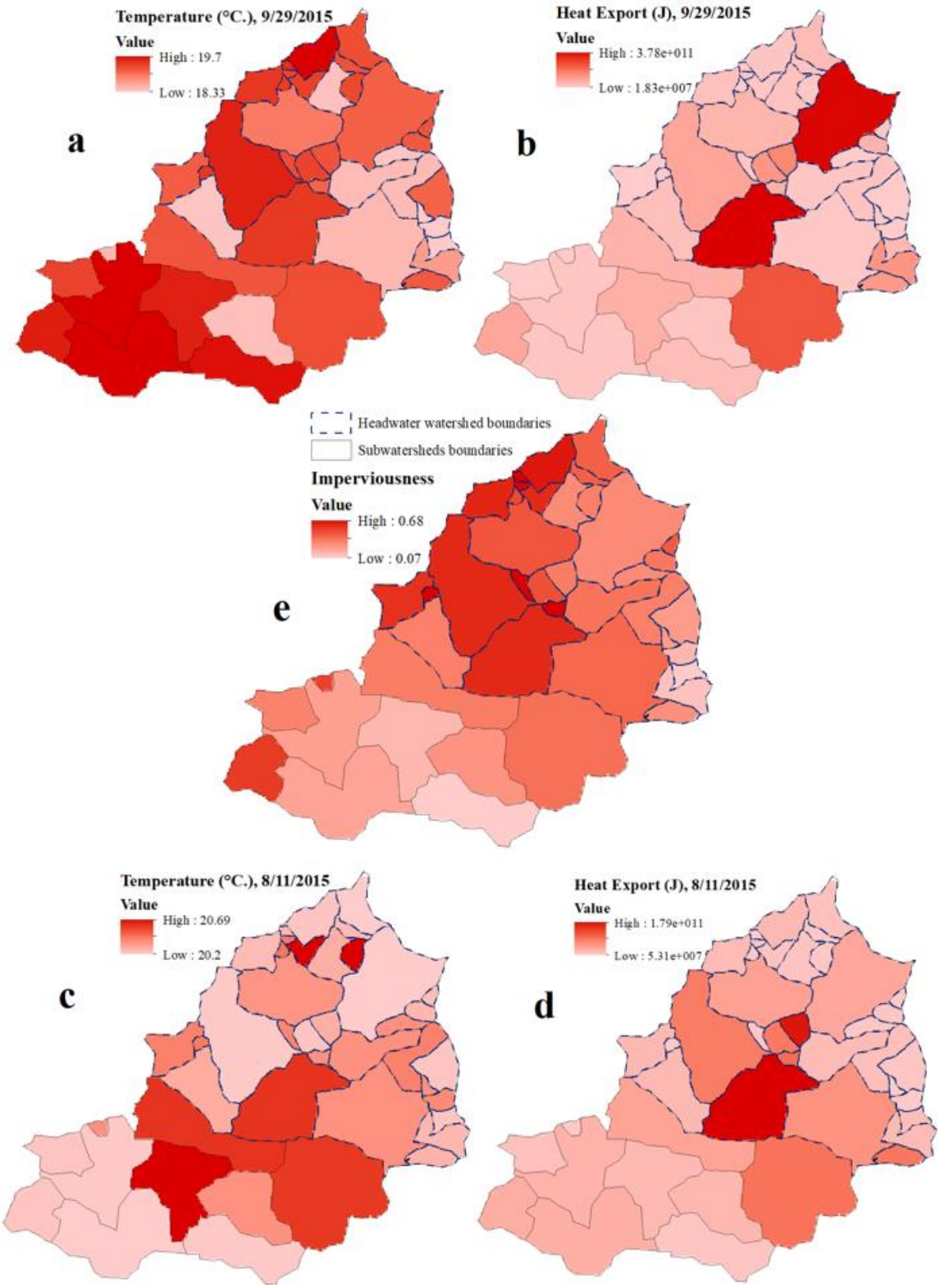

Figure 5.14. Temperature, heat export and imperviousness maps of Stroubles Creek subwatersheds: (a) Temperature map for Sep 29 storm, (b) Heat export map for Sep 29 storm, (c) Temperature map for Aug 11 storm, (d) Heat export map for Aug 11 storm, and (e) Imperviousness coefficients map.

Chapter 6.0 Utilizing Watershed-Scale Practices/Approaches to Mitigate Thermal Effects

In this chapter, the calibrated and validated SWMM and MINUHET models presented in Chapter 5 were utilized to apply watershed-scale infiltration practices and thermal mitigation approaches to reduce temperature and heat loads at the watershed outlet. Bioretention, various modified conventional pavements/roofing materials (referred to as "cool surfaces"), and increased vegetation canopies were used individually in a number of scenarios with the objective of mitigating predicted thermal pollution during the validation period (Summer 2015).

6.1 Cooling Effects of Various Pavements and Roofs Installation

Impervious conventional pavements consisting of either concrete and asphalt increase the peak surface temperature to 48-75°C (Ferguson et al., 2008). During daylight, heat builds and propagates downward in the pavement to the subsurface; this heat is later released as radiative heat during the night. Higher temperature pavements surfaces transfer this heat to runoff, which is discharged to local water bodies. In addition to pavements, residential and commercial roofs contribute to increased heat load of surface runoff. Urban runoff causes a host of aforementioned water quantity and quality issues in receiving streams (Walsh et al., 2005), including excessive temperatures which impair aquatic life (Li et al., 2013). Pavement and roof properties control the rate of heat absorption and are critical in mitigating hot pavements. Modified or "cool pavements/roofs" reflect solar radiation and lower the surface temperature when compared to unmodified conventional pavements/roofs.

A newly installed concrete pavement has a high magnitude solar reflectance which is generally considered as cool pavements (Mohegh et al., 2017). The albedo of a specific surface is the percentage of solar energy reflected by that surface. In addition to the pavement surface type, the albedo of the pavement affects its temperature below the pavement surface, since less heat is

available at the surface to be transferred downward. Concrete and asphalt conventional pavements have an approximate initial albedo of 5 and 35%, respectively (at the beginning of construction) (Ferguson et al., 2008). This is what these materials are assigned in MINUHET. Over time, use of the surfaces for foot and vehicle traffic dirty the cement causing it to darken during the life time of concrete pavement, gradually lowering the albedo; in contrast to concrete, asphalt tends to lighten as the binder oxidizes and the aggregate is exposed to weathering, which leads to higher albedo over time (Figure 6.1). Therefore, the actual albedo depends on pavement material and age (Ferguson et al., 2008). Generally, lighter pavements tend to have greater albedo, affecting surface temperatures considerably (Mohegh et al., 2017).

Thermal emittance of a surface is the radiant energy at a specific temperature per unit area. Unlike albedo, which is mostly dependent on color, thermal emittance correlates with surface material type and properties (Ferguson et al., 2008). Solar reflectance which is a term used for visible spectrum is an index representing effects of both albedo and thermal emittance combined. In addition, pavement thickness indicates how much heat is stored in a pavement, with thicker pavements storing more heat (Herb et al., 2009b). The typical unit of heat capacity is J/kg·°C, but MINUHET models heat capacity unit is in J/m^3·°C; hence the density of each material must be considered to compute the approximate heat capacity of each material (Table 6.1) (Ferguson et al., 2008; Herb et al., 2010).

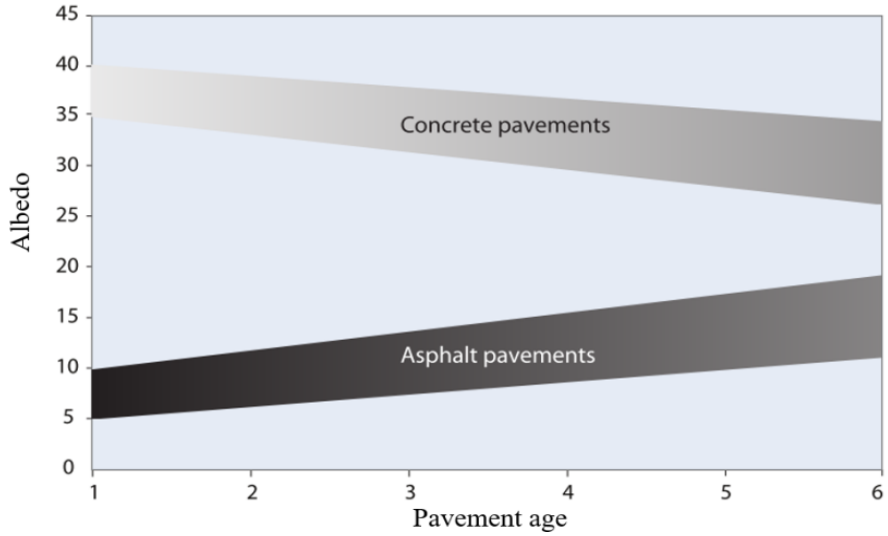

Figure 6.1. Asphalt and concrete pavements typical albedo over time (Ferguson et al., 2008)

Asphalt and concrete pavement types and commercial and residential rooftops are the dominant impervious surface types of the Stroubles Creek Watershed, which were used as input to the watershed module of MINUHET model. There is a limitation in MINUHET configuration, as there is no option to divide an impervious area of a subwatershed into various impervious land uses mentioned above. Hence, the designer has to choose only one of the aforementioned impervious land uses for each subwatershed as the dominant impervious surface type (Figure 6.2a); this could be a source of systematic bias in heat load simulation. The current dominate condition of the impervious surface type of each subwatershed is shown in Figure 6.2a (based on aerial imagery, field review, and Town of Blacksburg GIS layers information). After MINUHET calibration, various types of pavement and roofing materials were installed in the watershed through the calibrated MINUHET configuration to evaluate temperature and heat load variations downstream. Lastly, a combination of utilizing cool pavements installation and cool roofing materials (at the watershed-scale) was simulated in two individual scenarios to maximize heat load and temperature reduction downstream (Figure 6.1d, and scenarios 9 and 10 shown on Table 6.1).

Residential and commercial roofs were assigned to be asphalt shingles and metallic roofing, respectively, for the current condition (baseline scenario) of the watershed (based on aerial imagery as shown in Figure 6.2a). Thermal properties of baseline scenarios of residential and commercial roofs are shown in Table 6.1 under scenario 1 of category A. The baseline scenario of both residential and commercial roof types were converted to Acrylic Coated Galvalume (ACG) to reduce streamflow heat load and temperature downstream, while keeping asphalt and concrete thermal properties and roof areas constant (based on baseline scenario). This type of roofing has less thermal emittance and a greater albedo than conventional roof types. The thermal properties of ACG are mentioned in Table 6.1 under scenario 2 (http://www.berridge.com/colors/sri-values-for-berridge-cool-roof-colors/). Total heat load, average, median and maximum temperatures, were simulated for each of two scenarios during the validation period, and the total heat load reduction was calculated.

Asphalt and concrete pavements were installed in various scenarios with greater and lower pavement properties (thermal diffusivity, and heat capacity) compared to the current conditions (referred to as the baseline scenario). Changes in the thermal properties of pavements (scenarios 4, 5, 7, and 8) were based on an assumed change in the asphalt and concrete, which resulted in changes in thermal properties (Janke et al., 2013), with the goal being to evaluate how changing the pavement surface type affects streamflow temperature and heat load downstream (Table 6.1). All streets, roadways, parking lots, and sidewalks were assumed to be paved by either asphalt or concrete completely for categories B and C, respectively, while keeping residential and commercial roof thermal properties and roof areas constant, based on the baseline scenario (Table 6.1). Each category was assumed to have a number of scenarios of pavement properties (Table 6.1). Total heat load (THL), average, and maximum temperatures, and THL

reduction (compared to baseline scenario) were simulated for each of eight scenarios during the validation period (Table 6.2). Since asphalt and concrete have similar thermal emittance, the thermal emittance of both asphalt and concrete pavements was kept constant at a value of 91% (https://heatisland.lbl.gov/). Thermal diffusivity is the thermal conductivity of a pavement, which ranges from 5×10^{-7} to 30×10^{-7} m^2/s within MINUHET (Table 6.1). Pavement thickness is required to be at least 15 cm for semi-heavy traffic areas to meet structural stability (Iowa storm water management manual, 2008; Ketabchy et al., 2016b). The current MINUHET model input for asphalt and concrete pavement thickness was assumed to be 20 cm based on requirements for design standards of streets for Blacksburg, VA (Moore et al., 2016; Wakchaure et al., 2001).

Heat loads and temperature values of pavement and roof surfaces and percentage of time that temperature exceeded the 21°C threshold (PTTET) for each are provided in Table 6.2. Concrete pavement showed better performance in reducing mean temperature and total heat load compared to asphalt pavements (Table 6.2 and Figure 6.3). The albedo coefficient of concrete is far greater than asphalt (Table 6.1), resulting in lower total heat loads in all pavement scenarios. Thermal diffusivity is the rate of heat conductivity of pavement, and greater thermal diffusivity results in more heat energy transferred between the hot side and cold side of a pavement, thereby storing less heat energy through the pavement surface (which is exposed to stormwater) (Li et al., 2013). Specific heat capacity of pavements are less than wet soil and greater than dry soil (https://www.engineeringtoolbox.com/specific-heat-solids-d_154.html); therefore, build-up areas capture more thermal energy than undeveloped areas covered by dry soil. Hence, scenarios with higher specific heat capacity of pavements resulted in less stored heat (scenarios 4 and 7 of Tables 6.1 and 6.2). The sensitivity analysis results of thermal diffusivity and heat capacity mentioned in Table 5.1 confirm these results.

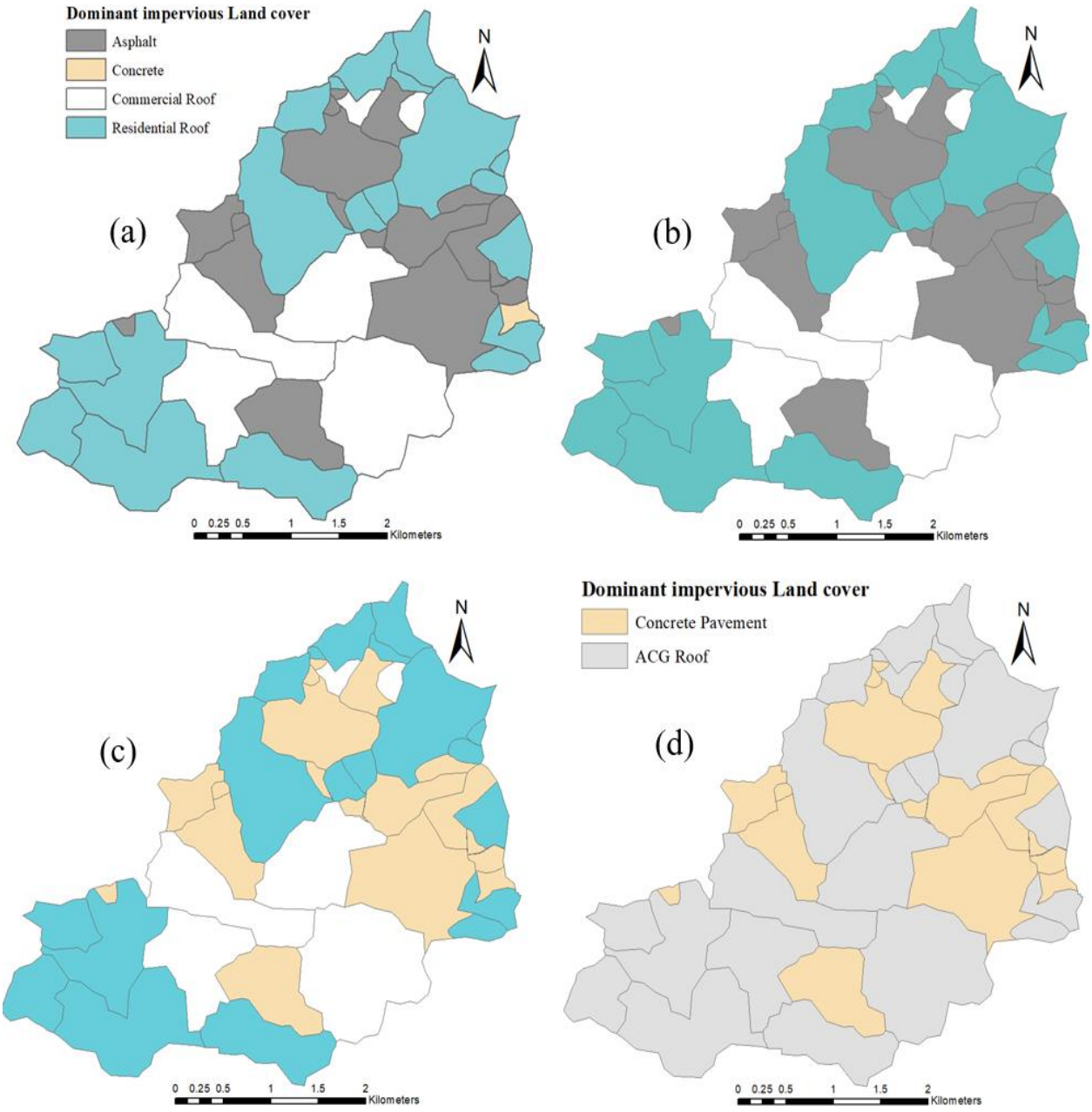

Figure 6.2. The dominant impervious surface type of each subwatershed as input to the MINUHET model for (a) Current condition or baseline scenario of watershed (based on aerial imagery, field review, and Town of Blacksburg GIS layers information), (b) Scenarios of Category B, (c) Scenarios of Category C (based on Table 6.1), and (d) scenarios of Category D (based on Table 6.1). Legends of (b) and (c) Figures are similar to that of (a).

Table 6.1. The properties of pavements and roofs, which are used as input to the MINUHET model, based on 10 scenarios.

Scenario No.	Albedo (%)	Thermal Emittance (%)	Surface Roughness*	Thermal Diffusivity (m^2/s)	Thickness (m)	~ Value of Heat Capacity ($J/m^{3}\cdot°C$)
Category A: scenarios of roof surfaces						
1**	RR***: 15	RR: 94	RR: 0.010	RR: 10.0×10^{-7}	RR: 0.01	RR: 3.0×10^{6}
	CR***: 30	CR: 70	CR: 0.010	CR: 04.2×10^{-6}	CR: 0.02	CR: 3.0×10^{6}
2	67 (H****)	0.20 (L****)	0.010	9.7×10^{-5} (H)	0.02	3.0×10^{6}
Category B: 100% of roadways, streets, parking lots, and sidewalks paved by asphalt						
3**	5	91	0.013	10×10^{-7}	0.20	3.0×10^{6}
4	5	91	0.013	15×10^{-7} (H)	0.20	4.0×10^{6} (H)
5	5	91	0.013	5×10^{-7} (L)	0.20	1.5×10^{6} (L)
Category C: 100% of roadways, streets, parking lots, and sidewalks paved by concrete						
6**	35	91	0.011	10×10^{-7}	0.20	3.0×10^{6}
7	35	91	0.011	15×10^{-7} (H)	0.20	4.0×10^{6} (H)
8	35	91	0.011	5×10^{-7} (L)	0.20	1.5×10^{6} (L)
Category D: scenarios 2 and 7 were combined for all roof and pavement surfaces of watershed						
9	GR***: 67	GR: 20	GR: 0.010	GR: 9.7×10^{-5}	GR: 0.02	GR: 3.0×10^{6}
	CP***: 35	CP: 91	CP: 0.011	CP: 15×10^{-7}	CP: 0.20	CP: 4.0×10^{6}
10*****	GR***: 67	GR: 20	GR: 0.010	GR: 9.7×10^{-5}	GR: 0.02	GR: 3.0×10^{6}
	CP***: 25	CP: 91	CP: 0.011	CP: 15×10^{-7}	CP: 0.20	CP: 4.0×10^{6}

*based on Herb et al. 2010 and Rossman, 2009
**represents the current properties of roofs/pavement, or baseline scenario of pavements/roofs properties;
***RR: Residential Roof; CR: Commercial Roof; GR: Galvalume Roof; CP: Concrete Pavement
****H: Higher than baseline scenario; L: Lower than baseline scenario.
***** Scenario 10 represents assumption of 6-year concrete age, while scenario 9 assumed concrete pavement newly constructed.

Scenario 7 resulted in the lowest total heat and water temperature between all scenarios of asphalt and concrete pavements. Scenario 7 showed better performance of urban heat island effect reduction compared to other scenarios. Overall, solar reflectance was the most critical parameter concerning how pavements interact thermally with the environment when exposed to stormwater, radiation and sunlight; thermal diffusivity and heat capacity of pavements count as second order factors (Iowa storm water management manual, 2008). Scenario 5 (asphalt pavement) resulted in increased heat load compared to scenario 0 (Current Condition) since thermal diffusivity and heat capacity increased. Scenario 8 (concrete pavement) resulted in lower heat reduction compared to scenarios 6 and 7, since the aforementioned thermal properties increased. Surprisingly, all concrete and asphalt scenarios performed similar in simulating maximum temperature of streamflow during the validation period, while PTTET of concrete scenarios were approximately 3% less than asphalt scenarios (Table 6.2 and Figure 6.3).

ACG was used as surface type for both commercial and residential roofs. ACG installation considerably reduced heat load of the watershed during validation period (-35.6%, as shown on Table 6.2 as scenario 2). Greater albedo, less thermal emittance (greater solar reflectance combined), and far greater thermal diffusivity compared to current condition of roofs resulted in better performance of heat reduction and PTTET (Table 6.2).

Pavements and roofs scenarios with the best performance (scenarios 2 and 7) were combined at the watershed-scale to minimize thermal pollution downstream, thus creating scenarios 9 and 10 (Table 6.1). Installations of ACG for roofs material and concrete for pavement were utilized to evaluate heat load and temperature downstream. Scenario 9, representing newly-constructed concrete pavements, resulted in 46% and 4.5% reduction in heat load and Percentage of Time Temperature Exceeded 21°C Threshold (PTTET), respectively

(compared to baseline scenario), which were greater than using either concrete pavement or ACG alone. Concrete pavement with 6 years of age assessed and used in scenario 10 to evaluate effect of pavement age on heat load of watershed (Tables 6.1 and 6.2). According to Ferguson et al. 2008, the albedo of concrete pavements declines by 25%, 6 years after construction (Figure 6.1). Hence, scenario 10 assumed concrete pavement to have an age of 6 years, thereby resulting in less reduction of total heat load than scenario 9 (which assumed concrete pavement was newly-constructed) (Figure 6.3).

Table 6.2. Heat load and temperature values of cool roof and pavement installation scenarios, at the outlet of the watershed, during the validation period.

Scenario No.	**Total Heat Load (J)**	**Heat Red.*** **(%)**	**Mean Temperature (°C)**	**Maximum Temperature (°C)**	**PTTET (%)**
0***	1.40×10^{13}	-	19.83	25.76	37.90
1	1.40×10^{13}	-	19.83	25.76	37.90
2	9.04×10^{12}	-35.60	18.93	25.76	34.88
3	1.40×10^{13}	~00.00	19.83	25.76	37.90
4	1.40×10^{13}	-00.38	19.82	25.74	37.82
5	1.42×10^{13}	01.05	19.84	25.76	37.90
6	1.28×10^{13}	-8.54	19.22	25.75	35.57
7	1.24×10^{13}	-11.40	19.08	25.48	35.34
8	1.33×10^{13}	-05.22	19.69	25.75	37.44
9	7.56×10^{12}	-46.10	18.71	25.72	33.73
10	8.41×10^{12}	-39.75	18.84	20.78	34.53

*Heat load percentage reduction compared to baseline scenario (reference temperature for heat load calculations is 17°C). The negative values represent heat load reduction while the positive values represents increased heat load; **threshold for trout; ***this scenario represents the Current Condition or baseline scenario of the watershed.

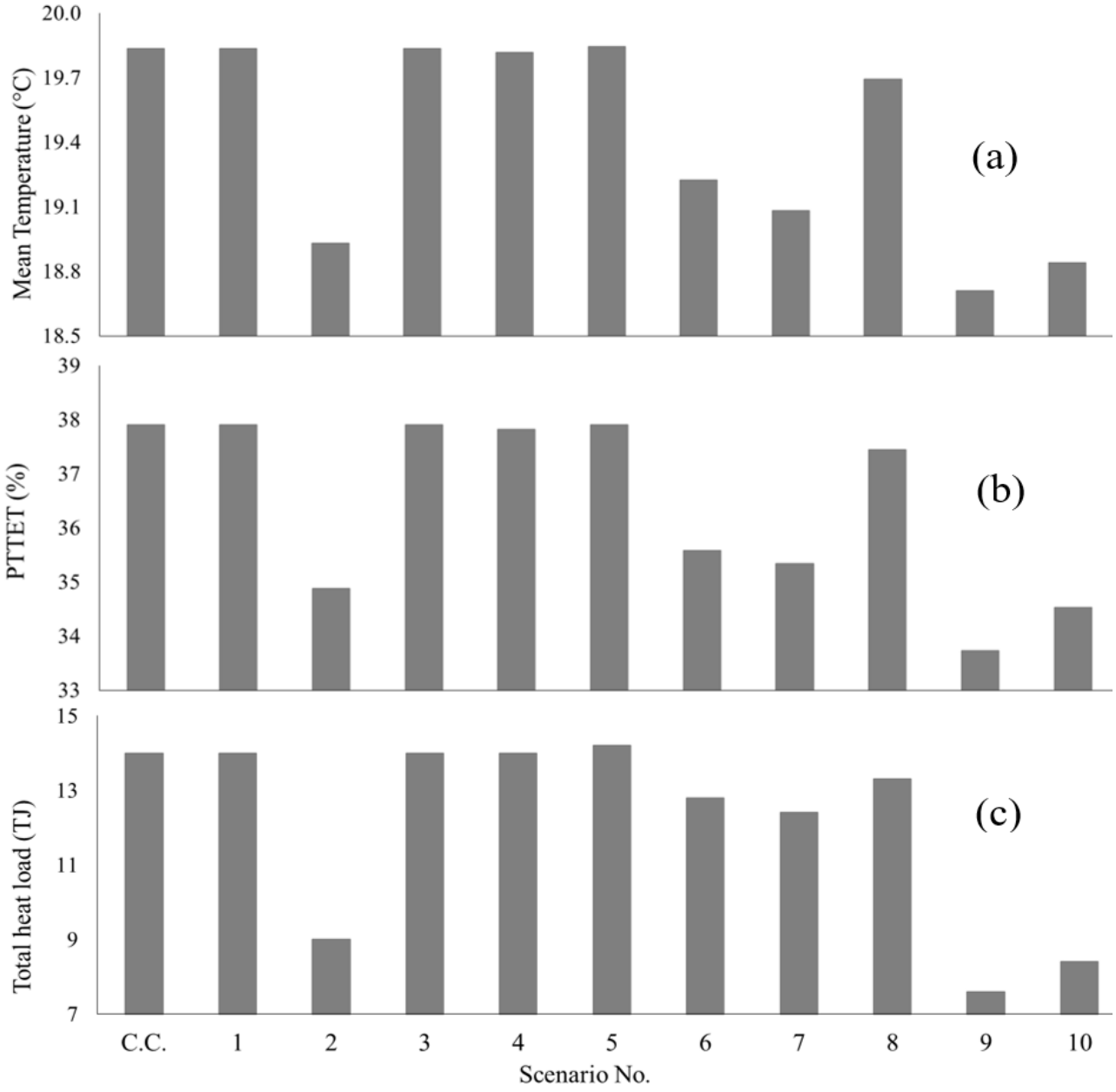

Figure 6.3. (a) Mean temperature of cool surfaces scenarios (b) PTTET for each scenario (c) Total heat load for all scenarios of cool surfaces during the validation period.

6.2 Bioretention Systems Hydrologic and Thermal Mitigation Effects

Bioretention cells are vegetated areas (with designed soil mixes or compost-amended native soils) designed to capture stormwater and rainfall, and reduce surface runoff temperature impacts. A bioretention cell allows runoff to infiltrate both through its treatment media and into

the native soil beneath it; this infiltrated water provides recharge for the shallow water table. Bioretention is a stormwater BMP that can moderate mean runoff temperature, i.e., keeping it cool in seasonally hot weather and prevents severe temperature fluctuations during cold months (Herb et al., 2010). This section evaluates the effectiveness of bioretention cells in reducing heat load and temperature through installation of bioretentions systems at the down-gradient end of a number of selected parking lots using the calibrated SWMM and MINUHET models. Schematic of a bioretention cell is shown in Figure 6.4.

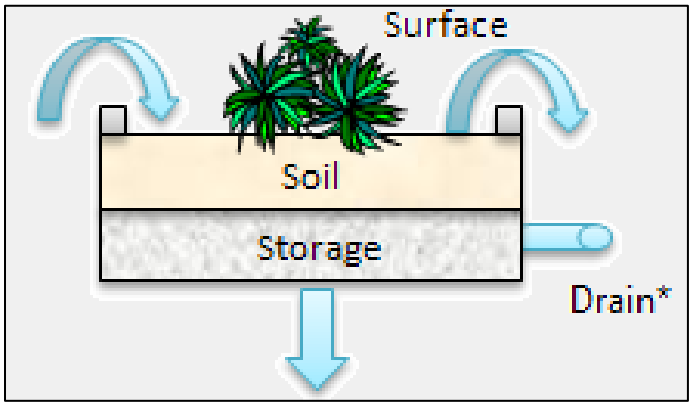

Figure 6.4. Schematic of a bioretention cell (Rossman, 2009).

Based on a specified bioretention system volume, depression storage is increased in the pervious part of the subwatershed (extra depressional storage = bioretention volume/pervious area). Bioretention cells were simulated in SWMM using the specific attributes listed in Table 6.3. Infiltration ponds were used instead of bioretention in the MINUHUET model because: 1) in the current configuration of MINUHET, only rooftops can be routed to a bioretention cell, while, in our watershed, the main portion of the impervious area is pavement; 2) Since infiltration ponds are external to a subwatershed within MINUHET, they are defined individually, which is similar to the SWMM approach; 3) There is a software issue in the data entry for bioretention

within the MINUHET model for English units; and 4) the bioretention cells in MINUHET affect stormwater quantity, but not stormwater temperature (Herb et al., 2010; Virginia Department of Conservation and Recreation, 1999). Hence, due to the four aforementioned reasons, infiltration ponds model were used in MINUHET model to represent bioretention systems to treat a substantial area of impervious parking lots. A total storage volume of the bioretention systems and an infiltration rate can be represented using the infiltration pond model. Pond bathymetry was developed to match the total amount of bioretention storage (above ground storage + soil pore storage) in the corresponding SWMM model. The point was to represent how much water could be stored during storm events, and then how fast it will drain down after the event. A detail that will be missed with the infiltration pond model is the speed at which the soil storage fills up (the infiltration pond model assumes that all storage is available immediately, whereas in reality, there is a finite rate at which the soil storage fills up). The infiltration ponds and bioretentions specifications simulated in the models are shown in Table 6.3. In developing the models, several assumptions were made including:

Parking lots area: Parking lots with at least 4645 m^2 or 50,000 ft^2 (53 in total) were selected for bioretention installations at their outlets. The location of each parking lot within the watershed is shown on Figure 6.5. Total area of parking lots in the watershed is 1.41×10^6 m^2, and the total parking lots area that was retrofitted is 7.36×10^5 m^2; therefore, 52% of the total parking lots area of the watershed were retrofitted by bioretention systems (Figure 6.5).

Bioretention to parking lots area proportion: For planning purposes, the surface area of each bioretention was approximately 5% of the impervious area of the respective parking lot (James et al., 2010). In addition, the entire area of the selected parking lots was assumed to be

treated by bioretention systems, and the overflow from the bioretention drained to the outlet of the subwatershed.

Width vs. length dimensions: Each bioretention systems dimensions was at least assumed to be of the ratio 1:2 (width vs. length) (James et al., 2010). For the current study, the width of each bioretention system was assumed 6.1 m (20 ft.).

Each bioretention unit area: A number of bioretention cell units were installed at the outlet of each selected parking lot to capture the surface runoff during storm events. Determination the number of units of each bioretention systems was based on the area of the respective parking lots in acres. In other words, one acre of each parking lots was assigned to one bioretention unit. For example, if there is a 20,000 m^2-parking lot (and 20,000 m^2 is approximately equivalent to 5.0 acres), and the total bioretention size assigned to this parking lot is 5% of 20,000 m^2 (i.e. 1000 m^2), therefore, the number of bioretention units would be five with each being 202 m^2 in terms of area. Hence, the standard area of each bioretention unit was chosen as 202 m^2. Since each bioretention unit width was assumed 6.1 m, length of each bioretention unit would be 33.1 m. The area of selected parking lots and bioretention systems, and the number of bioretention units for each parking lot are shown on Appendix C.

Bioretention soil moisture: The soil moisture within each bioretention cell was assumed to be dry, at the wilting point, initially (Rossman, 2009).

Media thickness: The Virginia Department of Environmental Quality specifies a minimum media thickness of 61 cm (24 in) and storage layer depth of 30 cm (12 in), so these were used (Table 6.3).

Media soil infiltration rate: this parameter was set at three engineered amount scenarios of 4.16, 25, and 41.6 mm/hr. (Table 6.3). The aforementioned infiltration rates represent sandy clay loam, sand, and sandy gravel conditions of media soil, respectively (Virginia Department of Conservation and Recreation, 1999).

Installation of underdrain systems: Since Virginia Department of Environmental Quality (DEQ) requires that all bioretention cells installed in karst areas (Blacksburg geology is karst) should be lined with either a synthetic or clay liner, underdrain systems were included for all the bioretention cells. Unlike SWMM, there is no built-in underdrain option for infiltration ponds in the MINUHET model, which can be a source of errors in temperature simulation. The underdrain page of the SWMM model requires the following input data: flow exponent (n), flow coefficient (C), and offset height ($H_{d,}$ mm). The outflow equation used for underdrain systems is as Eq. 6.1 (Rossman, 2009).

$$Q = C \times (h\text{-}H_d)^n \qquad \text{Eq. 6.1}$$

Where Q is outflow, mm/hr., and h is the height of stored water (mm). If the goal is to drain a fully saturated soil media in a specific amount of time, a typical value for n (flow exponent) would be 0.5 (which makes the drain act like an orifice). A rough estimate for C (flow coefficient) would be as Eq. 6.2 (Rossman, 2009).

$$C = \frac{2 \times D^{0.5}}{T} \qquad \text{Eq. 6.2}$$

Where D is the depth of stored water (mm) and T is the time in hours to drain. A typical value for T is 12 hr. Therefore, for the current study, n and offset height were chosen to be 0.5, and 0,

respectively; while C was calculated through the equation mentioned above for different depth of water in the storage layer (Rossman, 2009).

Scenarios of bioretention installation: Four scenarios to evaluate the effectiveness of bioretention cells were defined: 1) current condition of the watershed without retrofitting with bioretention systems (baseline scenario), 2) installing bioretention systems with soil media conductivity of 4.16 mm/hr., 3) installing bioretention systems with soil media conductivity of 25 mm/hr., and 4) installing bioretention systems with soil media conductivity of 41.6 mm/hr.

Model utilization: The calibrated SWMM and MINUHET models were used to simulate streamflow, and temperature, respectively. Then, a Hybrid approach was employed to simulate total heat load during the validation period, for each scenario.

Total streamflow (TSFs) and total heat load (THLs) for the bioretention installations are shown in Table 6.4. Scenario 1 represents the current water condition (simulated through Hybrid model), while scenarios 2, 3 and 4 represent media infiltration rates of 4.16, 25, and 41.6 mm/hr., respectively (Virginia Department of Conservation and Recreation, 1999). Scenario 3 resulted in approximately 11% heat reduction compared to current conditions. Surprisingly, total streamflow flow and consequently total heat load of scenario 4 was greater than scenario 3 (Table 6.4). Scenario 3 (with soil-media infiltration rate of 25 mm/hr., which represents sand and sandy loam soil type) resulted in better total heat reduction, while scenario 4 of bioretention installation performed better in mitigating mean temperature (Table 6.4). The PTTET index indicates the scenario 3 configuration of bioretention performed poorly in reducing thermal effects on trout habitats (Table 6.4). This performance of bioretention in reducing of average temperature and PTTET is similar to results from the Herb (2008) study on Vermillion River Watershed.

Table 6.3. Specifications of bioretention cells/infiltration ponds used in SWMM and MINUHET models to mitigate hydrologic and thermal loads to the Stroubles Creek watershed.

Specifications	Unit	Value	Reference
Shading/Sheltering	%	10 / 0	(Herb et al., 2010)
Surface Layer			
Berm height	cm	0	(Herb et al., 2010; Rossman, 2009)
Vegetative volume	Fraction	0.9	(Rossman, 2009)
Surface roughness for bioretention cells	Manning's n	0.24-0.41 (0.41 for current study)	(Rossman, 2009; Virginia Department of Conservation and Recreation, 1999)
Surface slope	Percent	0	(Herb et al., 2010; Rossman, 2009)
Soil Media Layer			
Thickness/depth	cm	61	(The Virginia Department of Environmental Quality, 2011)
Porosity	Volume fraction	0.4 (the same used for aquifer)	(Rossman, 2009; Virginia Department of Conservation and Recreation, 1999)
Field capacity	Volume fraction	0.24 (the same used for aquifer)	(Rossman, 2009)
Conductivity slope	-	1 (the same used for aquifer)	(Rossman, 2009)
Conductivity	mm/hr.	"Each bioretention media infil. rate can be engineered to a value between 4.16 and 41.6 (the mean is 25)"	(Rossman, 2009)
Wilting point	Volume fraction	0.086 (the same used for aquifer)	(Herb et al., 2010; Rossman, 2009)
Suction head	cm	"Each bioretention suction head is attributed to the respective subwatershed soil's properties, based on NRCS, 1999"	(Herb et al., 2010; Rossman, 2009)
Storage Layer			
Seepage rate	mm/hr.	"Each bioretention storage layer seepage rate is attributed to the respective subwatershed soil's properties based on NRCS, 1999"	(Herb et al., 2010; Rossman, 2009; Virginia Department of Conservation and Recreation, 1999)
Storage void ratio	-	0.4	(James et al., 2010)

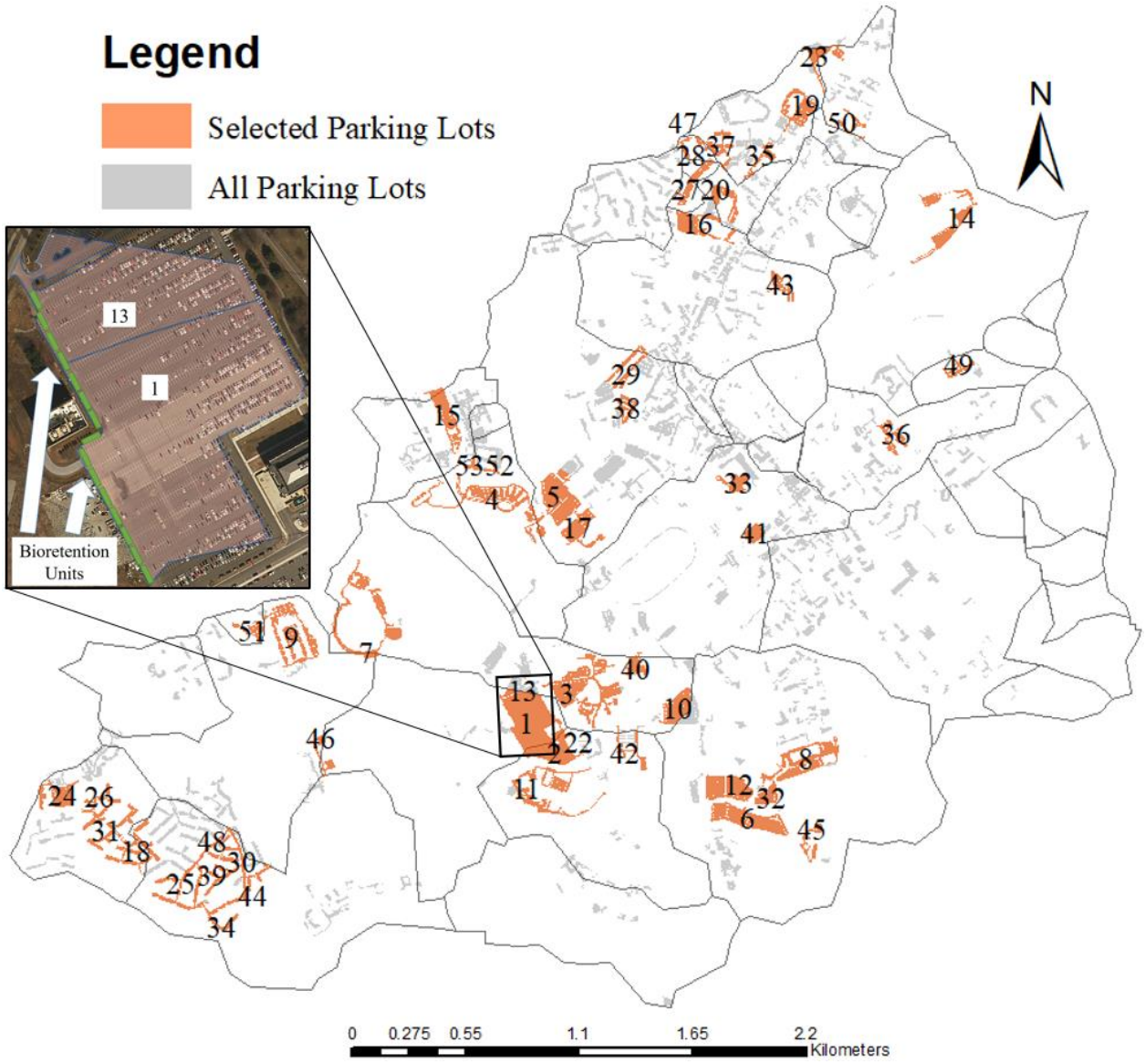

Figure 6.5. Location and numbering of the selected parking lots within the watershed with No. 1 being the largest and No. 53 being the smallest, and a schematic example of installing bioretention units for parking lots 1 and 13 (the green rectangular shapes represent bioretention units).

Table 6.4. Hydrologic and thermal results of installation of bioretention systems.

Scenario	Total Streamflow $(m^3)^2$	Total Heat Load $(J)^3$	Heat Reduction (%)	Mean Temperature (°C)	PTTET (%)
1[1]	1.95×10^6	1.80×10^{13}	-	19.83	37.90
2	1.89×10^6	1.76×10^{13}	-2.22	19.51	37.11
3	1.76×10^6	1.60×10^{13}	-11.11	19.48	37.02
4	1.90×10^6	1.74×10^{13}	-3.33	19.37	36.54

1. Represents the Current Condition or baseline scenario. 2. Simulated by SWMM model. 3. Simulated by Hybrid.

6.3 Canopy Thermal Effects

Vegetation and tree canopies reduce surface and air temperature through shading, sheltering, and evapotranspiration (Bell et al., 2009). Shading and sheltering reduce solar radiation and lower surface temperatures below canopies (which can be paved parking lots in urbanized area). These cooler surfaces result in a reduction of heat transmitted in the local atmosphere and building. Evapotranspiration reduces air temperature by using heat from air to evaporate water and add moisture to the atmosphere, which results in increased humidity levels. Various studies showed that peak air temperature in tree canopies is 5.0ºC less than open terrain areas, and suburban surface areas with mature tree canopies are cooler than those without tree canopies (Huang et al., 1990; Mcpherson et al., 2005; Sandifer and Givoni, 2002). This section evaluates the effectiveness of various pervious land cover types on the reduction of heat loads and temperatures at the watershed downstream, through the calibrated MINUHET model during the validation period. The Stroubles Creek watershed has three main land cover types for pervious area, which were used as input to the MINUHET model (Figure 6.6). Six scenarios of land cover type for pervious areas (including the current condition or baseline scenario) were designed to investigate the effects of vegetation on thermal processes within the watershed (Table 6.5). Three land cover types of bare soil, short grass, and forest canopies were selected. The scenarios were designed based on the current condition, minimum level, and maximum level of vegetation density (LVD), shading for impervious land (SIL), and shading for pervious land (SPL). The main difference between the scenarios of forest canopies (4, 5, and 6) are SIL and SPL values, which are mainly due to the height of forest canopies for each scenario (short forest canopies for scenario 4, and tall forest canopies for scenario 6). In addition and according to Herb et al. (2010), the actual maximum level of shading value would be 0.9. The current

condition of subwatersheds LVD, SIL, and SPL are illustrated on Figure 6.6 and more information concerning vegetation canopies of the watershed can be found on Appendix B.

Table 6.5. Various scenarios of using vegetation to reduce thermal effects in the watershed.

Scenario No.	Land cover of Watershed Pervious Land	Vegetation Density (%)	Shading for Impervious Land (%)	Shading for Pervious Land (%)
1	C.C.*	C.C.	C.C.	C.C.
2	Bare Soil	0	C.C.	0
3	Short Grass	100	C.C.	C.C.
4	Forest Canopies	100	C.C.	C.C.
5	Forest Canopies	100	C.C.	90
6	Forest Canopies	100	90	90

* Current Condition of the watershed (referred to as the baseline scenario).

The scenarios including forest canopies resulted in lower total heat loads and average temperatures than current conditions and short grass scenarios, primarily because of more shading on soil and impervious surfaces, and more evapotranspiration (Figure 6.7 and Table 6.6). Clearly, bare soil (scenario 2) resulted in higher heat loads and temperatures due to lower soil moisture and no shading/sheltering. SIL values of the bare soil scenario are primarily due to shading by buildings. Stream temperatures had low sensitivity to shading, while lower sensitivity for wind sheltering; in other words, stream temperature was least impacted by wind sheltering (approximately 0.0). SIL, such as roads with overhanging trees had the most sensitivity, since this can drop the temperature of the pavement prior to a storm, and the temperature of the runoff itself in the first part of a storm. Compared to impervious areas, the SPL has less of an effect, since there is less runoff from these areas. Hence, the total heat loads of scenarios 4 and 5 are similar in magnitude (SIL of scenario 5 was assumed equal to current conditions and SPL was increased to 90%). In contrast, scenario 6 resulted in far less total heat load compared to scenario 4 due to increased percentage of SIL of the watershed (Figure 6.7 and Table 6.6).

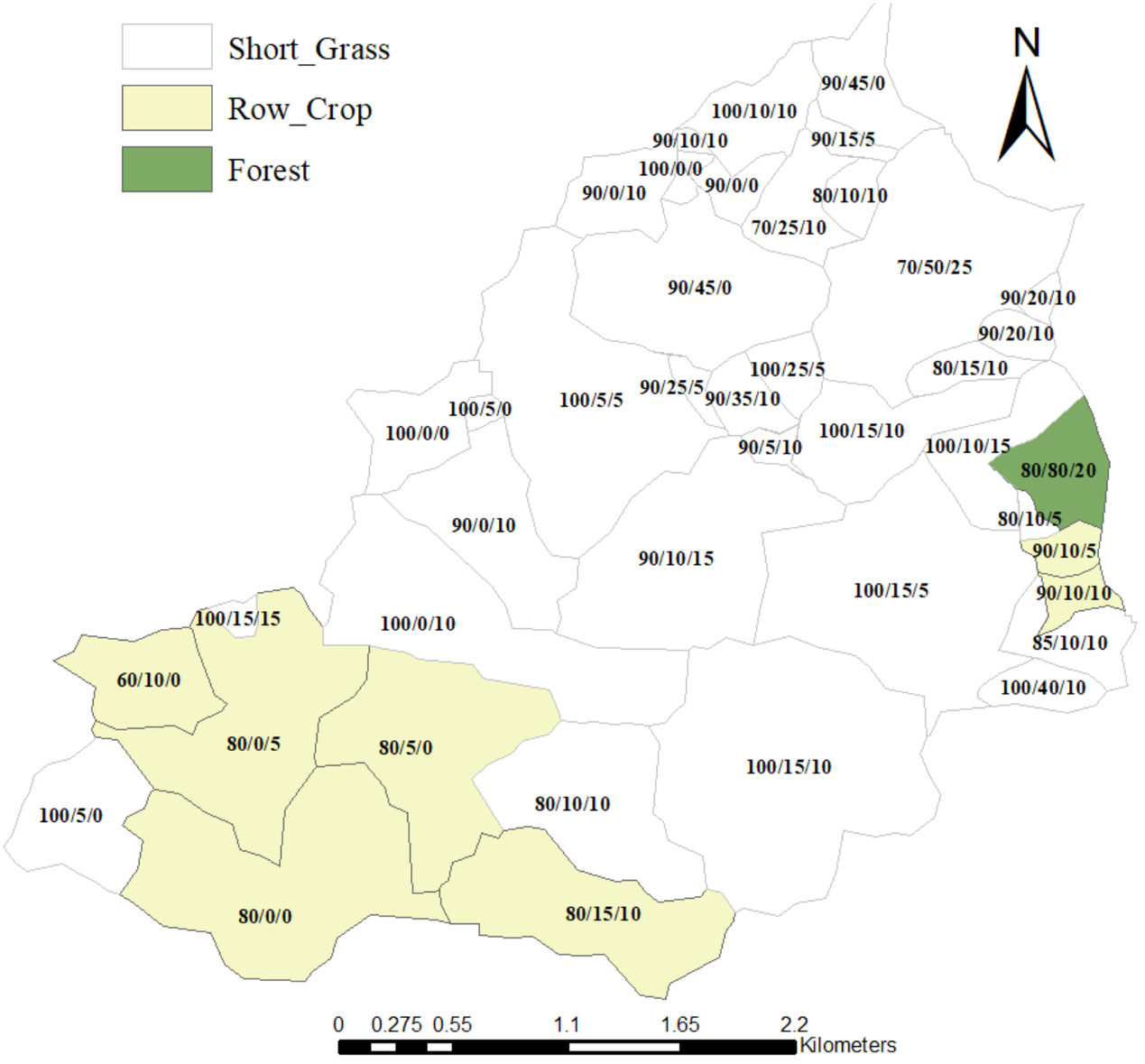

Figure 6.6. The current dominant land cover of pervious areas of each subwatershed (based on aerial imagery and field review); the three numbers on each subwatershed represent the approximate percentage of respective land cover type of pervious area, shading percentage of subwatershed pervious area, and shading percentage of impervious area, respectively.

Employing forest canopies in all pervious areas of the Stroubles Creek watershed and assuming shading of the pervious and impervious lands of 90% yielded a 24% reduction in total heat load from the watershed. The percentage of time temperature exceeded 21°C, which is a threshold for trout habitats, was 33.56% for scenario 6. There was an approximately 3.5% decrease in the aforementioned criteria compared to the baseline scenario.

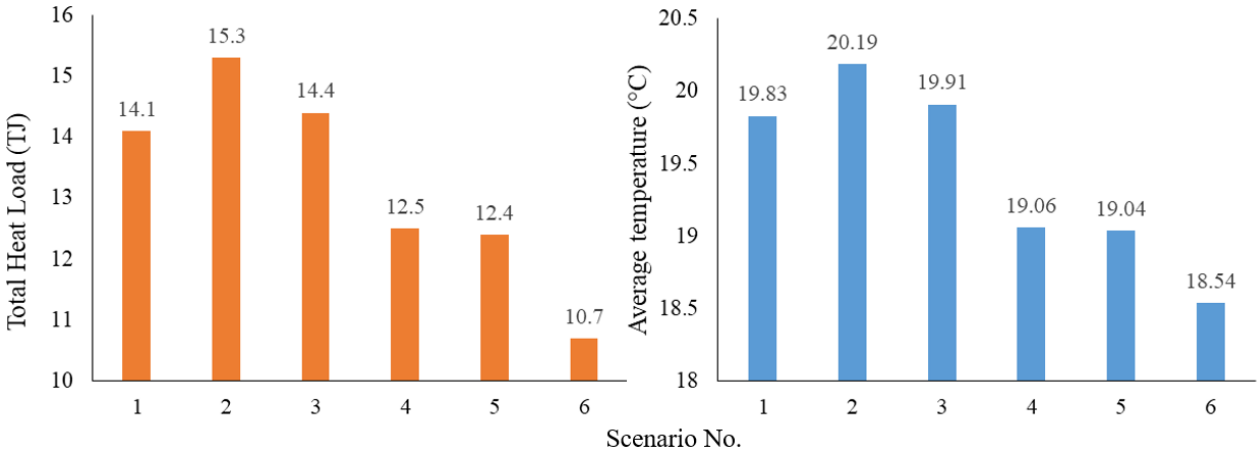

Figure 6.7. Total heat load and average temperature for the vegetation scenarios.

Table 6.6. Heat load and temperature values of canopies scenarios.

Scenario No.	**Total Heat load (J)**	**Heat Red.* (%)**	**Mean Temperature (°C)**	**PTTET (%)**
1***	1.40×10^{13}	-	19.83	37.90
2	1.53×10^{13}	8.75	20.19	39.40
3	1.44×10^{13}	2.48	19.91	38.04
4	1.25×10^{13}	-11.05	19.06	36.22
5	1.24×10^{13}	-12.29	19.04	36.18
6	1.07×10^{13}	-24.03	18.54	33.56

*Heat load percentage reduction compared to baseline scenario (reference temperature for heat load calculations is 17°C). The negative values represent heat load reduction while the positive values represents increased heat load; **threshold for trout; ***Current Condition or baseline scenario.

6.4 A Comprehensive Plan to Mitigate Thermal Pollution

According to the simulated results concerning the effectiveness of infiltration practices and watershed-based approaches (i.e. bioretention systems, concrete pavement/cool roofs, and planting forests), they can be applied through a comprehensive plan to mitigate the thermal effects of urbanization. In other words, a combination of aforementioned approaches with optimum performance can be employed to decrease the thermal impacts of urbanization within the Stroubles Creek watershed. Hence, the best of all scenarios of pavement/roofs installation, bioretention practices, and vegetation canopies were employed in a single combined scenario. The combined effects of utilizing concrete pavement and ACG roofing (scenario 9 of Table 6.1) on the impervious lands, installing bioretention systems at the outlets of selected parking lots (scenario 3 of Table 6.4), and planting trees in pervious areas (scenario 6 of Table 6.5), resulted in better performance of total heat load and mean temperature reduction than any single scenario.

Total heat load reduction, mean temperature, and PTTET index of the comprehensive plan were -69.2%, 18.02°C, and 26.61%, respectively. Using the comprehensive plan, the water temperatures violated the temperature standard for trout approximately 13% less than the scenario without any infiltration practices and watershed-based approaches. In other words, there would be less (in terms of percentage of time) thermal stress on trout population.

Chapter 7.0 Conclusion and Future Works

SWMM and MINUHET are simulation models for routing stormwater and heat loads, respectively, through urbanized mixed-land use watersheds. SWMM and MINUHET models produce high-resolution time series of streamflow and heat loads, respectively, at the outlet of a watershed. To date, MINUHET has not been evaluated for an urbanized watershed of the scale and size of the Stroubles Creek Watershed, approximately 14.1 km^2 in area. Thus, in this study MINUHET and SWMM were used to simulate streamflows and/or thermal effects of the Stroubles Creek Watershed to serve as a case study. Further, strength of each model (i.e. streamflow for SWMM and temperature for MINUHET) were combined in a unique hybrid approach to increase the accuracy of heat load simulations. The models demonstrated an ability to effectively simulate streamflow, water temperature, and heat load.

Overall, concrete pavement and ACG roof installation performed better at reducing mean temperature, heat load, and PTTET index than bioretention systems and forest canopies in the Stroubles Creek watershed. The comprehensive plan of utilizing infiltration practices and watershed-based approaches resulted in lower heat reduction and outlet mean temperature than any single scenario concrete pavement and ACG roofing, bioretention systems, and forest canopies.

The following recommendations are made for future applications of the current models:

Incorporating MINUHET routines in SWMM submodules: A catchment-based stream temperature model with hourly time step resolution and capability of utilizing a broad range of LID practices is required to evaluate temperature and heat load variations of streamflow. Since SWMM performed better at streamflow simulation, and it has a larger number of LID

submodels, it is recommended that SWMM be modified to incorporate thermal modeling capability. Hence, the mentioned method allows investigation the possible stream temperature variations impacted due to urbanization by incorporating temperature routines for both sheet and channel flow as well as runoff routines from MINUHET into SWMM.

Conducting uncertainty analysis to identify areas in which estimates of parameters needs to be improved: The sensitivity analysis conducted in this study determined the key parameters and weather variables that had a substantial impact on model simulations. Hence, any uncertainty in these parameters has the potential to considerably affect MINUHET and SWMM simulation results. Sensitivity analysis should be conducted with the key input parameters and weather parameters for a couple of large storm events, to investigate the extent to which input uncertainties may affect simulation results. The sensitivity analysis conducted in this study would provide reasonable error limits for expected uncertainties in the models inputs. Eventually, uncertainty analysis could produce a probability distribution for the models simulated results to assist in risk analysis.

Assess various thermal mitigation strategies with life cycle cost to identify the most cost-effective options: Although the effectiveness of infiltration practices and watershed-based approaches were demonstrated in this study in a number of scenarios, there is a need to assess their implementation and maintenance costs and balance these with benefits.

Evaluate the effects of combined land use and climate changes in an analysis of uncertainty for temperature and heat load: The potential for increases in stream heat loads and temperature across the Stroubles Creek Watershed as a result of combined land use and climate changes can cause challenges for the survival of sensitive aquatic species. Simulated changes to

the thermal and hydrologic regime of Stroubles Creek can be evaluated in response to a variety of scenarios of projected changing climate and land use, and consider implications of thermal stresses to sensitive aquatic species such as Trout.

Application of the models in a smaller watershed: Application of MINUHET, SWMM, and Hybrid models in a smaller watershed would likely result in a more accurate output of streamflow, heat load, and temperature. This is due to more accurate delineation of pavement/roof, and vegetation canopies areas. A smaller watershed within the main Stroubles Creek watershed could be selected, and portable gauging stations and temperature measurements conducted at its outlet. Corresponding MINUHET, SWMM and Hybrid models could then be developed, calibrated and validated. Infiltration practices and watershed-based thermal reduction approaches can be assessed at a smaller scale.

Literature Cited

Abiy, A.Z., Demissie, S.S., MacAlister, C., Dessu, S.B., Melesse, A.M., 2016. Groundwater Recharge and Contribution to the Tana Sub-basin, Upper Blue Nile Basin, Ethiopia, in: Landscape Dynamics, Soils and Hydrological Processes in Varied Climates. pp. 463–481. doi:10.1007/978-3-319-18787-7_22

Agersborg, H.P.K., 1930. The Influence of Temperature on Fish. Ecology 11, 136–144. doi:10.2307/1930786

Ahmadisharaf, E., Tajrishy, M., Alamdari, N., 2016. Integrating flood hazard into site selection of detention basins using spatial multi-criteria decision-making. J. Environ. Plan. Manag. 59, 1397–1417. doi:10.1080/09640568.2015.1077104

Al-Abed, N., Al-Sharif, M., 2008. Hydrological modeling of Zarqa River Basin - Jordan using the hydrological simulation program - FORTRAN (HSPF) model. Water Resour. Manag. 22, 1203–1220. doi:10.1007/s11269-007-9221-9

Alamdari, N., Sample, D., Steinberg, P., Ross, A., Easton, Z., 2017. Assessing the Effects of Climate Change on Water Quantity and Quality in an Urban Watershed Using a Calibrated Stormwater Model. Water 2017, Vol. 9, Page 464 9, 464. doi:10.3390/W9070464

Barco, J., Wong, K.M., Stenstrom, M.K., 2008. Automatic Calibration of the U.S. EPA SWMM Model for a Large Urban Catchment. J. Hydraul. Eng. 134, 466–474. doi:10.1061/(ASCE)0733-9429(2008)134:4(466)

Beaufort, A., Moatar, F., Curie, F., Ducharne, A., Bustillo, V., Thiéry, D., 2016. River Temperature Modelling by Strahler Order at the Regional Scale in the Loire River Basin, France. River Res. Appl. 32, 597–609. doi:10.1002/rra.2888

Bell, R., Cole, D., Deangelo, B., Desaultes, L., Dickerhoff, E., Estes, M., Heisler, G., Hitchcock, D., Klunich, K., Kollin, C., Lewis, M., Magee, J., Mcpherson, G., Nowak, D., Rodbell, P., Rosenthal, J., Sarkovich, M., Wolf, K., Yarbrough, J., Zalph, B., 2009. Reducing Urban Heat Islands: Compendium of Strategies: Trees and Vegetation.

Bogan, T., 2003. Stream temperature-equilibrium temperature relationship. Water Resour. Res. 39, 1–12. doi:10.1029/2003WR002034

Caissie, D., 2006. The thermal regime of rivers: A review. Freshw. Biol. 51, 1389–1406. doi:10.1111/j.1365-2427.2006.01597.x

Company, B.M., 2002. BERRIDGE SRI VALUES [WWW Document]. doi:http://www.berridge.com/colors/sri-values-for-berridge-cool-roof-colors/

Cooter, E.J., Cooter, W.S., 1990. Impacts of greenhouse warming on water temperature and water quality in the southern United States. Clim. Res. 1, 1–12.

Dietz, M.E., Clausen, J.C., 2005. a Field Evaluation of Rain Garden Flow and Pollutant Treatment. Water. Air. Soil Pollut. 167, 123–138.

Eckhardt, K., 2008. A comparison of baseflow indices, which were calculated with seven different baseflow separation methods. J. Hydrol. 352, 168–173. doi:10.1016/j.jhydrol.2008.01.005

Elliott, J.M., Elliott, J.A., 1995. The effect of the rate of temperature increase on the critical thermal maximum for parr of Atlantic salmon and brown trout. J. Fish Biol. 47, 917–919. doi:10.1111/j.1095-8649.1995.tb06014.x

Evans, E.C., McGregor, G.R., Petts, G.E., 1998. River energy budgets with special reference to river bed processes. Hydrol. Process. 12, 575–595. doi:10.1002/(SICI)1099-1085(19980330)12:4<575::AID-HYP595>3.0.CO;2-Y

Ferguson, B., Fisher, K., Golden, J., Hair, L., Haselbach, L., Hitchcock, D., Kaloush, K., Pomerantz, M., Tran, N., Waye, D., 2008. Reducing Urban Heat Islands: Compendium of Strategies, Cool Pavements.

Gorney, R.M., Williams, M.G., Ferris, D.R., Lance, R., Gorney, R.M., Williams, M.G., 2012. The University of Notre Dame The Influence of Channelization on Fish Communities in an Agricultural Coldwater Stream System Source : The American Midland Naturalist , Vol . 168 , No . 1 (July 2012), pp . 132-143 Published by : The University of Notre Da.

Green, W.H., Ampt, G., 1911. Studies on soil physics: I. Flow of air and water throught soils. J. Agric. Sci. 4, 1–24.

Gupta, Vijai, H., Sorooshian, S., Yapo, Ogou, P., 1999. Status of Automatic Calibration for Hydrologic Models: Comparison with Multilevel Expert Calibration. J. Hydrol. Eng. 4, 135–143.

Herb, W.R., 2008. Analysis of the effect of stormwater runoff volume regulations on thermal loading to the Vermillion River. St. Anthony Falls Lab. Proj. Reports 1–34.

Herb, W.R., Janke, B., Mohseni, O., Stefan, H.G., 2010. MINUHET (Minnesota Urban Heat Export Tool) USER MANUAL.

Herb, Erickson, T., Stefan, H.G., 2009a. Stream Temperature Modeling of Miller Creek , Duluth , Minnesota by, ST. ANTHONY FALLS LABORATORY Engineering, Minnesota Pollution Control Agency.

Herb, Janke, B., Mohseni, O., Stefan, H.G., 2009b. Runoff Temperature Model for Paved Surfaces. J. Hydrol. Eng. 14, 1146–1155. doi:10.1061/(ASCE)HE.1943-5584.0000108

Herb, Mohseni, O., Stefan, H.G., 2009c. Simulation of temperature mitigation by a stormwater detention pond. J. Am. Water Resour. Assoc. 45, 1164–1178. doi:10.1111/j.1752-1688.2009.00354.x

Hester, E.T., Bauman, K.S., 2013. Stream and Retention Pond Thermal Response to Heated Summer Runoff From Urban Impervious Surfaces. J. Am. Water Resour. Assoc. 49, 328–342. doi:10.1111/jawr.12019

Hester, E.T., Doyle, M.W., 2011. Human impacts to river temperature and their effects on biological processes: A quantitative synthesis. J. Am. Water Resour. Assoc. 47, 571–587. doi:10.1111/j.1752-1688.2011.00525.x

Hofmeister, K.L., Cianfrani, C.M., Hession, W.C., 2015. Complexities in the stream temperature regime of a small mixed-use watershed, Blacksburg, VA. Ecol. Eng. 78, 101–111. doi:10.1016/j.ecoleng.2014.05.019

Huang, Y.J., Akbari, H., Taha, H., 1990. The wind-shielding and shading effects of trees on residential heating and cooling requirements, in: Proceedings of the ASHRAE Winter Conference. United States, pp. 11–14.

Huber, W.C., Dickinson, R.E., 1988. Storm Water Management Model , Version 4 : User's Manual 720. doi:EPA/600/3-88/001a

Iowa storm water management manual, 2008. Iowa storm water management manual.

James, L., Burges, S., 1982. Selection, calibration, and testing of hydrologic models. Hydrol. Model. small watersheds.

James, W., Rossman, L.A., James, W.R.., 2010. User's guide to SWMM5.

Janke, B.D., Herb, ; William R., Mohseni, ; Omid, G., S. and H., 2013. Case Study of Simulation of Heat Export by Rainfall Runoff from a Small Urban Watershed Using MINUHET. J. Hydrol. Eng. 18, 995–1006.

Janke, B.D., Herb, W.R., Mohseni, O., Stefan, H.G., 2009. Simulation of heat export by rainfall-runoff from a paved surface. J. Hydrol. 365, 195–212. doi:10.1016/j.jhydrol.2008.11.019

Johnson, S., 2004. Factors influencing stream temperatures in small streams: substrate effects and a shading experiment. Can. J. Fish. Aquat. Sci. 61, 913.

Jones, M., Hunt, W., 2009. Bioretention impact on runoff temperature in trout sensitive waters. J. Environ. Eng. 577–585. doi:10.1061/41009(333)80

Jones, M.P., Hunt, W.F., 2010. Effect of Storm-Water Wetlands and Wet Ponds on Runoff Temperature in Trout Sensitive Waters. J. Irrig. Drain. Eng. 136, 656–661. doi:doi:10.1061/(ASCE)IR.1943-4774.0000227

Jones, M.P., Hunt, W.F., Winston, R.J., 2012. Effect of Urban Catchment Composition on Runoff Temperature. J. Environ. Eng. 138, 1231–1236. doi:doi:10.1061/(ASCE)EE.1943-7870.0000577

Kavianipour, A., Beck, J. V., 1977. Thermal property estimation utilizing the Laplace transform

with application to asphaltic pavement. Int. J. Heat Mass Transf. 20, 259–267. doi:10.1016/0017-9310(77)90212-5

Ketabchy, M., Nayeb Yazdi, M., Ahamdisharaf, E., 2016a. An Overview on Geographic Information System (GIS) Application in Environmental Management , Case Study : Algae Growth Assessment in Tampa Bay. Casp. Sea J. 10, 8–13.

Ketabchy, M., Tajrishy, M., Ahmadisharaf, E., 2016b. Development of Permeable Pavement Design Model (PPDM) for Runoff Reduction and Pollutant Removal Efficiency Prediction, in: EWRI Congress Annual Meeting Abstract. West Palm Beach, FL. doi:http://eventscribe.com/2016/ASCE-EWRI/ajaxcalls/presentationinfo.asp?pres=140280

Kinouchi, T., Yagi, H., Miyamoto, M., 2007. Increase in stream temperature related to anthropogenic heat input from urban wastewater. J. Hydrol. 335, 78–88. doi:10.1016/j.jhydrol.2006.11.002

Kong, F., Ban, Y., Yin, H., James, P., Dronova, I., 2017. Modeling stormwater management at the city district level in response to changes in land use and low impact development. Environ. Model. Softw. 95, 132–142. doi:http://dx.doi.org/10.1016/j.envsoft.2017.06.021

Li, H., Harvey, J.T., Holland, T.J., Kayhanian, M., 2013. Corrigendum: The use of reflective and permeable pavements as a potential practice for heat island mitigation and stormwater management. Environ. Res. Lett. 8, 49501. doi:10.1088/1748-9326/8/4/049501

Long, D.L., Dymond, R.L., 2014. Thermal Pollution Mitigation in Cold Water Stream Watersheds Using Bioretention. J. Am. Water Resour. Assoc. 50, 977–987. doi:10.1111/jawr.12152

Lott, D.A., Stewart, M.T., 2016. Base flow separation: A comparison of analytical and mass balance methods. J. Hydrol. 535, 525–533. doi:10.1016/j.jhydrol.2016.01.063

Luca, J., Mrawira, D., 2005. New Measurement of Thermal Properties of Superpave Asphalt Concrete. J. Mater. Civ. Eng. ASCE 17, 72–79. doi:10.1061/(ASCE)0899-1561(2005)17

Mcpherson, G., Simpson, J.R., Peper, P.J., Maco, S.E., Xiao, Q., 2005. Municipal Forest Benefits and Costs in Five US Cities. J. For.

Mohegh, A., Rosado, P., Jin, L., Millstein, D., Levinson, R., Ban-Weiss, G., 2017. Modeling the climate impacts of deploying solar reflective cool pavements in California cities. J. Geophys. Res. Atmos. 122, 6798–6817. doi:10.1002/2017JD026845

Moore, W., Mirshahi, M., Bates, K., Thrasher, B., 2016. 2016 Road and Bridge Specifications. doi:http://www.virginiadot.org/business/resources/const/VDOT_2016_RB_Specs.pdf

Moriasi, D.N., Arnold, J.G., Van Liew, M.W., Binger, R.L., Harmel, R.D., Veith, T.L., 2007. Model evaluation guidelines for systematic quantification of accuracy in watershed simulations. Trans. ASABE 50, 885–900. doi:10.13031/2013.23153

Morrill, J.C., Bales, R.C., Conklin, M.H., 2005. Estimating stream temperature from air temperature: Implications for future water quality. J. Environ. Eng. 131, 139–146. doi:10.1061/(asce)0733-9372(2005)131:1(139)

Mostaghimi, S., Benham, B., Brannan, K., Dillaha, T.A., Wagner, R., Wynn, J., Y., G., Zeckoski, R., 2003. Benthic TMDL for Stroubles Creek in Montgomery County, Virginia.

Nash, J.E., Sutcliffe, J. V, 1970. River Flow Forecasting Through Conceptual Models Part I-a Discussion of Principles*. J. Hydrol. 10, 282–290. doi:10.1016/0022-1694(70)90255-6

Nayeb Yazdi, M., Delavarrafiee, M., Arhami, M., 2015. Evaluating near highway air pollutant levels and estimating emission factors: Case study of Tehran, Iran. Sci. Total Environ. doi:10.1016/j.scitotenv.2015.07.141

Neff, B.P., Day, S.M., Piggott, A.R., Fuller, L.M., 2005. Base flow in the Great Lakes basin. U.S. Geol. Surv. Sci. Investig. Rep. 32.

NRCS, 2007. National Engineering Handbook Chapter 7 Hydrologic Soil Groups, United States Department of Agriculture. doi:https://directives.sc.egov.usda.gov/OpenNonWebContent.aspx?content=17757.wba

NRCS, 1986. Urban Hydrology for Small Watersheds TR-55. USDA Nat. Resour. Conserv. Serv. Conserv. Engeneering Div. Tech. Release 55 164. doi:Technical Release 55

Rawls, W.J., 2006. Infiltration properties, 2nd Ed. ed. Taylor and Francis, Boca Raton, FL.

Rossman, L.A., 2009. Storm Water Management Model: User's Manual. doi:https://www.epa.gov/water-research/storm-water-management-model-swmm

Sandifer, S., Givoni, B., 2002. THERMAL EFFECTS OF VINES ON WALL TEMPERATURES-COMPARING LABORATORY AND FIELD COLLECTED DATA, in: Proceedings of the Annual Conference of the American Solar Energy Society. Reno, NV.

Selbig, W.R., 2015. Simulating the effect of climate change on stream temperature in the Trout Lake Watershed, Wisconsin. Sci. Total Environ. 521–522, 11–18. doi:10.1016/j.scitotenv.2015.03.072

Singh, J., Knapp, H.V., Arnold, J.G., Demissie, M., 2004. Hydrologic Modeling of the Iroquois River Watershed Using HSPF and SWAT. J. Am. Water Resour. Assoc. 41, 343–360. doi:10.1111/j.1752-1688.2005.tb03740.x

Stefan, H.G., Herb, W.R., Janke, B., Mohseni, O., Stefan, H.G., 2008. Thermal Pollution of Streams by Runoff From Paved Surfaces. Hydrol. Process. 22, 987–999. doi:10.1002/hyp.6986

Taylor, C.A., Stefan, H.G., 2009. Shallow groundwater temperature response to climate change and urbanization. J. Hydrol. 375, 601–612. doi:10.1016/j.jhydrol.2009.07.009

The Virginia Department of Environmental Quality, 2011. VA DEQ STORMWATER DESIGN SPECIFICATION NO. 9 BIORETENTION. doi:http://www.vwrrc.vt.edu/swc/documents/2013/DEQ%20BMP%20Spec%20No%209_BIORETENTION_FinalDraft_v1-9_03012011.pdf

Thompson, A.M., Kim, K., Vandermuss, A.J., 2008. Thermal characteristics of stormwater runoff from asphalt and sod surfaces. J. Am. Water Resour. Assoc. 44, 1325–1336. doi:10.1111/j.1752-1688.2008.00226.x

Virginia Department of Conservation and Recreation, 1999. Virginia Stormwater Management Handbook Volume I I, 619.

Wakchaure, A.S., Randolph, J., Zahm, D., Carstensen, L.W., 2001. An ArcView tool for simulating Land Subdivision for Build Out Analysis. Virginia Tech. doi:https://vtechworks.lib.vt.edu/bitstream/handle/10919/37156/Ashwini_W_Project.pdf?sequence=1

Walsh, C.J., Allison, H.R., Feminella, J.W., Cottingham, P.D., Groffman, P.M., Ii, R.P.M., 2005. The urban stream syndrome: current knowledge and the search for a cure. J. North Am. Benthol. Soc. 24, 706–723. doi:10.1899/04-028.1

Wanielista MP, 1997. Hydrology and water quality control, 2nd edn. ed. Wiley, New York.

Webb, B., Zhang, Y., 1999. Water temperatures and heat budgets in Dorset chalk water courses. Hydrol. Process. 13, 309–321. doi:10.1002/(sici)1099-1085(19990228)13:3<309::aid-hyp740>3.0.co;2-7

Wehrly, Wang, L., Mitro, M., 2007. Field-Based Estimates of Thermal Tolerance Limits for Trout: Incorporating Exposure Time and Temperature Fluctuation. Trans. Am. Fish. Soc. 136, 365–374. doi:10.1577/T06-163.1

Xin, Z., Kinouchi, T., 2013. Analysis of stream temperature and heat budget in an urban river under strong anthropogenic influences. J. Hydrol. 489, 16–25.

Xing, W., Li, P., Cao, S., Gan, L., Liu, F., Zuo, J., 2016. Layout effects and optimization of runoff storage and filtration facilities based on SWMM simulation in a demonstration area. Water Sci. Eng. 9, 115–124. doi:http://dx.doi.org/10.1016/j.wse.2016.06.007

Appendix A. The geologic map of the Stroubles Creek Watershed

The geologic map of the Stroubles Creek Watershed (georeferenced and digitized as a hard copy from the Geology and Mineral Resources Division of Commonwealth of Virginia, 1985) is displayed in Figure A.1 (https://www.dmme.virginia.gov/dgmr/mapspubs.shtml). Below are the descriptions regarding the geologic characteristics of areas of the watershed; the followings description can be used as legend for Figure A.1.

Al (Alluvium; the area along the Stroubles Creek, which is represented by red yellow color): Floodplain deposits of stratified light-gray to light-brown, unconsolidated sand, silt, and clay with beds and lenses of pebbles and cobbles. Thickness: 0-9.2m.

Td (Talus deposits; the area beneath the ponds of the watershed, which is represented by yellow): Unconsolidated, unsorted boulder fields composed of 0.3-1.8m thick angular boulders of quartzite, siliceous sandstone and quartzes conglomerate. This detritus has been derived from nearby state of Mississippian, Silurian and Devonian age. Thickness: 0-9.2m.

Ce (Elbrook Formation; which is represented by red color): The uppermost part of the formation is characterized by interbedded sandy, commonly crossbed, fine-grain dolomite containing thin (1-10cm) lenses of fine to medium-grained sandstone and 0.3-1.2m thick ribbon-banded limestone dolomite.

Cr (Rome Formation; the area mostly at the eastern portion of the watershed, which is represented by red color and black lines): Consists of interbedded mottled, maroon and green phylittic mudstone, fine-grained sandstone and siltstone, and dark-gray, fine-grained dolomite.

Ccr (Copper Ridge Formation; the area upstream of the watershed, which is represented by yellow color): inter-bedded medium-gray, fine to medium-grained locally grained, massive dolomite, supper siliceous oolite and quartzose sandstone. Total thickness is about 366m.

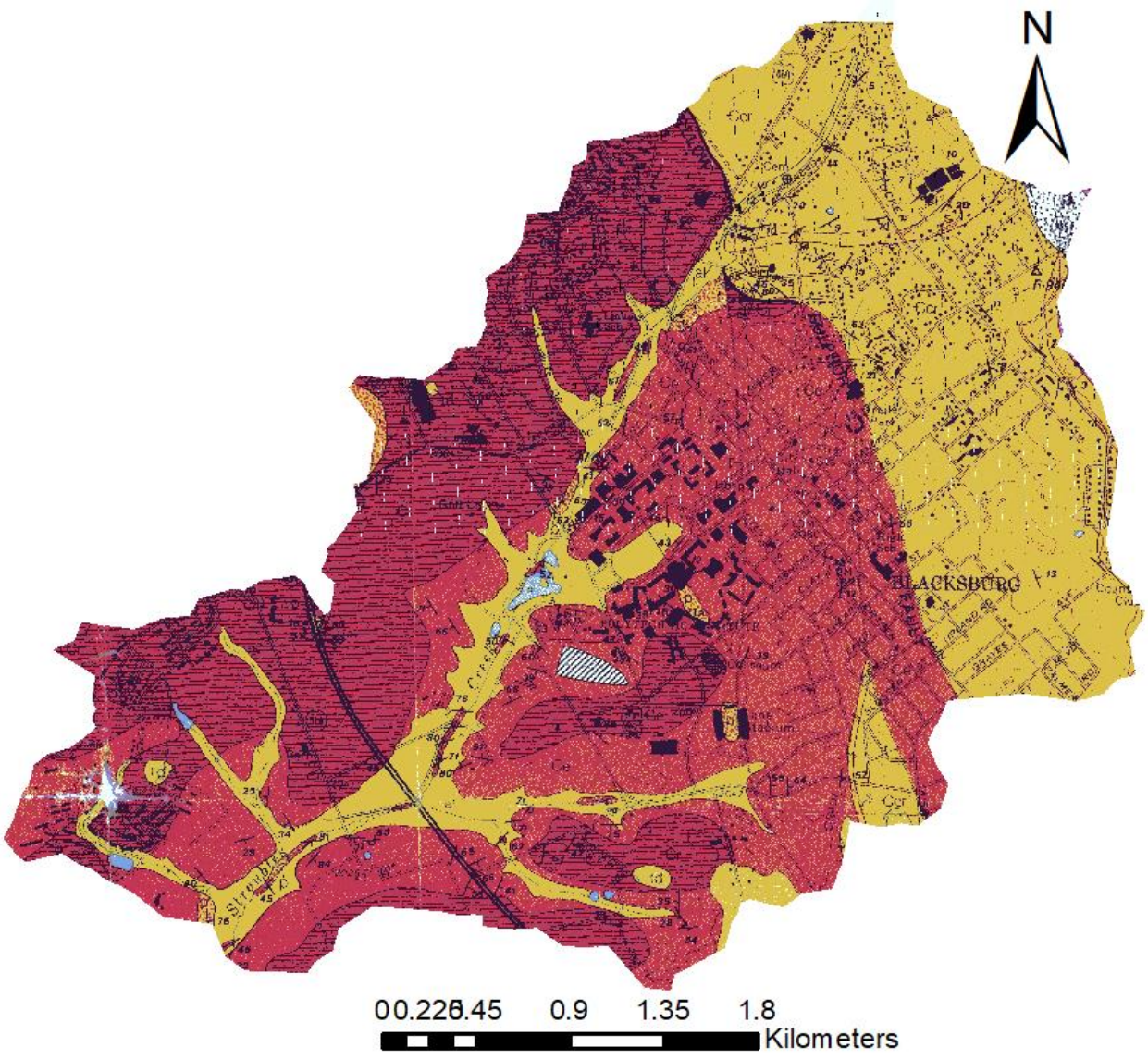

Figure A.1. The geologic map of the Stroubles Creek Watershed.

Appendix B. Watershed Characteristics as Input to the SWMM Model

The subwatershed characteristics, which were used as input to the Calibrated SWMM Model, are shown in Figure B.1 and Table B.1. In addition to SWMM, the input data used for subwatershed characteristics of MINUHET model are shown in Table B.2. Area, length, width, roughness and slope parameters values used for pervious and impervious lands of SWMM model were used as input for MINUHET model as well; hence, the parameters mentioned above are not included in Table B.2.

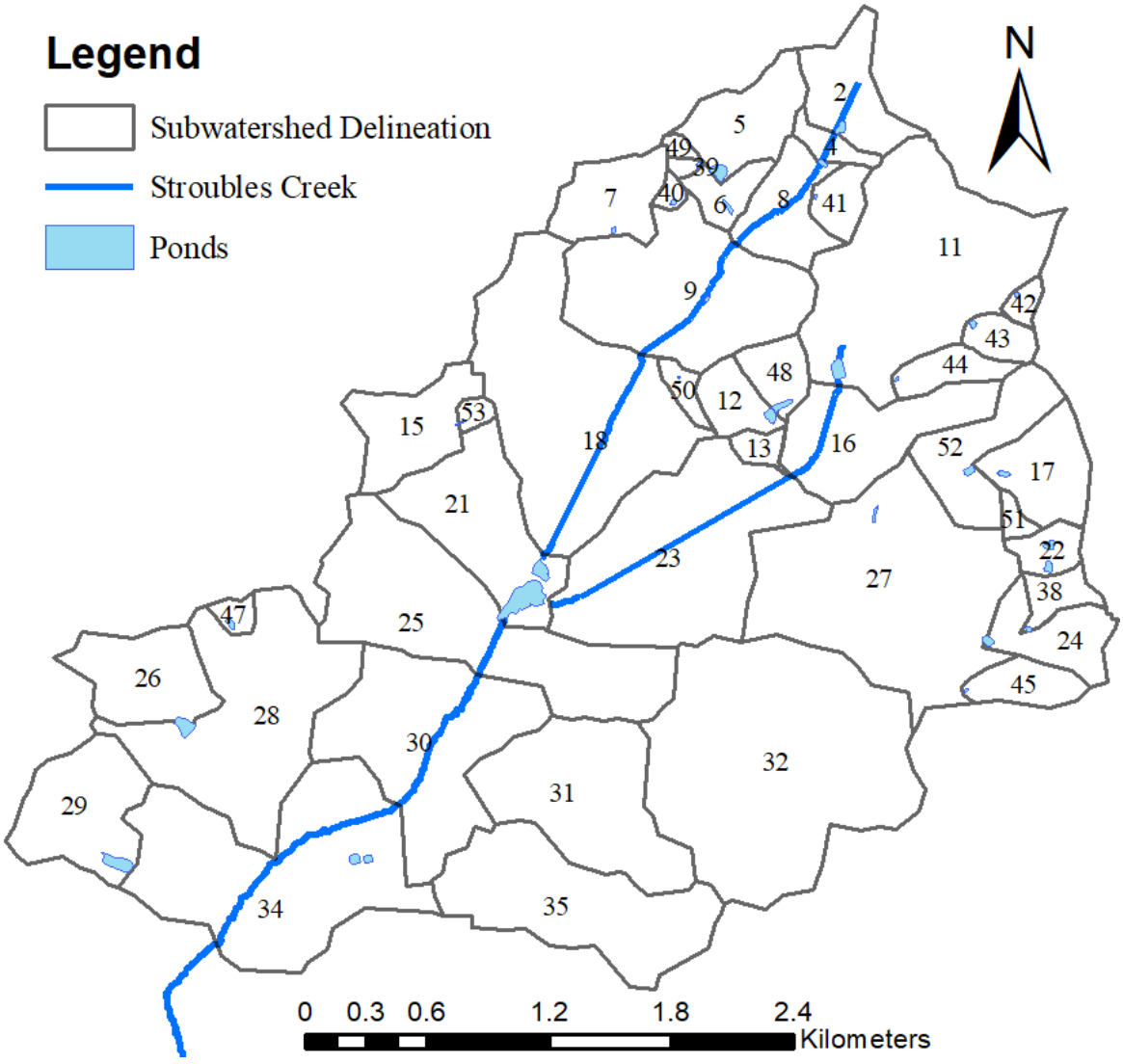

Figure B.1. The subwatershed delineation; the numbers on each subwatershed represent subwatershed No.

Table B.1. The input watershed parameters for the calibrated SWMM model.

Wat. No.*	Area (m^2)	Width (m)	Slope (%)	Imperv. (%)	N Imperv.*	N Perv.*	Suction Head (cm)	Conductivity (mm/hr.)	Initial Deficit (frac.)
2	2.14E+05	620	1.12	37	0.010	0.239	16.99	7.87	0.284
4	5.07E+04	354	1.25	37	0.012	0.342	16.99	6.15	0.284
5	2.21E+05	271	0.81	53	0.009	0.365	14.00	7.98	0.237
6	8.07E+04	213	0.94	50	0.013	0.369	16.99	7.29	0.284
7	1.95E+05	946	0.89	51	0.011	0.348	14.00	9.53	0.237
8	1.94E+05	304	1.46	26	0.011	0.355	24.00	5.84	0.284
9	6.68E+05	772	1.10	40	0.013	0.343	24.00	5.94	0.284
11	9.10E+05	733	1.40	26	0.009	0.220	24.00	4.37	0.284
12	1.04E+05	203	0.58	41	0.014	0.350	21.50	1.30	0.244
13	3.93E+04	231	0.46	55	0.010	0.231	24.00	0.81	0.321
15	2.36E+05	957	0.60	48	0.009	0.339	08.53	20.14	0.147
16	3.63E+05	583	0.98	32	0.010	0.305	14.00	10.36	0.237
17	2.12E+05	661	1.74	22	0.014	0.386	6.10	34.34	0.105
18	9.60E+05	674	0.78	50	0.008	0.245	14.00	7.32	0.237
21	4.24E+05	551	0.86	29	0.012	0.326	24.00	6.10	0.284
22	7.06E+04	512	1.18	15	0.012	0.356	09.14	11.46	0.170
23	8.18E+05	568	0.73	50	0.011	0.218	32.00	0.05	0.378
24	1.74E+05	1161	1.76	12	0.011	0.291	19.48	4.14	0.264
25	8.04E+05	930	0.85	30	0.011	0.341	24.00	6.63	0.284
26	2.72E+05	392	0.83	28	0.013	0.292	07.90	21.16	0.140
27	1.02E+06	830	0.99	35	0.012	0.329	11.00	12.80	0.190
28	7.56E+05	541	0.98	21	0.013	0.291	11.00	11.51	0.190
29	3.37E+05	403	0.96	46	0.013	0.279	14.00	5.87	0.237
30	6.92E+05	695	0.73	15	0.014	0.354	14.00	6.65	0.237
31	5.60E+05	605	0.89	24	0.012	0.280	14.00	9.58	0.237
32	1.32E+06	915	0.80	33	0.013	0.260	12.93	5.16	0.264
34	9.43E+05	732	0.78	20	0.011	0.366	14.00	11.43	0.237
35	5.93E+05	510	0.92	10	0.008	0.275	14.00	8.71	0.237
38	6.99E+04	244	1.80	7	0.009	0.291	12.93	3.25	0.264
39	1.33E+04	182	0.77	61	0.013	0.300	12.93	3.63	0.264
40	1.96E+04	294	0.85	43	0.009	0.229	10.29	10.36	0.180
41	7.82E+04	418	1.29	29	0.008	0.316	14.00	9.98	0.237
42	2.99E+04	253	1.56	38	0.010	0.262	14.00	6.93	0.237
43	6.78E+04	240	1.75	31	0.013	0.302	19.48	4.01	0.264
44	9.22E+04	222	1.50	26	0.008	0.341	11.00	15.21	0.190
45	1.07E+05	176	0.96	25	0.010	0.364	21.50	1.47	0.244
47	3.16E+04	200	0.93	44	0.012	0.344	05.97	44.73	0.090
48	9.70E+04	435	0.80	30	0.010	0.286	21.50	1.40	0.244
49	1.58E+04	72	0.77	55	0.010	0.274	14.00	7.67	0.237

Continuation of previous page

50	4.06E+04	110	0.98	68	0.013	0.388	14.00	7.34	0.237
51	2.61E+04	73	2.02	22	0.014	0.385	06.10	33.81	0.105
52	2.49E+05	447	1.61	29	0.012	0.366	11.00	8.92	0.190
53	2.43E+04	141	0.69	62	0.009	0.232	24.00	7.92	0.284

*Wat: Watershed; N Imperv.: Manning's n for impervious area; N Perv.: Manning's n for pervious area.

Table B.2. The input watershed parameters for the calibrated MINUHET model.

	Pervious Land					**Impervious Land**	
Wat. No.[1]	**Shading (%)[2]**	**Soil Type[3]**	**Soil moisture status[4]**	**Vegetation density (%)[5]**	**Dominant Land use[6]**	**Shading (%)**	**Dominant Land use[7]**
2	45	C	nor[8]	90	S.G[10]	0	RR[9]
4	15	C	nor	90	S.G	5	RR
5	10	B	nor	100	S.G	10	RR
6	0	C	nor	90	S.G	0	CR[9]
7	0	C	nor	90	S.G	10	RR
8	25	C	nor	70	S.G	10	A[9]
9	45	C	nor	90	S.G	0	A
11	50	C	nor	70	S.G	25	RR
12	35	C	nor	90	S.G	10	RR
13	5	C	nor	90	S.G	10	A
15	0	C	nor	100	S.G	0	A
16	15	C	nor	100	S.G	10	A
17	80	C	nor	80	F[10]	20	RR
18	5	C	nor	100	S.G	5	RR
21	0	C	nor	90	S.G	10	A
22	10	C	nor	90	R.C	5	A
23	10	C	nor	90	S.G	15	CR
24	10	C	nor	85	S.G	10	RR
25	0	C	nor	100	S.G	10	CR
26	10	C	nor	60	R.C	0	RR
27	15	C	nor	100	S.G	5	A
28	0	B	nor	80	R.C	5	RR
29	5	B	nor	100	S.G	0	RR
30	5	B	nor	80	R.C	0	CR
31	10	B	nor	80	S.G	10	A
32	15	C	nor	100	S.G	10	CR
34	0	B	nor	80	R.C[10]	0	RR
35	15	B	nor	80	R.C	10	RR
38	10	C	nor	90	R.C	10	C[9]
39	10	C	nor	90	S.G	0	A
40	0	C	nor	100	S.G	0	A
41	10	B	nor	80	S.G	10	CR
42	20	C	nor	90	S.G	10	RR
43	20	C	nor	90	S.G	10	RR

Continuation of previous page

44	15	C	nor	80	S.G	10	A
45	40	C	nor	100	S.G	10	RR
47	15	B	nor	100	S.G	15	A
48	25	C	nor	100	S.G	5	RR
49	10	C	nor	90	S.G	10	RR
50	25	C	nor	90	S.G	5	A
51	10	C	nor	80	S.G	5	A
52	10	C	nor	100	S.G	15	A
53	0	C	nor	100	S.G	0	A

1. Wat: Watershed.
2. The degree of shading from trees and buildings, 0.0 = no shading, 100= full shading.
3. USDA hydrologic soil group.
4. Near surface soil moisture prior to storm events.
5. The vegetation canopy density, 0.0 = no vegetation, 100 = full vegetation.
6. The dominant pervious land use for the watershed.
7. The dominant impervious surface type.
8. Normal.
9. RR: Residential Roof, CR: Commercial Roof, A: Asphalt, C: Concrete.
10. S.G: Short Grass, F: Forest, R.C: Row_Crop

Appendix C. Areas of parking lots and bioretention systems, and number of bioretention units for each parking lots

Table C.1. Areas of parking lots and bioretention systems, and number of bioretention units for each parking lots.

Parking Lot No.	Parking Lot Area (m^2)	Total Bioretention are (m^2)[1]	No. of Bioretention Units[2]
1	46016	2301	11
2	46016	2301	11
3	40491	2025	10
4	31425	1571	8
5	28706	1435	7
6	27538	1377	7
7	25693	1285	6
8	24386	1219	6
9	24353	1218	6
10	23009	1150	6
11	22952	1148	6
12	21504	1075	5
13	20837	1042	5
14	19437	972	5
15	16998	850	4
16	16334	817	4
17	14790	739	4
18	13396	670	3
19	12723	636	3
20	12108	605	3
21	11810	590	3
22	11810	590	3
23	11492	575	3
24	11271	564	3
25	10870	544	3
26	9443	472	2
27	9344	467	2
28	9344	467	2
29	9026	451	2
30	8865	443	2
31	8380	419	2
32	8036	402	2
33	7642	382	2
34	7321	366	2
35	7276	364	2
36	7167	358	2

Continuation of previous page

37	7159	358	2
38	6298	315	2
39	6228	311	2
40	6214	311	2
41	6119	306	2
42	6114	306	2
43	5878	294	1
44	5781	289	1
45	5677	284	1
46	5505	275	1
47	5437	272	1
48	5433	272	1
49	5429	271	1
50	5327	266	1
51	5250	263	1
52	5128	256	1
53	5038	252	1

1. It represents 5% of respective parking lot area. 2. Each bioretention unit area is assigned to 202 m^2.

Appendix D. The baseflow separation method

Baseflow separation involves separating stream hydrograph into baseflow and runoff. The most widely used methods of baseflow separation are analytical methods (Lott and Stewart, 2016). A hydrograph is composed of long and short waves; analytical methods assume that the long waves are due to baseflow with a lower amplitude, while direct runoff makes shorter waves with greater frequency variability of streamflow (Abiy et al., 2016). Eckhardt, (2008) developed a two parameters equation through numerical analysis for baseflow separation, which is provided in Eq. 5

$$b_k = \frac{(1-BFI_{\max})ab_{k-1}+(1-a)BFI\times y_k}{1-aBFI_{max}} \quad \text{Eq. D.1}$$

Where *a* is, the groundwater recession constant, y is the total streamflow, b is the baseflow, and k is the time step number. There are three values for maximum baseflow index (BFI_{max}) parameter; 0.80 for perennial streams with porous aquifers, 0.50 for ephemeral streams with porous aquifers, and 0.25 for perennial streams with hard rock aquifers. In the current study, a web-based hydrograph analysis tool (WHAT) was used for baseflow separation using the Eckhardt method (Eckhardt, 2008). The aforementioned method is able to separate baseflow more accurate than other numerical methods, since it utilizes two-parameter filters (Eckhardt, 2008; Neff et al., 2005). Since the current stream study is perennial with porous aquifers underneath, a BFI_{max} of 0.80 was applied.